Plasma Phys. Control. Fusion **50** (2008) 043001 (87pp) doi:10.1088/0741-3335/50/4/043001

REVIEW ARTICLE

Application of dimensionless parameter scaling techniques to the design and interpretation of magnetic fusion experiments

T C Luce[1], **C C Petty**[1] **and J G Cordey**[2]

[1] General Atomics, PO Box 85608, San Diego, CA 92186-5608, USA
[2] UKAEA Fusion, Culham Science Centre, Abingdon, Oxfordshire, OX14 3DB

Received 20 August 2007, in final form 13 February 2008
Published 10 March 2008
Online at stacks.iop.org/PPCF/50/043001

Abstract

A review of the application of dimensionless parameter scaling techniques to magnetic fusion experiments is presented. Because the methods of this type of analysis are not generally known, a detailed discussion of the basis for these techniques is given, including examples. The primary applications and successes of these methods in magnetic fusion research are in the area of transport of energy and particles across surfaces of constant magnetic flux. The experimental justification for the use of these techniques to describe transport is given, and the applications are reviewed. The two key applications of these techniques, the identification of the underlying physical mechanisms that cause transport and the projection of the transport in future devices from present-day experiments, are extensively discussed. Comparison of the results of dimensionless parameter scaling experiments with the regression analysis of multi-machine databases points to limitations in the databases and the analysis of them as the source of the discrepancies. These discrepancies have significant implications for the design optimization of tokamaks, which are discussed here. Finally, the application of dimensionless parameter scaling techniques to plasma stability, to the boundary region between closed and open field lines and to divertor operation in the open field line region are reviewed and discussed.

(Some figures in this article are in colour only in the electronic version)

1. Introduction

Dimensionless parameter scaling techniques are a robust method for obtaining qualitative and quantitative information about complex physical systems when complete mathematical descriptions of the systems cannot be found. Two distinct situations where such complete descriptions cannot be obtained are commonly encountered. The first case is when a mathematical model describing the quantity of interest does not yet exist. If a set of parameters

that are believed to determine the behavior of this quantity can be written down, based on intuition or experimentation, then application of established techniques for finding appropriate dimensionless parameters can provide significant information on the relationships among the original set of empirical parameters. In the second case, the governing equations are established, but they are impossible to solve analytically or numerically in the situation of interest. Again, the use of dimensionless parameter scaling techniques can lead to the identification of a few key parameters that characterize the behavior of the system. Both of these situations are encountered routinely in plasma physics. Once dimensionless parameter techniques have been applied, the results are especially useful for predicting the physical behavior in situations that would be impractical (or undesirable) to test directly by experiment. The application of dimensionless parameter scaling techniques in a specific area of plasma physics—the design and interpretation of magnetic fusion experiments—is the subject of this review.

Dimensionless parameter scaling techniques appear under a variety of names. The names dimensional analysis, scale invariance and similarity correspond to the situations outlined above. As will be explained in more detail in the following section in the context of plasma physics, each of these techniques requires different types of input and yields differing information about the system under consideration. The power of these techniques is a direct result of the simple yet profound truth that the behavior of a physical system cannot depend on the choice of physical units employed to measure it.

An awakening to the power of dimensionless parameter techniques appears to have occurred in the early part of the twentieth century. Papers promoting the use of these techniques appeared almost simultaneously in the United States [1,2] and the United Kingdom [3]. While these authors provide little attribution to prior work, the style of writing indicates that these techniques were at least under wide discussion at the time of their writing. The paper by Buckingham [2] has achieved a more lasting renown, perhaps because it has a more tutorial style[3]. By the mid-century, the techniques appeared in standard texts in physics [5, 6] and engineering [7], primarily in topics related to fluid behavior.

Theoretical problems lend themselves rather naturally to dimensionless parameter techniques, but experimentalists have been somewhat slower to adopt these methods. Lord Rayleigh, in the opening lines of his paper entitled 'The Principle of Similitude' [3], takes his contemporaries to task:

> I have often been impressed by the scanty attention paid... to the great principle of similitude. It happens not infrequently that results in the forms of 'laws' are put forward as novelties on the basis of elaborate experiments, which might have been predicted a priori after a few minutes' consideration.

A 'few minutes' consideration' of Rayleigh's paper shows that he neither explains his methods nor refers the interested reader to an explanation. These techniques often appear mysterious and arbitrary to those who see them for the first time, which is a significant obstacle to their adoption. Sedov, in his book on the application of these techniques to mechanics, states that the situation in his field had improved in the intervening years [6, p 2]:

> In fact it is out of the question to formulate and carry out experiments nowadays without making use of similarity and dimensionality concepts.

The experience in fusion research is somewhat different from that of Sedov, in that the consideration of dimensionless parameter techniques was absent from the design of

[3] Readers may benefit from the exposition of dimensional analysis following Buckingham's approach in a monograph containing lectures to graduate students at Yale University by Bridgman [4].

experiments before 1990. However, a later comment by Sedov more accurately describes the situation reviewed here [6, p 2]:

> [I]n spite of their simple and elementary character, the methods of dimensional analysis and similarity theory require considerable experience and ingenuity on the part of the investigator, when probing into the properties of some new phenomenon.

It is the collective experience and ingenuity of plasma physics investigators who have applied these techniques that this review seeks to make accessible to the community. Therefore, this review begins with a brief tutorial on dimensionless parameter scaling techniques in section 2, including specific examples relevant to familiar situations and to plasma physics. The main application of these techniques to date in magnetic fusion experiments has been to the local analysis of the transport of energy and particles, which are reviewed in section 3. Related methods are applied to global energy confinement databases both for analysis and interpretation of the results of regression. This work is discussed in section 4, along with a comparison of the results of the local and the global analysis. The success of dimensionless parameter scaling in describing energy transport in plasmas has motivated the application in other areas of magnetic fusion research. A summary of the use of these methods and preliminary experiments in the areas of H-mode transitions and pedestals, scrape-off layer and divertor behavior, and magnetohydrodynamic (MHD) stability is given in section 5, along with suggestions for how future experiments might be carried out. Finally, a brief summary of the most significant experimental findings and some conclusions about the use of dimensionless parameter scaling techniques in magnetic fusion plasmas are offered in section 6.

2. Conceptual basis for the application of dimensionless parameter scaling in plasmas

Dimensionless parameter scaling techniques are used in many branches of physics. As noted in the introduction, they are used extensively in fluid dynamics and aeronautics; however, their widespread use in plasma physics is fairly recent. Two practical applications are predominant. One application is applying the dimensionless parameter scaling techniques to design an appropriate scale model, so that information can be obtained on the behavior of a full-scale device. Testing of the aerodynamic properties of a material object in a wind tunnel is a familiar example of this application. Another application is the identification of the boundaries of regimes where the behavior of a physical system changes, based on changes in the values of the dimensionless parameters. The transition from laminar flow to turbulent flow of a fluid at critical value of the Reynolds number is one such example. In both cases, the procedure is first to identify the key variables that control the physical process under study. From these dimensional variables, a set of dimensionless variables is then constructed. Two related methods, dimensional analysis and scale invariance, are commonly used to find the appropriate dimensionless parameters. Once these parameters have been determined, the concept of similarity is needed to determine what constitutes an appropriate scale model. In this section, these three methods—dimensional analysis, scale invariance and similarity—will be introduced. The historical development of the application of dimensionless parameter scaling to fusion plasmas will serve as examples of these various concepts.

2.1. Dimensional analysis

The first author to formalize the technique of dimensional analysis was Buckingham [2], elucidating what became known as the Π theorem. Any physical system can be described by

Table 1. Variables considered for determining the range of a spherical projectile in air.

Variable	Symbol	Dimensions
Range	R	Length
Diameter	d	Length
Surface perturbation size	δ	Length
Projectile mass	m	Mass
Projectile speed	V	Length/time
Angular frequency of the projectile	ω	1/time
Mass density of air	ρ	Mass/(length)^3
Viscosity of air	μ	Mass/length·time
Wind speed	u	Length/time
Gravitational acceleration	g	Length/(time)^2

an equation of the general form

$$f(Q_1, Q_2, Q_3, \ldots, Q_M) = 0, \tag{2.1}$$

where the quantities Q_i have physical dimensions. If any of these quantities have the same dimensional units, then they can be treated in the function f as ratios r_i to a chosen one of the Q_i. The general equation then becomes

$$f(Q_1, Q_2, Q_3, \ldots, Q_N; r_1, r_2, r_3, \ldots, r_{M-N}) = 0. \tag{2.2}$$

In general, combinations of the dimensional quantities Q_i can only appear in physically realistic equations as products or as sums of like dimensional terms and not as the arguments of any transcendental functions. Therefore, the arbitrary function f in equation (2.2) can be replaced by a sum of products of the dimensional quantities. A general form of these products can be defined as

$$\Pi = Q_1^{\mathrm{a}} Q_2^{\mathrm{b}} Q_3^{\mathrm{c}} \ldots, \tag{2.3}$$

where the product Π is required to be dimensionless. The requirement that Π be dimensionless follows from the principle that all terms in a sum must have the same units. Returning to the original Q_N dimensional variables, there are only k independent variables needed to evaluate the quantities $\{Q_i\}$, where k is determined by the number of physical units (mass, length, time, etc) required for evaluation of the $\{Q_i\}$. The other N-k variables can be considered as derived from the set $\{Q_1, \ldots, Q_k\}$. These variables will now be denoted as the set $\{P_i\}$. Then, any 'complete' equation describing a physical system can be expressed in the form:

$$\psi(\Pi_1, \Pi_2, \Pi_3, \ldots, \Pi_{N\text{-}k}) = 0, \tag{2.4}$$

where the products Π_i are the complete set of independent dimensionless variables. These products are determined from equations of the form

$$\Pi_i = Q_1^{\mathrm{a}} Q_2^{\mathrm{b}} \ldots Q_k^k P_i. \tag{2.5}$$

The fact that Π must be dimensionless yields unique constraint equations for the exponents of the Q_i for each Π_i.

While this treatment is general, it is not obvious how to apply it to a real physical problem or whether it will yield any valuable information. Before taking on plasma physics, an example from the field of mechanics may be enlightening. A simple problem of interest is the range of a spherical projectile in air. Following Buckingham's approach, the first task is to choose a list of dimensional variables that will be treated as a comprehensive list. Table 1 lists the set of variables chosen for this problem. The first step is to convert all but one of the variables that have the same dimensions to ratios of like quantities. From table 1, the variables R, d and δ all have

Table 2. Evaluation of dimensionless parameters for various spherical projectiles. Properties of air used are typical of sea level ($\rho = 1.23\,\mathrm{kg\,m^3}$, $\mu = 1.73 \times 10^{-5}\,\mathrm{kg\,m^{-1}\,s^{-1}}$). Typical values for V and ω were chosen by search of various sources.

Projectile	m (kg)	V ($\mathrm{m\,s^{-1}}$)	ω ($\mathrm{rad\,s^{-1}}$)	$(\mathrm{m^2 g\,\mu^{-2}})^{1/3}$ (m)	Π_2	Π_3	Π_4	Π_3'	Π_4'
Table tennis ball	0.0027	30	1000	62	1.8	1.59×10^{10}	1.09×10^{8}	146	9.2×10^{-9}
Golf ball	0.046	50	300	410	0.49	7.3×10^{9}	1.85×10^{9}	4.0	5.4×10^{-10}
Tennis ball	0.057	50	400	470	0.40	2.2×10^{10}	2.3×10^{9}	9.4	4.4×10^{-10}
Baseball	0.142	50	100	870	0.159	8.4×10^{8}	5.7×10^{9}	0.147	1.75×10^{-10}
Cricket ball	0.160	50	100	940	0.141	9.4×10^{8}	6.4×10^{9}	0.147	1.55×10^{-10}
Football (soccer ball)	0.43	30	30	1820	0.0113	6.8×10^{7}	1.73×10^{10}	4.0×10^{-3}	5.8×10^{-11}
Basketball	0.60	5	10	2300	3.8×10^{-5}	3.5×10^{6}	2.4×10^{10}	1.46×10^{-4}	4.1×10^{-11}

units of length, while V and u both have units of length/time. Since R is the quantity of interest, it must be retained, and d and δ will only appear as ratios to it. Likewise, the projectile velocity V seems to be a primary variable compared with the wind speed; therefore, u will appear only in u/V. The complete set of $\{Q\}$ for equation (2.2) is now $\{R, m, V, \omega, \rho, \mu, g\}$, while the set $\{r\}$ consists of $\{d/R, \delta/R, u/V\}$. Note that quantities such as the relative directions of the projectile velocity and wind velocity or the velocity vector and the rotation vector are naturally dimensionless and, if explicitly included, would appear in $\{r\}$. The next step is to pick those variables that are considered fundamental and which are considered derived. From table 1, there are three units of dimension (mass, length, time); therefore, there will be three fundamental and four derived variables. The choice of which variables to consider as fundamental and which as derived is not critical, except that the quantity of interest, in this case the range, must appear in the derived variable list. Other combinations of dimensionless parameters are formally related to the set chosen by an algebraic transformation of variables. Here, the quantities $\{m, \mu, g\}$ will be considered the fundamental variables. Starting with R, equation (2.5) implies that the quantity $m^{\mathrm{a}}\mu^{\mathrm{b}}g^{\mathrm{c}}R$ must be dimensionless. This implies that the exponents for each dimensional unit must sum to 0:

$$\begin{aligned} &\text{Mass}: \ a + b = 0, \\ &\text{Length}: \ -b + c + 1 = 0, \\ &\text{Time}: \ -b - 2c = 0. \end{aligned} \tag{2.6}$$

The solution to this system of equations is $a = -2/3$, $b = 2/3$, $c = -1/3$. By convention, fractional exponents are not used, so the resulting dimensionless parameter is $\Pi_1 = \mu^2 R^3/m^2 g$. Applying the same method, the other three dimensionless parameters are $\Pi_2 = \mu V^3/mg^2$, $\Pi_3 = m\omega^3/\mu g$ and $\Pi_4 = mg\rho/\mu^2$. Putting these into equation (2.4), the equation for the range of a spherical projectile in air must take the form

$$R = (m^2 g/\mu^2)^{1/3} F(\mu V^3/mg^2, m\omega^3/\mu g, mg\rho/\mu^2), \tag{2.7}$$

if the list of variables chosen is complete.

At this point, it is instructive to show what can and cannot be learned from this exercise by evaluating the dimensionless parameters for some typical parameters. Table 2 shows the values of $\{\Pi\}$ for some common spherical projectiles, from which some important observations regarding the use of dimensional analysis can be drawn. One might expect that dimensionless parameters that are appropriate to the problem would be of O(1) and that ignorable dimensionless parameters would be either very small or very large. This is more

of a guideline than a rule, since the set $\{r\}$ may contain quantities that could be used to scale Π_i. From table 2, the values of parameter Π_2 are O(1) in most cases, but those of Π_3 and Π_4 are very large, but of similar magnitude. It is important to remember that combinations of these dimensionless parameters are equally valid, so an O(1) dimensionless parameter $\Pi_3' = \Pi_3/\Pi_4$ can be defined. Rather than Π_4, its reciprocal can be used (Π_4'). To arrive at the set $\{\Pi_2, \Pi_3', \Pi_4'\}$, some physical intuition and art have been applied. The quantities Π_2 and Π_3' have been used, rather than their reciprocals or a product and a ratio of the two, because it is likely to be of interest to compare the relative effect on the range of V and ω on an equal footing. The use of Π_4' rather than Π_4 is more stylistic in order to give the impression how important the parameter is in the sense of a perturbation expansion in a small quantity. The conclusion that Π_4' may be ignorable is not too surprising, since it is composed of 'variables' that are constant for a given projectile under standard conditions.

Looking now at the set $\{\Pi_2, \Pi_3', \Pi_4'\}$, the dimensionless parameters describe the behavior that is well known to practitioners of the various sports. The relative size of Π_3' to Π_2 indicates that the motion of the lighter projectiles (table tennis, golf, tennis) will be influenced strongly by the spin. The baseball and cricket ball have similar values of the dimensionless parameters pertaining to speed and spin, so subtle changes in these parameters could result in quite different trajectories. Also, it is observed that golf balls and batted baseballs travel farther at high altitude. The viscosity of air μ changes little with pressure, but the density ρ varies linearly at constant temperature. Therefore, a variation in altitude changes Π_3' while leaving Π_2 unchanged, indicating that the range of these projectiles is influenced significantly by spin, as predicted by the dimensional analysis. This may also explain the difficulty that baseball pitchers have at high altitude with their pitches taking a straighter trajectory, since the delicate balance between V and ω to get a ball to break after a certain distance of travel varies with altitude. The football (or soccer ball to Americans) seems to have a stronger influence from the speed, but it is known that a talented player can use spin to influence the trajectory, due to the cubic dependence on V and ω. Note that all of the $\{\Pi\}$ for the basketball are small, which is consistent with the intuition that the motion of such a slow, heavy projectile is not influenced by the presence of the air. Along these same lines, there is no obvious method to reduce these dimensionless parameters suitable for air at standard conditions to the limit of a projectile in vacuum. Applying the Buckingham technique to the set $\{R, m, g, V\}$, the correct answer for the case of a projectile in vacuum, $R \propto V^2/g$, is obtained.

Finally, it is important to note that dimensional analysis is silent about certain phenomena that are known to impact the projectile motion significantly. Surface irregularities such as dimples on golf balls or seams and scuffmarks on baseballs or cricket balls have long been demonstrated to influence the motion of these balls. A dimensional parameter to account for this was included in the original set (δ), but it was immediately eliminated because it had the same units as other quantities in the list. As a general rule, dimensional analysis cannot yield any information on the dependence of phenomena on the set of ratios $\{r\}$. Despite this limitation, the example detailed above indicates that dimensional analysis can give considerable insight into the physical origin of phenomena and thereby guide a more detailed mathematical analysis of the behavior.

Encouraged by the example above, a set of dimensionless parameters that describe the behavior of plasmas will now be derived. Dimensional analysis of the type demonstrated in the previous example was first applied to tokamak plasmas by Kadomtsev [8, 9]. He chose the following set of dimensional parameters to describe tokamak behavior $\{a, R, B, B_P, c, e, m_e, m_i, T_e, T_i, n\}$, where a is the minor radius of the tokamak, R the major radius, B is the toroidal magnetic field, B_P is the poloidal magnetic field, c is the speed of light in vacuum, e is the charge of the electron, m_e is the mass of the electron, m_i is the mass of the ion (assuming

a single component plasma), T_e is the electron temperature, T_i is the ion temperature and n is the plasma density[4]. Without any explanation, Kadomtsev then presented a set of eight dimensionless parameters that he proposed to be relevant to tokamak behavior. In modern notation, they are:

1. Poloidal ion Larmor radius normalized to machine size: $\rho_{*P} \equiv \rho_{Pi}/a$.
2. Normalized collision frequency: $\nu_{mfp} \equiv qR/\lambda_e$ with λ_e the 'electron mean free path', defined as the product of the Debye length and the number of particles in the Debye sphere.
3. Ratio of kinetic to poloidal magnetic pressure $\beta_P \equiv 2\mu_0 nT/B_P^2$.
4. Aspect ratio: R/a.
5. Temperature ratio: T_e/T_i.
6. Safety factor (in the cylindrical approximation): $q = aB/RB_P$.
7. Mass ratio: m_e/m_i.
8. Number of particles in Debye sphere: $N = (4\pi/3)\lambda_D^3 n$.

These form a complete, but not unique, set of dimensionless parameters, given the choice of dimensional parameters.

It is instructive to apply Buckingham's techniques directly to the Q_i chosen by Kadomtsev (plus ε_0 for MKS units). Four ratios of like parameters are noted immediately:

$$\{r\} = \{R/a,\ B_P/B,\ m_e/m_i,\ T_e/T_i\}. \tag{2.8}$$

From the four ratios of like parameters, the quantities a, B, m_i and T_i will be retained in the set $\{Q\}$. For the set of quantities to stand for the units, the set $\{a, c, e, m_i\}$ will be used. This leaves four more dimensionless parameters to be derived. Applying the technique described above, the following parameters are obtained:

$$\{\Pi\} = \{eBa/m_i c,\ T_i/c^2 m_i,\ na^3,\ ac^2 m_i \varepsilon_0/e^2\}. \tag{2.9}$$

These quantities $\{\Pi\}$ can be recognized as standard plasma parameters: $\Pi_1 = (1/\rho_*)(v_{th,i}/c)$, $\Pi_2 = (v_{th,i}/c)^2$ and $\Pi_4 = (\delta/a)^2(m_i/m_e)\Pi_3$, where ρ_* is the ion gyroradius normalized to a, $v_{th,i}$ is the ion thermal velocity, and δ is the skin depth. The quantity $\Pi_3 = na^3$ is essentially the number of particles in the plasma. These parameters can be transformed to give Kadomtsev's set of parameters or vice versa, illustrating that the set $\{\Pi\}$ is complete, but not unique.

2.2. Scale invariance

If the equations governing the behavior of a plasma are assumed to be known, then the technique of scale invariance can be used to derive the necessary dimensionless relationships between the variables that appear in the equations. Connor and Taylor [10] formalized this analysis to obtain the scaling of a confinement time in several different limits. To illustrate the technique of scale invariance, a simple example for the limiting case of electrostatic, collisionless plasmas will be given here.

[4] Kadomtsev's paper employed CGS units; in MKS units, either the permittivity of the vacuum (ε_0) or the permeability of the vacuum (μ_0) must also be included. For simplicity, the discussion here is restricted to singly charged ions. A more general formulation will appear later. Also, the notation chosen here anticipates that the dimensionless scaling methods have been applied almost exclusively to toroidal magnetic confinement systems with a dominant toroidal field. The analysis presented is easily adapted to linear systems, cusp geometries, reversed-field pinches, or spherical tokamaks where the approximation that the magnitude of the magnetic field B is given by the magnitude of a single component of B (in this case the toroidal component) does not hold. In these cases, the true magnitude of B should be retained as the fundamental quantity and the components of B in the directions of the chosen coordinate system appear as ratios of like quantities.

In the electrostatic, collisionless limit, the plasma is assumed to be described by the Vlasov equations for the distribution functions f_j of electrons ($j = \mathrm{e}$) and ions ($j = \mathrm{i}$, multiple species possible):

$$\frac{\partial f_j}{\partial t} + \boldsymbol{v} \cdot \nabla f_j + \frac{e_j}{m_j}(\boldsymbol{E} + \boldsymbol{v} \times \boldsymbol{B}) \cdot \frac{\partial f_j}{\partial \boldsymbol{v}} = 0 \qquad j = \mathrm{i}, \mathrm{e}, \tag{2.10}$$

where the magnetic field $\boldsymbol{B}$ is fixed and the electrostatic field $\boldsymbol{E}$ is determined by the quasi-neutrality condition

$$\sum_j e_j \int \mathrm{d}^3 v f_j = 0. \tag{2.11}$$

The quantities e_j and m_j are the charge and mass of each component of the plasma, and $\boldsymbol{v}$ is the particle velocity. The principle of scale invariance implies that scale transformations of the form

$$f_j \to \alpha f_j, \qquad \boldsymbol{v} \to \beta \boldsymbol{v}, \qquad x \to \gamma x, \qquad t \to \delta t, \qquad \boldsymbol{E} \to \mu \boldsymbol{E}, \qquad B \to \nu B, \tag{2.12}$$

that leave equations (2.10) and (2.11) invariant are dimensionally correct. (Here α, β, γ, δ, μ and ν are simply multiplicative constants to define the transformations here and should not be confused with plasma parameters defined later in this paper using the same symbols.) There are three independent transformations of this type that may be expressed as

$$\begin{aligned} &A_1 : f_j \to \alpha f_j, \\ &A_2 : \boldsymbol{v} \to \beta \boldsymbol{v}, \qquad \boldsymbol{B} \to \beta \boldsymbol{B}, \qquad t \to \beta^{-1} t, \qquad \boldsymbol{E} \to \beta^2 \boldsymbol{E}, \\ &A_3 : \boldsymbol{x} \to \gamma \boldsymbol{x}, \qquad \boldsymbol{B} \to \gamma^{-1} \boldsymbol{B}, \qquad t \to \gamma t, \qquad \boldsymbol{E} \to \gamma^{-1} \boldsymbol{E}. \end{aligned} \tag{2.13}$$

The particular specifications A_1 through A_3 are arbitrary to the extent that any three independent products of these transformations would also leave equations (2.10) and (2.11) invariant. Now the scale invariance principle implies that any variable derived from these equations, such as a confinement time, must transform appropriately under A_1 through A_3. Consider a power-law scaling for the confinement time of the form

$$\tau \sim n^p T^q B^r a^s, \tag{2.14}$$

where the density n and temperature T are taken to be characteristic values of these quantities, for example the value at the plasma mid-radius. Such characteristic values are sufficient since the profiles of these quantities are determined by the equations under investigation. The quantity a is again a measure of the plasma size. It follows, recalling the definitions $n \equiv \int \mathrm{d}^3 v f$ and $nT \equiv \int \mathrm{d}^3 v (m v^2/3) f$, that the four indices p, q, r and s are constrained by the three transformations to satisfy the relations

$$p = 0, \qquad 2q + r = -1, \qquad s - r = 1. \tag{2.15}$$

Therefore, only one index (q) is independent and

$$B\tau = F(T/a^2 B^2). \tag{2.16}$$

Note that this exercise determines the relationships among the dimensional parameters that must hold on both sides of the equation, but still requires the addition of dimensional constants of nature (m_j, e_j) to yield dimensionless parameters. For the left-hand side of equation (2.16), the cyclotron frequency $\Omega \equiv e_j B/m_j$ provides a convenient normalization, since it has the correct units and is proportional to B. The quantity in the parenthesis on the right-hand side of

equation (2.16) can be recognized as the square of the gyroradius $\rho \equiv \sqrt{Tm_j}/e_j B$ normalized to the physical size of the plasma a. Writing this result in a fully dimensionless form gives

$$\Omega\tau = F(\rho_*), \tag{2.17}$$

where $\rho_* \equiv \rho/a$. The above result may be extended to include the effects of collisions by the addition of a Fokker–Planck operator into the Vlasov equations. Finite β effects may be included by introducing a self-consistent magnetic field that satisfies the Maxwell equations. The dimensionless confinement time then has the more general form

$$\Omega\tau = F(\rho_*, \nu_*, \beta, \{r_i\}), \tag{2.18}$$

where ν_* is a normalized collision frequency and the $\{r_i\}$ are ratios of quantities with like dimensions. The scalings of the dimensionless confinement time arising from other plasma models are listed in the review by Connor [11]. Experimental evidence that equation (2.18) is sufficiently general to adequately describe the energy transport in magnetic fusion plasmas will be presented in section 3.

2.3. Comparison of dimensional analysis and scale invariance

While the papers cited above are the most prominent in the development of dimensionless parameter scaling techniques in the field of plasma physics, earlier applications of these techniques exist. An early attempt to obtain the appropriate dimensionless parameters to describe plasma behavior was by Beiser and Raab [12]. They analyzed two systems of equations—one composed of the Maxwell equations plus the Navier–Stokes equation of motion and the other the Boltzmann kinetic equation. But, rather than finding the scale invariance properties of this system of equations by inspection like Connor and Taylor, they used Buckingham's Π theorem [2] to derive the dimensionless variables associated with these systems of equations. A similar treatment was developed by Lacina [13], using the Vlasov equation for electrons and ions plus the Maxwell equations. Lacina's work was quite general in that it included a steady electric field as well as the confining magnetic field, due to an interest in describing plasmas in mirror devices where non-ambipolar transport is important. It also assumed that collisions of charged particles with a neutral gas background dominated over binary charged particle collisions. These assumptions lead to different dimensionless parameters than discussed above. Unfortunately, these pioneering works that applied the methods of dimensionless parameter scaling appear to have gone unnoticed. The use in both papers of Buckingham's Π theorem to find the scale invariant solutions for a known system of equations introduces the question of how dimensional analysis and scale invariance are related.

The general technique of dimensional analysis requires that the practitioner supply a dimensional quantity whose behavior is of interest and a list of variables on which the behavior could depend. Then, Buckingham's Π theorem gives a systematic method by which a complete set of dimensionless variables can be obtained, given the choice of variables. Complete does not imply unique or correct, but simply denotes that the dimensionless parameters determined by the method are sufficient to describe the situation, if the choice of variables is sufficient. Evaluation of these dimensionless parameters for the situation of interest then shows which variables are important and which can be ignored. On the other hand, the application of the concept of scale invariance to find dimensionless parameters that describe the behavior of some variable of interest requires that a complete set of equations governing the behavior of the system of interest be known. In this case, the ignorable dimensionless parameters have already been removed from view by the approximations applied in the derivation of the governing equations. The techniques of dimensional analysis can be used as a method to find the scale invariant quantities (as in Beiser and Raab or Lacina), or the scale invariants can be found by

other means (like Connor and Taylor). This difference in approach explains the appearance in Kadomtsev's work of a large number of dimensionless parameters, while only one variable appears in the simple example from Connor and Taylor. The catalogue of equations analyzed by Connor [11] is equivalent to ignoring various combinations of Kadomtsev's dimensionless parameters. One potential weakness of the scale invariance approach is that some essential dimensionless parameters may appear only in the boundary conditions of the equations. The dimensional analysis method can account for these directly by the choice of the set of relevant variables.

2.4. Similarity and identity experiments

Given the indeterminacy in the methods described above, it is legitimate to question whether the techniques have any real practical value beyond the qualitative speculations of the type given at the beginning of section 2.1. As mentioned at the beginning of this section, dimensional scaling techniques are applied in two areas—the creation of suitable scale models to study behavior in systems not directly testable and the determination of the domain of applicability of equations and critical parameters. These exercises are often described in terms of 'similarity' or 'identical' systems. As will be shown below, these two concepts are not independent, but arise from the differing points of view of dimensional analysis and scale invariance.

Starting from the dimensional analysis approach, it is assumed that the chosen set of parameters (including the ratios) is complete, in the sense that it uniquely specifies the plasma of interest. However, it is often the case that one dimensionless parameter can be ignored, such as the reciprocal of the number of particles in a Debye sphere in Kadomtsev's list. Then one of the dimensional variables can be treated as a parameter to generate a family of plasmas that are similar, in that they have the same values of the dimensionless parameters, except the ignorable one. For example, if $1/N$ is ignored in Kadomtsev's list of dimensionless variables and the plasma size a is taken as a parameter, then the other dimensionless variables define how T, B and n must change to keep the plasma behavior similar as the size changes. This is called a one-parameter family of similarity.

Likewise, the scale invariance approach defines a set of parameters that describe the plasma behavior, based on the choice of governing equations. Because the ignorable parameters have been removed in the approximations leading to the governing equations, two plasmas should be identical in their behavior if they have the same values of the dimensionless parameters. In the example given above from Connor and Taylor, only the quantity $T/(Ba)^2$ is important, so the normalized confinement time should be the same at any values of T, B and a as long as this combination has the same value. It should be clear from this discussion that the concepts of similar plasmas and identical plasmas are not distinct, but arise from complementary views based on the type of dimensionless scaling method used.

The discussion of similarity and identical plasmas also suggests how dimensionless parameter scaling techniques can be applied in practice. From the dimensional analysis approach, all plasmas with variations of one or more of the dimensionless parameters will be distinct if all of the dimensionless parameters are important. If one of the dimensionless parameters is assumed to be ignorable, one can carry out in two or more devices of different sizes a realization of the one-parameter similarity concept to validate this assumption. The magnetic field, density, and temperature can be adjusted to compensate for the change in size to give the same dimensionless parameters in both devices. If the resultant plasma behavior is indeed the same, the plasmas are indeed similar, and the chosen parameters are deemed sufficient to describe the plasma behavior. (Caveats to this statement will be discussed with respect to definite experiments, rather than attempting a general discussion here.) Likewise, from the

scale invariance approach, one can make identical plasmas (ones with equal values of the dimensionless parameters determined by scale invariance) and determine whether the plasma behavior is identical. If indeed the plasmas are identical, the approximations used to obtain the assumed governing equations are validated, and the resulting dimensionless parameters are sufficient to describe the plasmas. Once similarity or identity has been established, experiments can be carried out to determine the scaling of plasma behavior with respect to the important dimensionless parameters.

The use of dimensionless parameter scaling in fusion plasma experiments began in earnest after it was noted that the scaling of plasma performance from present-day devices to plasmas suitable for energy production could be reduced to a single dimensionless parameter. In scaling from a smaller to a larger toroidal device Waltz [14] showed that the only parameter that changes significantly is the normalized gyroradius ρ_*; the remainder of the dimensionless parameters can be kept fixed. Going from a medium-size tokamak DIII-D ($B = 2\,\mathrm{T}$, $a = 0.6\,\mathrm{m}$) to the largest tokamak JET ($B = 3\,\mathrm{T}$, $a = 1\,\mathrm{m}$), ρ_* decreases by roughly a factor of 2. Continuing on to a burning plasma experiment such as ITER ($B = 5\,\mathrm{T}$, $a = 2\,\mathrm{m}$), ρ_* is reduced by a further factor of 3. Hence, in predicting the performance of a larger device from the present-day devices, determining the scaling with ρ_* is crucial.

3. Local analysis of energy and particle transport

Most of the applications in fusion plasma research of dimensionless parameter scaling techniques have been in the area of energy and particle transport. In this section, experiments designed explicitly to determine the scaling of energy and particle transport with respect to dimensionless parameters will be reviewed. As discussed in the previous section, empirical justification for the dimensionless scaling approach relies on identity experiments as the demonstration of its utility. The standard dimensionless variables for energy and particle transport scaling will be introduced in section 3.1, and their use will be justified by a series of identity experiments in section 3.2. In the later subsections, the scaling experiments with respect to various dimensionless parameters will be reviewed. In general, the experiments concerning each individual dimensionless parameter are reviewed in chronological order.

3.1. Dimensionless parameters for energy transport

Energy transport in magnetic fusion plasmas is generally larger than that predicted by theories treating binary collisions in realistic magnetic geometries ('neoclassical' theory) [15–17]. The enhanced transport over collisional theory is attributed normally to the effects of a turbulent spectrum of waves supported by the plasma and driven by its free energy [18, 19]. While there has been significant progress in obtaining a first-principles calculation of the effects of the turbulence, a comprehensive calculation of the turbulence is still beyond the capabilities of present-day computers, due to the nonlinearities and the range of spatial and temporal scales of relevance. One goal of the dimensionless parameter scaling experiments is to test whether the scale invariance of the equations used in these calculations is reflected in the resultant energy transport.

Based on the discussion of section 2, a formal approach to finding an appropriate set of dimensionless parameters to describe energy and particle transport could be undertaken. But the historical development of research in this area led to a common set of dimensionless parameters from what effectively is a scale invariance approach. Rather than starting afresh and ignoring this work, this common set will be adopted here and then justified from both the scale invariance and the dimensional analysis point of view.

Table 3. Definitions of dimensionless parameters used for energy transport scaling in terms of dimensional variables.

Dimensionless parameter	Definition in dimensional parameters	Description
$\rho_{*,j}$	$(m_j T_j)^{1/2}/Ba$	Gyroradius normalized to the minor radius
β	$(\sum n_j T_j)/B^2$	Energy density normalized to the magnetic energy density
ν_{C}	$n_{\mathrm{e}} R/T_{\mathrm{e}}^2$	Electron collision frequency normalized to the toroidal transit time
q	$(Ba^2\kappa)/IR$	Safety factor (elongation dependence is approximate)
M	$\omega_{\mathrm{tor}} R m_{\mathrm{i}}^{1/2}/T_{\mathrm{e}}^{1/2}$	Toroidal rotation velocity normalized to the ion sound speed
ε	a/R	Inverse aspect ratio
κ		Ratio of the plasma height to width
A	m_j/m_{p}	Ratio of particle mass to proton mass
Z	e_j/e	Ratio of the particle charge to the electron charge

Examination of the theoretical literature indicates that both fluid and kinetic treatments of transport effectively adopt an approximation that the equilibrium is in local thermodynamic equilibrium. This means that equations governing moments of the momentum distribution function higher than the second moment (temperature) are ignored. Only fluctuations of these lowest moments of the distribution function about their equilibrium values are considered in evaluating the transport. This is implicit in both the dimensional analysis approach of Kadomtsev and the scale invariance approach of Connor and Taylor discussed in section 2. In both cases, the parameters of interest included density and temperature, but no higher moments of the distribution function. A standard set of dimensionless parameters to characterize energy and particle transport can be identified that is consistent with both the dimensional analysis of Kadomtsev (section 2.1) and the scale invariance approach of Connor and Taylor (section 2.2). From a purely mathematical standpoint, the choices are arbitrary in that products with other dimensionless parameters are also valid, and therefore a transformation of variables can be applied to generate a different set of parameters. However, as will become clearer as the experiments are reviewed, some choices of parameters better reflect both the plasma behavior and the design of the experiments. The set of dimensionless parameters used here are the gyroradius normalized to the smallest dimension of the plasma cross-section (ρ_*), the total plasma pressure normalized to the magnetic field pressure (β), the collision frequency normalized to the toroidal transit time (ν_{C}), the safety factor (q), the inverse aspect ratio (ε), the toroidal flow speed normalized to the local ion sound wave speed (M) and the elongation of the plasma cross-section (κ). In addition, provision must be made for the existence of electron and multiple ion species. A table of the definitions of these dimensionless parameters as used in this review is found in table 3.

In order to quantify energy transport, both the absolute value and the scaling with dimensionless parameters, a quantity known as the thermal diffusivity (χ) will be defined in terms of the heat flux q and the gradient of the temperature T:

$$q = -n\chi\nabla T. \tag{3.1}$$

This can be defined separately for electrons and ions or as an 'effective' diffusivity for the total heat flux. The diffusivity can be parametrized in terms of the dimensionless parameters in the form:

$$\chi/\chi_{\mathrm{B}} \propto \rho_*^{\alpha_\rho}\beta^{\alpha_\beta}\nu_{\mathrm{C}}^{\alpha_\nu}M^{\alpha_M}q^{\alpha_q}\varepsilon^{\alpha_\varepsilon}\kappa^{\alpha_\kappa}A^{\alpha_A}Z^{\alpha_Z}, \tag{3.2}$$

where $\chi_{\mathrm{B}} \equiv T/ZeB$ is the Bohm diffusivity (up to a numerical coefficient). The experiments reviewed here seek to evaluate the various exponents (α_ρ, α_β, etc), typically by variations in

only one dimensionless parameter while holding the others constant. The choice of a power-law form for the dependence of χ on the dimensionless parameters is not required by dimensional analysis, but arises from the convenience of comparison with the traditional power-law scalings applied to the engineering variables. In principle, experiments could be carried out with nearly continuous variation of a single dimensionless parameter while holding all others fixed in order to determine the true dependence of the diffusivity on that parameter without recourse to an assumed mathematical form. In practice, this is not feasible in magnetic fusion experiments, and as will be seen later the power-law form is suitable for describing the results of the limited scans that can be done. It is possible (and often necessary) to describe the transport of energy in the electrons and ions separately. When defining χ_e and χ_i separately, they can be written in terms of ρ_* and χ_B for each species, or the values for one species and the ratio T_i/T_e can be specified, where all ions are assumed to have the same temperature. To study the energy confinement time rather than the local diffusivity, the relationship between the two is taken to be $\tau_E \propto a^2/\chi$. This form implicitly assumes that losses other than that described by a diffusion equation, such as line radiation, bremsstrahlung, synchrotron radiation or charge exchange with neutral atoms, contribute a negligible amount to the global energy confinement. This assumption is generally very good for present-day experiments, but could give rise to a systematic difference between the scalings found for χ (where the analysis corrects for these effects) and the scalings found for τ_E. Recalling the normalization of the confinement time by the cyclotron frequency Ω (equation (2.18)), the scaling of confinement with dimensionless parameters can be written as

$$\Omega\tau_E \propto \rho_*^{-2-\alpha_\rho} \beta^{-\alpha_\beta} \nu_C^{-\alpha_\nu} M^{-\alpha_M} q^{-\alpha_q} \varepsilon^{-\alpha_\varepsilon} \kappa^{-\alpha_\kappa} A^{-\alpha_A} Z^{-\alpha_Z}, \tag{3.3}$$

where the exponents in equations (3.2) and (3.3) are the same. Equation (3.3) is valid whether the electron or ion quantities are used.

The question of inclusion of spatial gradients of the density, momentum or temperature in the construction of dimensionless parameters is an important one. The free energy for driving the instabilities thought to be responsible for transport above the collisional level is measured by these gradients. Even in the collisional picture, the gradients represent the potential for transport to occur. In a perfectly local fluid model, the gradients do play an essential role. However, in both the collisional and the turbulent wave models, transport arises because of non-local spatial effects—finite orbit excursions and finite spatial correlations, respectively. The philosophy followed in this review is that the dimensionless parameters to be used must be matched over a spatial distance that is several times the intrinsic scale size of the underlying cause of the transport. This matches automatically the gradients of the fluid moments, and therefore to include them in the dimensionless parameter set would be redundant. From a practical experimental point of view, this philosophy also leads to matching quantities directly measured by the plasma diagnostics and not their derivatives, which facilitates a more straightforward evaluation of the quality of the match during the execution of the experiments and a clearer path to evaluation of the uncertainties in the full analysis.

Analysis of multi-experiment databases of global energy confinement has traditionally focused on finding the scaling with engineering variables in a power-law form similar to equation (3.3). In section 4, the transformation of these scalings into dimensionless parameter scalings of the form of equation (3.3) will be developed. The discussion of how these transformed scalings compare with the results of the experiments explicitly designed to isolate the scaling with single dimensionless parameters will be deferred to that section also. However, in the summary plots of the experimental results for the individual dimensionless parameter scalings shown in this section, the transformed database results for a benchmark H-mode

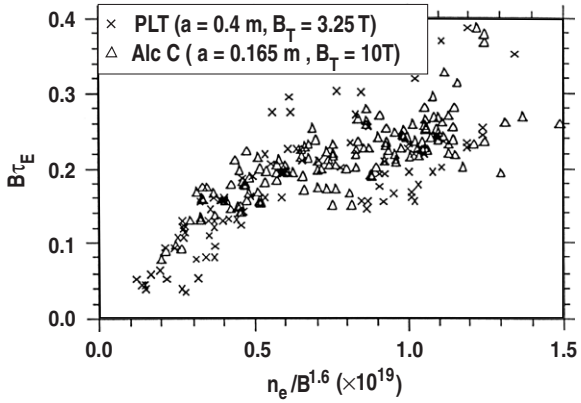

Figure 1. Comparison of ohmic discharges in PLT (×) and Alcator C (Δ) scaled to test the identity discharge conditions. The vertical axis is the dimensionless energy confinement time and the horizontal axis is a combination of the conditions na^2 and $Ba^{5/4}$ that must be constant for identical discharges. Reprinted from [22] by permission.

scaling [20] known as IPB98(y, 2) (equation (4.3)) and a benchmark L-mode scaling [21] (equation (4.4)) known as ITER97-L will be indicated on the plots.

3.2. Identity experiments

As described in section 2.4, the fundamental test of the suitability of the chosen set of dimensionless parameters is to construct an identity test. The basic principle is that two plasmas with dissimilar control parameters (B, I, a, n, ω_{tor}, ...) but identical dimensionless parameters (ρ_*, β, ν_{C}, q, M, ...) should have an identical amount of transport, with the appropriate normalization to make it dimensionless. This is the essence of equations (3.2) and (3.3). The practical implications of matching the dimensionless parameters can be derived as follows. Consider two toroidal plasmas of identical magnetic geometry (q, ε, κ) and the same ion species (A, Z). To make the ρ_*, β, ν_{C} and M profiles match in both plasmas, the following relations must be constant: na^2, $Ta^{1/2}$, $Ba^{5/4}$ and $\omega_{\mathrm{tor}}a^{5/4}$, where the physical size of the plasma is used for the parametric variation and the dimensional constants have been omitted for clarity. The local transport should then scale with $a^{3/4}$ or, equivalently, $\chi a^{-3/4}$ should be the same in both plasmas (from equation (3.2)). Equation (3.3) implies $B\tau_E$ should be constant. Writing τ_E as W/P, this is equivalent to the relation $Pa^{3/4}$ constant, where P is the transport loss power.

The first attempts to make identical discharges were done by comparing global energy confinement in ohmic tokamak plasmas. This might seem to be a futile effort since the ohmic power cannot be independently varied from the other control parameters. However, the ohmic power can be approximated as $P_\Omega \propto I^2\mathcal{R} \propto a^{-3/4}$ using $Ia^{1/4}$ as a constant to keep q fixed and $\mathcal{R} \propto a^2/T^{3/2}$, where $\mathcal{R}$ is the plasma resistance. Therefore, the ohmic power in identity experiments scales by coincidence exactly as needed to keep other dimensionless parameters fixed, assuming they are an appropriate set to describe transport.

Comparison of selected ohmic discharges from PLT and Alcator C [22] showed that the global confinement scaled as expected from the identity conditions for a wide variation of normalized density (figure 1). The value of ε is not matched in these two tokamaks (0.30 for PLT versus 0.26 for Alcator C). This introduces some potential systematic error. In [23], it is

stated that the Alcator C data show no variation of energy confinement with q, so it appears that mismatches in q were simply ignored. Given the correlation of the ohmic power and the temperature discussed in the previous paragraph, the variation in temperature required for identical discharges is likely redundant with the match of the dimensionless confinement time. Attempts to extend this comparison to include TFTR data were less successful [23]. A substantial difference in the shape of the measured density profiles between TFTR and the two smaller tokamaks (between which the density profiles were well matched) was noted (figure 2 of [23]). This would indicate that the dimensionless parameters were not matched across the plasma radius, but only in the integrated global sense. It is not possible to give a definitive explanation for this mismatch, but variations in the particle source between TFTR and the smaller machines could give rise to the difference. Comparisons of discharges made in TFTR by matching the identity conditions during a 50% increase in physical size were reported to yield good matches of dimensionless energy confinement time over a range of densities [24], but further details of this experiment were not published.

Of more interest is the validation for tokamak plasmas with auxiliary heating. The majority of the reported global confinement results are for ELMing H-mode conditions[5] with neutral beam injection (NBI). Results comparing JET and DIII-D show very good agreement in the scaled confinement times when the other parameters are matched in a global sense [25, 26]. The scaled global confinement time matches to better than 10%, which is smaller than the measurement accuracy. Attempts to demonstrate matches between JET and ASDEX-Upgrade [27] and between JET and Alcator C-Mod [28] were less successful, apparently due to less accurate matches in β (and q in the JET/Alcator C-Mod case). The results are still indicative that the confinement time scaling inferred from the dimensionless scaling arguments is valid. Comparison of L-mode auxiliary heated discharges between DIII-D and Alcator C-Mod are also indicative that the inferred scaling is appropriate [26].

Matching of the global scalings provides motivation to attempt a match of the local parameters, which is a more sensitive test of the scaling principle. Because the underlying turbulence that causes heat transport is likely driven by the density and temperature gradients, the success of the global scaling test could be coincidental, since only the volume integrals of the dimensionless parameters are used. The accuracy with which the profiles can be matched for H-mode discharges in DIII-D and JET is illustrated in figure 2 [26]. The raw data from each machine are fitted to a smooth curve at many times within a discharge, spanning several energy confinement times. The times of the best matches are selected by comparing the fitted data for each machine. The match is very good for many correlation lengths in the regions where there are no MHD instabilities. The profile diagnostic information is not available with sufficient time resolution to calculate the time-dependent power balance between sawtooth crashes or ELMs. Therefore, information about the transport will only available in the regions undisturbed by these instabilities. In this case, this region lies between the diamond symbols in figure 2. (This restriction applies generally to all of the transport experiments discussed in this review.) The resulting power balance estimates of the local heat diffusivity of the time of the best match are shown in figure 3. Across the region where the profiles match, the scaled local diffusivity also matches. Similar comparison of L-mode discharges from Alcator C-Mod and DIII-D shows agreement to within the estimated uncertainties [26]. The conclusion is that the dimensionless parameters chosen to describe the plasma are sufficient to explain the observed changes in absolute heat transport in these plasmas.

[5] In many magnetic fusion experiments with external heating sources, especially in tokamaks, there are two confinement regimes with distinct characteristics. The low (L) mode has lower confinement than the high (H) mode. The transition from L mode to H mode occurs when a threshold in power is exceeded. In H mode, repetitive instabilities called ELMs are observed.

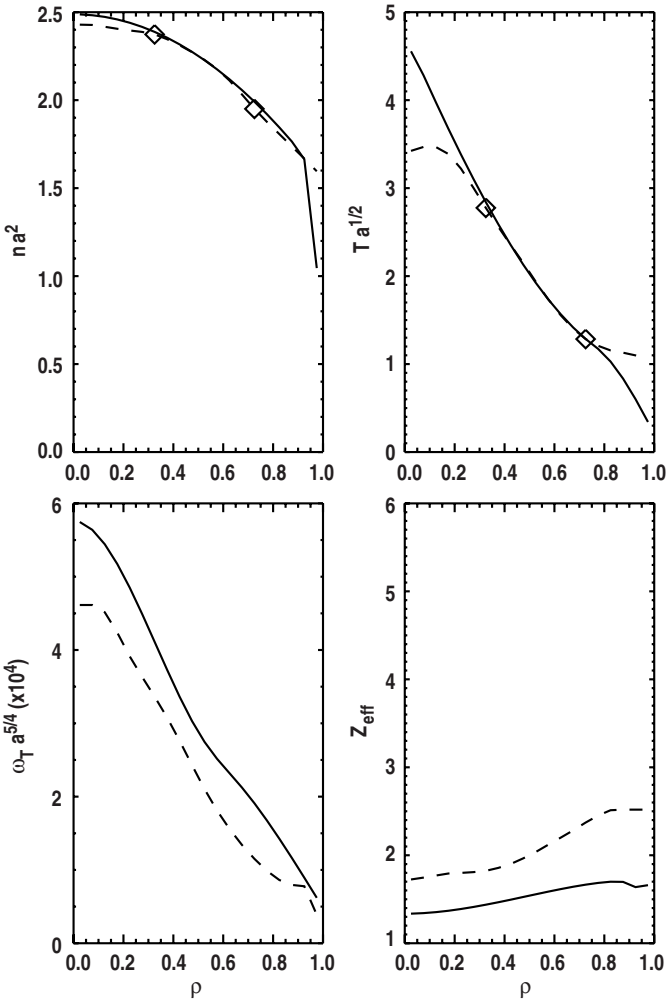

Figure 2. Comparison of the radial profiles of the normalized density, temperature, toroidal rotation and effective charge profiles for DIII-D (——) and JET (- - - -). The radial coordinate ρ is the square root of the toroidal flux normalized to the boundary value. (The symbol ω_T in the figure corresponds to the symbol ω_{tor} used for the toroidal angular frequency used in this paper.) Reprinted from [26] by permission.

The sensitivity of the scaling to the choice of dimensionless parameters can be illustrated by an example where the choice of parameters does not yield a reasonable scaling. The success of a simple empirical formula to describe the density limit in tokamaks has been well documented [29]. It has been noted that transport degrades in many cases as the limit is approached and that enhanced transport may explain the limit itself. Therefore, replacing the normalized collision frequency ν_C with density normalized to the empirical density limit (n/n_{DL}), where $n_{DL} \propto I/a^2$, could yield a more useful parameter set. To test this hypothesis, identity discharges that match this alternative set of dimensionless parameters have been found in DIII-D and JET [30]. Comparison of the scaled global energy confinement shows the scaled confinement differs in the two machines by about 25%, and the scaled thermal diffusivities differ strongly outside $\rho = 0.6$ (figure 3 of [30]). Looking to the local profile matches

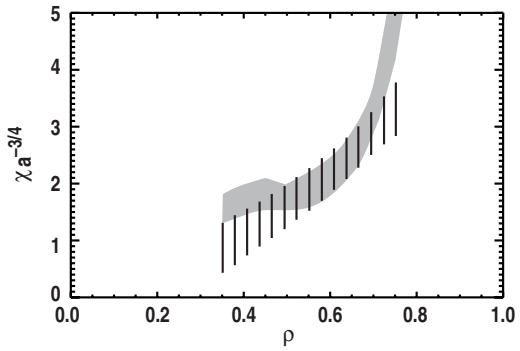

Figure 3. Radial profiles of the normalized diffusivity for DIII-D (dashed region) and JET (shaded region). The bands indicate the estimated uncertainty due to random error. Reprinted from [26] by permission.

(figure 4), the profile shapes are clearly different, especially the density profiles. The mismatch is taken as evidence that the chosen dimensionless parameters are not adequate to describe the local heat transport under these conditions. This is perhaps not too surprising, since n_{DL} does not depend on local parameters. The conclusion is that the density normalization through the collision frequency gives a significantly better description of the transport than normalization to the empirical density limit. This analysis, however, does not shed any light on the question of the origin of the empirical density limit.

Based on the identity experiments where good matches of the dimensionless parameters were obtained, the choice of ρ_*, β, ν_{C} and M gives an adequate description of the heat transport at both the global and the local scales. The fact that dimensionless parameters can be matched between tokamaks of different size across a large fraction of the minor radius provides substantial validation of the fundamental principles of dimensionless parameter scaling in hot plasmas.

3.3. ρ_* scaling experiments

3.3.1. Energy transport. Having justified the variables ρ_*, β, ν_{C} and M as appropriate scaling variables for energy transport by means of the identity test, it is now feasible to examine the scaling with respect to each one, holding the others fixed. The scaling with ρ_* is the most important scaling to determine for projections of energy confinement of future experiments, since present-day plasmas can match the values of β, ν_{C} M and geometry anticipated for future devices [14]. The ρ_* scaling of energy transport essentially quantifies the benefits of increasing the effective size of the plasma. Because ρ_* decreases with increasing physical size and increasing B, either means of increasing the effective size is equivalent. If the ρ_* dependence of the local energy transport is characterized by $\chi \propto \rho_*^{\alpha_\rho}$, then the global energy confinement has the dependence $\Omega\tau_E \propto \rho_*^{-(2+\alpha_\rho)}$. Beyond the convenience of a one-parameter projection to future designs, the strong dependence of the global energy confinement on ρ_*makes determination of the scaling with ρ_* a high priority.

The scaling of local energy transport with ρ_* also has significant implications for theoretical descriptions of the processes that govern the transport. Transport of particles and energy across the magnetic field is believed to be due to turbulence arising from unstable plasma waves. The fundamental equations that describe these waves exhibit uniformly a scaling of $\alpha_\rho = 1$. This dependence is known as gyro-reduced Bohm scaling (or 'gyroBohm') because

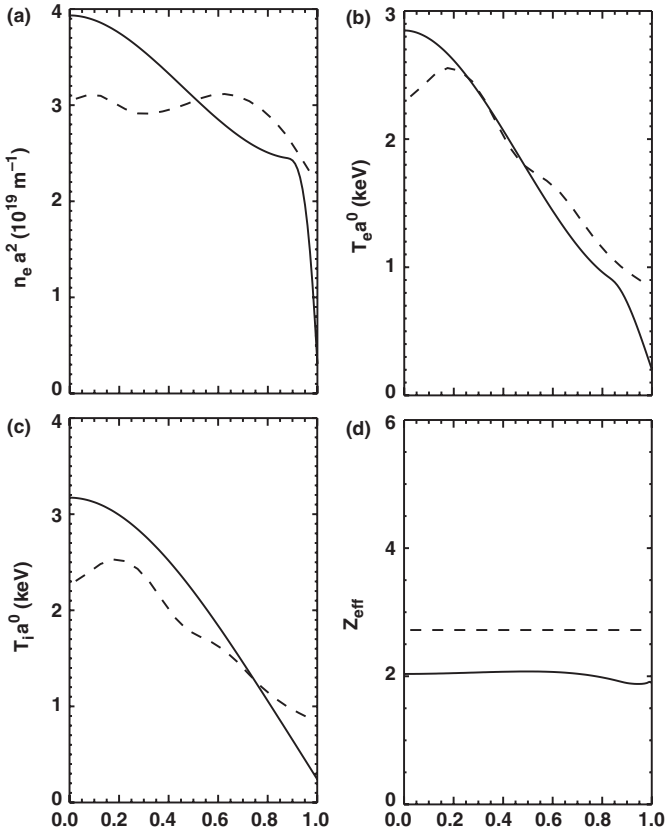

Figure 4. Normalized profiles from DIII-D (——) and JET (- - - -) of (*a*) electron density, (*b*) electron temperature, (*c*) ion temperature and (*d*) effective ion charge for the test of similarity at fixed n/n_{DL}. Reprinted from [30] by permission of the Institute of Physics.

the Bohm scaling normalization (explained below) is reduced by a linear factor proportional to the gyroradius. Simple estimates of the transport from turbulence, based on random-walk arguments, yield gyroBohm scaling because both the radial correlation length and the correlation time scale with ρ_*. This sets a clear expectation that the ρ_*-scaling experiments should yield $\alpha_\rho = 1$. However, as discussed below, early experiments found global ρ_* scalings closer to $\alpha_\rho = 0$ or 'Bohm' scaling. Heuristically, Bohm scaling can be obtained in two ways. First, if the random-walk step size scales with the plasma dimensions rather than the gyroradius, Bohm scaling results. Second, if a particle undergoes a random walk with the step size given by the gyroradius each gyroperiod, Bohm scaling is obtained. In this sense, Bohm scaling represents the worst possible scaling for magnetized plasmas with magnetic flux surfaces. If the transport takes place in a magnetic field that is stochastic, rather than having nested flux surfaces, the energy confinement is dominated by the parallel diffusion along the field, and $\alpha_\rho = -1$. Many attempts have been made to introduce a mechanism that yields a Bohm scaling in the gyroBohm theory. Numerical calculations with large ρ_* can exhibit Bohm-like behavior. However, it is still a hotly debated issue whether this is a feature of the saturated strong turbulence or an effect of the artificial boundary conditions and constraints required for the computations. The approach employed here will be to seek a consensus in the experimental values for α_ρ to guide extrapolations, then attempt to interpret the experiments in light of this

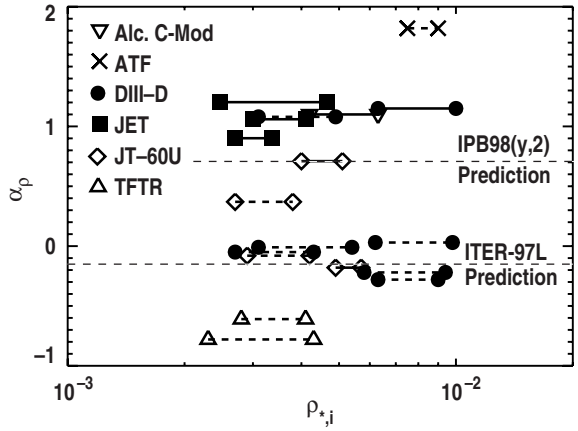

Figure 5. Plot of the ρ_*-scaling exponent for the global energy confinement versus the normalized ion gyroradius ($\rho_{*,\mathrm{i}}$). The scaling exponent is defined by $\tau_E \propto \rho_*^{-(2+\alpha)}$ as discussed in the text. The machine from which the data are obtained is denoted by the symbols given in the legend. The horizontal line type indicates a scan in H-mode (——) or L-mode (- - - -). The breadth of the scan in $\rho_{*,\mathrm{i}}$ is indicated by the length of the line.

theoretical background. It is beyond the scope of this review to critique or even catalogue exhaustively the large body of theoretical work in this area. The theories cited are intended as examples only.

The execution of a ρ_*-scaling experiment requires the local density, temperature, rotation and magnetic field to be adjusted to keep β, ν_{C} and M constant. This implies holding the physical geometry fixed, $n \propto B^{4/3}$, $T \propto B^{2/3}$, and $\omega_{\mathrm{tor}} \propto B^{1/3}$. With these relations, $\rho_* \propto B^{-2/3}$. To keep the magnetic geometry fixed, B_{p}/B must be constant everywhere. In standard tokamak operation, the central value of q remains close to 1, due to the effects of the sawtooth instability. Therefore, keeping q constant near the plasma edge is sufficient to give a match in B_{p}/B. This implies $I \propto B$. As will become clear, it is important to deal separately with the electrons and ions when possible. This implies that $T_{\mathrm{i}}/T_{\mathrm{e}}$, Z_{eff} and $m_{\mathrm{i}}/m_{\mathrm{e}}$ all must remain fixed.

The simplest analysis that can be carried out for ρ_*-scaling experiments is determination of α_ρ from the global energy confinement, where $\Omega\tau_E \propto \rho_*^{-(2+\alpha_\rho)}$ from equation (3.3). However, as can be seen in figure 5, which summarizes the results from many experiments, the outcome of this analysis is somewhat confusing. From such a plot, it would be tempting to conclude that dimensionless parameter scaling is not a particularly useful method, despite the success of the identity experiment. In fact, the experiments unraveling the effects that lead to the variation of α_ρ from -1 to 1 at fixed ρ_* give validation to the underlying equations that govern transport and lead to clear conditions for interpretation of the data. The remaining mysteries pose a significant test for theories that claim to describe plasma energy transport.

It should be noted, however, that some of the variation could be due to the choice of how to transform the results into a scaling. At least two choices have been used. The first is to assume that the profiles of ρ_* are changed by a fixed ratio determined by the change in B. The second is to use the measured ratio by which ρ_* changed. In the limit of the perfect ρ_* scan, this distinction obviously vanishes, but the reader should be aware that this choice can introduce systematic differences in the quoted scaling, especially in cases where the correct relationship among the fluid variables is not maintained. It is beyond the scope of this review to try to remove this potential source of systematic error; in fact, some authors do

not clearly state which method was used to determine the scaling. This caveat applies not just to ρ_* scans, but to all of the dimensionless parameter scaling experiments discussed in this review.

The first issue to resolve is the source of the large variation in α_ρ for L-mode discharges with roughly equivalent $\rho_{*,i}$. The first ρ_* scaling experiments in L-mode from the DIII-D [14], and JET [31] tokamaks reported that the global energy confinement scaling was roughly consistent with Bohm scaling, while TFTR tokamak data [23] showed a confinement scaling consistent with a non-dimensional formulation of Goldston scaling, which is even worse than Bohm with increasing size ($\alpha_\rho = -0.5$). These results for the global scaling were somewhat discouraging, given the uniform prediction of theory that the transport should exhibit gyroBohm scaling, although the local transport analysis of the DIII-D discharges [14] was consistent with gyroBohm scaling out to a normalized radius $\rho = 0.6$. The local analysis of the JET and TFTR data was more consistent with the reported global scaling. Similar L-mode results were reported from hydrogen discharges in ASDEX-Upgrade [32]. The inferred effective diffusivity was consistent with Bohm scaling or even $\alpha_\rho < 0$. The first result showing gyroBohm scaling in both the global confinement time and local transport analysis was from electron cyclotron heating (ECH) discharges in the Wendelstein VII-AS stellarator [33]. This result led to many speculations about the difference between tokamak and stellarator transport. Subsequent experiments in ATF [34] showed scaling even stronger than gyroBohm in the global confinement, although with large uncertainty. Experiments in LHD [35] and comparisons of LHD and CHS [36] also yielded gyroBohm scaling in both local transport and global confinement scaling. However, soon after the WVII-AS results were published, discharges with ECH and fast wave electron heating (FWEH) in the DIII-D tokamak also showed gyroBohm scaling in both local transport and global confinement scaling [37] under similar conditions to the WVII-AS results (strong electron heating). These results showed clearly that Bohm versus gyroBohm scaling was not determined by the confinement device nor by heating method, since JET had used ion cyclotron heating (ICH) [31].

The observation that regimes dominated by transport in the electron fluid exhibited gyroBohm scaling, while other regimes had Bohm scaling or worse, led to a key experiment on the DIII-D tokamak [38]. Three separate ρ_* scans were carried out. The first two employed ECH and FWEH at low density (electron heat flux dominant) and higher density (roughly equal electron and ion heat fluxes). The third had roughly equal electron and ion heat fluxes, but through neutral beam injection (NBI) rather than electron heating and collisional coupling. The results (figure 6(a)) show clearly that the global confinement scaling went from gyroBohm scaling when the heat flux was dominated by the electron heat flux to Bohm scaling when the electrons and ions shared the heat flux. The collisional coupling term, while large enough to transfer significant flux to the ions in the higher density case, was not so large as to prevent independent analysis of the electrons and ion transport by local power balance[6]. Treating the heat flux as purely diffusive, the electrons were found to have gyroBohm scaling in each case, while the ions always had a scaling consistent with the non-dimensional projection of the Goldston global scaling $\alpha_\rho = -0.5$ discussed above. This showed that the probable source of the variation in α_ρ shown in figure 5 was different ρ_* scalings for electrons and ions, combined with a continuous variation in the division of the heat flux between electrons and ions. The global confinement scaling or the effective one-fluid scaling can vary between the electron and

[6] In plasmas with strong collisional coupling, the uncertainties in the electron and ion temperature measurements can lead to a large uncertainty in the amount of energy transferred between the electron and ion fluids, that depends on the difference in the temperatures. This uncertainty propagates into the evaluation of the electron and ion thermal diffusivities and, when large, precludes any meaningful determination of the scaling of the individual diffusivities. In that case, the plasma must be treated as a single fluid.

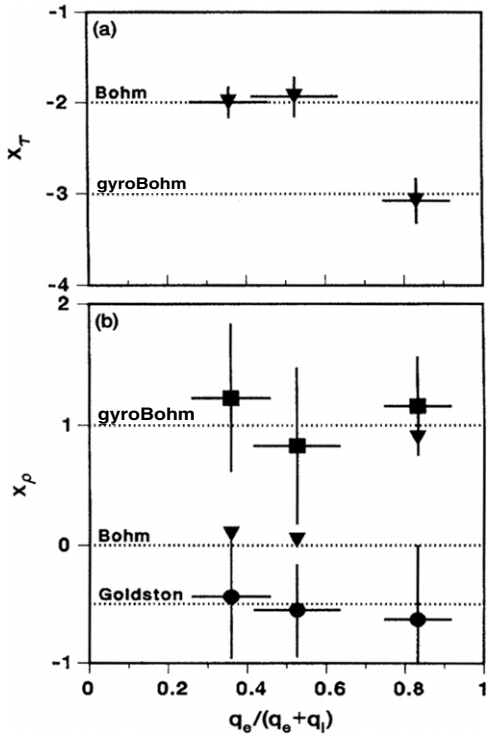

Figure 6. Gyroradius scaling exponents from DIII-D L-mode experiments for (*a*) global confinement, (*b*) electron (■), ion (●) and effective (▲) diffusivities as a function of the fraction of heat conduction in the electron channel. The quantity x_ρ corresponds to α_ρ in this paper. The quantity x_τ corresponds to $-(2+\alpha_\rho)$. The horizontal bars indicate the variation in the electron heat conduction fraction across the plasma radius. Reprinted from [38] by permission of the American Physical Society.

ion scaling values as shown in figure 6. Therefore, two-fluid analysis is needed to properly interpret ρ_* scaling experiments.

Equipped with the knowledge that two-fluid analysis is needed, subsequent experiments reported ρ_* results individually for both fluids when possible. The first L-mode results from JT-60U [39] showed trends similar to the DIII-D results [38]. The ion ρ_* scaling for plasmas with $q_{95} = 4.5$ and $q_{95} = 6.0$ was consistent with Bohm scaling, while the electron ρ_* scaling was between Bohm and gyroBohm scaling in both cases. The direction of the difference between the ion ρ_* scaling and the electron ρ_* scaling is the same as in the DIII-D experiment, but the magnitude of the difference is smaller in the JT-60U experiments. The match in JT-60U of β for the electrons in the $q_{95} = 4.5$ case and ions in the $q_{95} = 6.0$ case was not very accurate. The effect of this mismatch is difficult to estimate.

Similar results were obtained in L-mode experiments in helium on the Tore Supra tokamak [40]. The ion temperature was not measured, but inferred from the electron profile measurements and the total energy content. The profile was determined by applying an unspecified ion transport model with a multiplier varied to give the correct total stored energy. The heating at the high magnetic field was ion cyclotron resonance heating, while lower hybrid waves were used to heat the plasma at the low magnetic field. Both heating methods were assumed to give a centrally peaked heating profile. Global analysis indicated a ρ_* scaling that

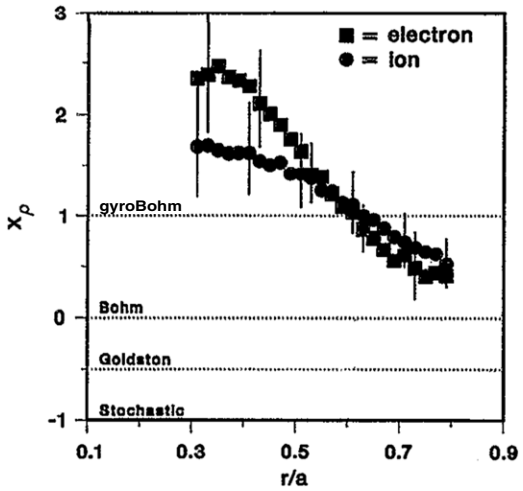

Figure 7. Measured value of the ρ_*-scaling exponent x_ρ (corresponds to α_ρ in this paper) for both the electron (filled squares) and ion (filled circles) heat diffusivity for DIII-D H-mode discharges. Reprinted with permission [41], Copyright 1995, American Institute of Physics.

was weaker than gyroBohm. The local transport analysis showed the electron ρ_* scaling to be near gyroBohm, but slightly weaker, while the inferred ion ρ_* scaling was between Bohm scaling and Goldston scaling. These results are consistent with the DIII-D and JT-60U results reported previously.

Historically, the next step in the ρ_* scaling was to move from L-mode experiments designed to understand the technique and study transport physics to H-mode experiments to provide data for extrapolation to future tokamaks such as ITER. The first H-mode ρ_* scaling results were reported from the DIII-D tokamak [41,42, (see discussion section)]. As shown in figure 7, both the electron and ion diffusivities change as expected for gyroBohm scaling, but with significant radial variation. The global energy confinement also has gyroBohm scaling. Results consistent with gyroBohm were subsequently reported on JET [43, 44], ASDEX-Upgrade [45], Alcator C-Mod [46] and JT-60U [47]. In order to assess the apparent agreement of these results, the methodology and quality of each of these experiments will now be discussed.

The DIII-D ρ_* scaling experiment [41] was carried out using NBI heating exclusively. The parameters were chosen to match the design point of the ITER baseline scenario at that time. However, in order to maintain central penetration of the NBI, the density in the low ρ_* case was limited to around $6 \times 10^{19}\,\mathrm{m}^{-3}$. In order to match the ITER ν_C, the plasma current was limited, resulting in $q_{95} = 3.7$ rather than the ITER value of 3.0. The NB voltage was reduced in the high ρ_* case in order to match T_i/T_e. In contrast to the previous L-mode results [38], there is a significant radial variation in the ρ_*-scaling exponent (figure 7). As discussed in more detail below (section 3.3.3), later reanalysis of these data in light of the effects of shear in the $\boldsymbol{E} \times \boldsymbol{B}$ flows indicated that the mismatch in the Mach number in these cases could affect the ρ_* scaling [48]. However, the radial variation in the ρ_*-scaling exponent is in both the electron and ion heat diffusivities, while the $\boldsymbol{E} \times \boldsymbol{B}$ flow shear was found to only affect the ion transport. Examining the dimensionless parameter matches (figure 7 in [41]), the mismatch in the density profile, leading to mismatches in ν_C and β, could be the source of this radial dependence. The radial variation of the ρ_* scaling is somewhat enhanced by showing the exponent rather than the ratio of the diffusivities, as in [38]. Due to the quality of match of the temperature profiles and the correspondence of the global energy confinement ρ_* scaling

and the local heat diffusivity scalings, the conclusion that the H-mode heat transport has a gyroBohm scaling for both the electrons and the ions seems to be warranted.

The JET experiments confirmed the gyroBohm scaling in H-mode under conditions designed to match the DIII-D experiments [43,49]. These plasmas were also heated exclusively by NBI. The matches of the dimensionless parameters were not published, so it is not possible to assess the quality of the match. Only the effective or one-fluid diffusivity is reported, presumably because of the errors in separating the two fluids in the high-density case due to the collisional coupling. The ratio of diffusivities corresponds across the entire radius to the expectation from gyroBohm scaling. Since the one-fluid diffusivity scales as expected from gyroBohm scaling, it seems likely that the electrons and ions scale individually with a gyroBohm scaling, based on the evidence that the electron scaling is found to be close to gyroBohm in all cases where the fluids can be separated. These experiments also revealed an important constraint on the application of ρ_* scaling—that the ρ_* scaling path must remain sufficiently far above the power required to maintain H-mode. If the ρ_* scaling trajectory approaches the L–H transition boundary, the apparent scaling of the core transport will reflect the scaling of the L–H transition power rather than the transport scaling [50]. This will be discussed further in section 3.3.3.

Recent experiments on JET [44] have verified that the ρ_* scaling in H mode with both Type III and Type I ELMing edge is consistent with gyroBohm scaling under conditions otherwise similar to those expected in ITER. Both scans were carried out at $q_{95} = 2.8$ at low collisionality ($\nu_*/\nu_{*,\mathrm{ITER}} \approx 1.7$ and 3.5, respectively). The scan with Type III ELMs had modest β ($\beta_\mathrm{N} \approx 0.7$), while the scan with Type I ELMs had $\beta_\mathrm{N} \approx 1.7$, which is closer to the expected value for the ITER baseline scenario. As was the case with the previous JET ρ_* scan, the profiles of the dimensionless parameters are not shown, so it is not possible to assess the quality of the matching of the parameters to be held fixed. For the plasmas with Type III ELMs, a four-point scan was analyzed only for the scaling of the global energy confinement. Regression analysis indicated $B\tau_E \propto \rho_*^{-2.9\pm0.5}$, consistent with gyroBohm scaling. The scan with Type I ELMs was analyzed only with local transport analysis, due to variation in the deposition profile of the NBI. In this case, a seven-point scan was obtained. A regression analysis of the effective heat diffusivity yielded $\chi/\chi_\mathrm{B} \propto \rho_*^{1.2\pm0.4}$, again consistent with gyroBohm scaling.

The H-mode ρ_* scaling experiments in ASDEX-Upgrade [45] also indicated a gyroBohm scaling of the effective heat diffusivity. The heating scheme was again NBI, and the plasma current and magnetic field were chosen to give $q_{95} \sim 4$. The scan in ρ_* was only a factor of 1.3, compared with a factor of 1.6 in the earlier DIII-D and JET scans. In these scans, the global energy confinement was worse than $\alpha_\rho = -0.5$ in the cases where the core profiles of β and ν_C matched. The profile matches were not published, so it is not possible to assess the quality of the matches. The NB voltage was adjusted to try to maintain a fixed deposition profile. However, this was not successful, due to the high-density operation, which also precluded separating the electron and ion diffusivities. Analysis of the effective diffusivity showed that it scaled as expected from gyroBohm scaling in the radial region where the profiles of β and ν_C matched (figure 6 of [45]). This illustrates a point discussed earlier, namely, that the dimensionless parameters need only match over a sufficiently large region to be meaningful for the process under study. In this case, a radial region of several radial correlation lengths of the underlying turbulence should be sufficient. The global energy confinement time is weighted strongly to the edge, which is evidently not well matched for these scans. This same issue was encountered in the original L-mode ρ_*-scaling experiments in DIII-D [14,51].

The ρ_*-scaling experiments in Alcator C-Mod [46] were similar to the scans discussed above, with the notable difference of plasma heating by ion cyclotron resonance heating on a hydrogen minority in deuterium plasmas. Because this heating scheme does not apply

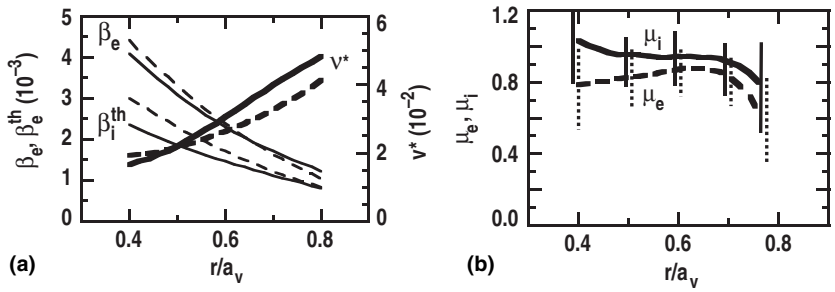

Figure 8. (*a*) Radial profiles of electron and ion β (thin curves) and electron ν_* (thick curves) for JT-60U H-mode ρ_* scaling experiments at $q_{95} = 3.7$. (*b*) Radial profiles of the electron and ion ρ_*-scaling exponent (corresponds to α_ρ in this review). Reprinted from [47] by permission of the Institute of Physics.

momentum to the plasma, the Mach numbers should be matched or small enough to be neglected. The result reported for the effective diffusivity was again gyroBohm scaling across most of the plasma (figure 1 of [46]). The densities in Alcator C-Mod are high enough that separation of the heat flux into electron and ion components was not possible. The radial dependence of the one-fluid diffusivity was similar to that reported in DIII-D [41], in that the value inside the half-radius indicated a scaling even stronger than gyroBohm. The profile matches of the dimensionless parameters unfortunately are not available, so it is not possible to correlate these data with the hypothesis discussed above about the DIII-D result that the radial variation arose from the mismatch in the density profile. However, it would seem reasonable that any mismatch in Mach number is not the explanation in this case.

The H-mode experiments in JT-60U [47] were able to separate the electron and ion transport and confirmed the original DIII-D result that both species exhibit a gyroBohm scaling. The heating method in these experiments is NBI. The matches of β and ν_C are shown in figure 8(*a*), for the case at $q_{95} = 3.7$ (similar to the DIII-D experiment). The ρ_* scaling is near gyroBohm in electrons and ions (figure 8(*b*)). The slight mismatch in β is in the direction to move the scaling closer to gyroBohm scaling, if the additional power required to increase β in the high ρ_* case is taken into account. A scan at $q_{95} = 3.0$ (similar to the ITER baseline design) showed a ρ_* scaling closer to Bohm scaling, which was attributed to the change in ELM behavior and triangularity. This result is probably consistent with the JET ρ_* scan that encountered the L–H threshold condition at low ρ_*. This topic will be discussed further in section 3.3.3. The second scan also had a significant mismatch in ν_C (almost a factor of 2). Given the weak ν_C scaling seen in most experiments (section 3.5), the mismatch may not be too significant, even one this large. However, it is in the direction to make the ρ_* scaling appear closer to Bohm scaling, if the mismatch is accounted for using the ν_C scaling reported in [47].

The local electron transport results from L-mode and H-mode experiments are summarized in figure 9(*a*). Although the uncertainties in the analysis are substantial, the clear interpretation is that the local electron transport scaling is consistent with gyroBohm scaling and is not consistent with Bohm scaling. The ion ρ_* scalings are not as uniform as the results for the electron ρ_* scaling (figure 9(*b*)). This implies that the variation in α_ρ in figure 5 has a component due to an intrinsic variation in the ion ρ_* scaling in addition to the variation due to the fractional heat flux in each channel.

The fact that all experiments that could resolve the electron heat diffusivity scaling observed the electron ρ_* scaling was gyroBohm, in combination with the ion ρ_* scaling varying from Goldston scaling in L-mode plasmas to gyroBohm in H-mode plasmas, suggested

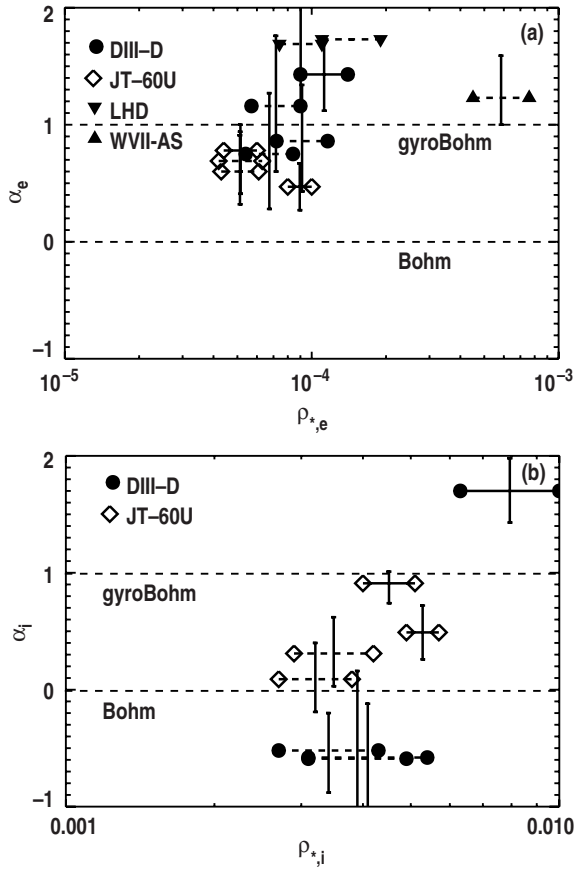

Figure 9. (*a*) Plot of the ρ_*-scaling exponent for the electron heat diffusivity evaluated at the half-radius versus the normalized electron gyroradius ($\rho_{*,e}$). The scaling exponent is defined by $\chi_e \propto \chi_B \rho_{*,e}^{\alpha}$ as discussed in the text. (*b*) Plot of the ρ_*-scaling exponent for the ion heat diffusivity evaluated at the half-radius versus the normalized ion gyroradius ($\rho_{*,i}$). In both plots the machine from which the data are obtained is denoted by the symbols given in the legends. The horizontal line type indicates a scan in H-mode (——) or L-mode (- - - -). The breadth of the scan in ρ_* is indicated by the length of the line.

a hypothesis to explain these variations. The electron ρ_* is small—$<10^{-3}$ in WVII-AS and $<2 \times 10^{-4}$ in all other experiments. Perhaps the electron gyroradius is small enough that the electron responds to the turbulence as if the machine were infinitely large. On the other hand, the ion ρ_* is larger—between 2×10^{-3} and 10^{-2} in the present dataset. Drift wave calculations usually associate the transport with long perpendicular wavelength modes (10–20 ρ_i), which would give only $\sim$10 wavelengths across the machine in extreme cases. If the equilibrium scale lengths associated with drift waves such as the density scale length ($L_n \equiv n/|\nabla n|$) or the magnetic shear length ($L_q \equiv q/|\nabla q|$) are less than a, then the free energy or mode spectrum available to the turbulence could be modified from that calculated for a uniform gradient model. The original two-fluid ρ_* scaling results from DIII-D were obtained in L-mode discharges (short L_n) with high q_{95} (short L_q). The H-mode results had flat density profiles (large L_n) at low q_{95} (large L_q). Perhaps in the H-mode case, the ions, despite having larger ρ_* than in the L-mode discharges, behaved as if they were in an infinitely large machine due to the flat density and q profiles.

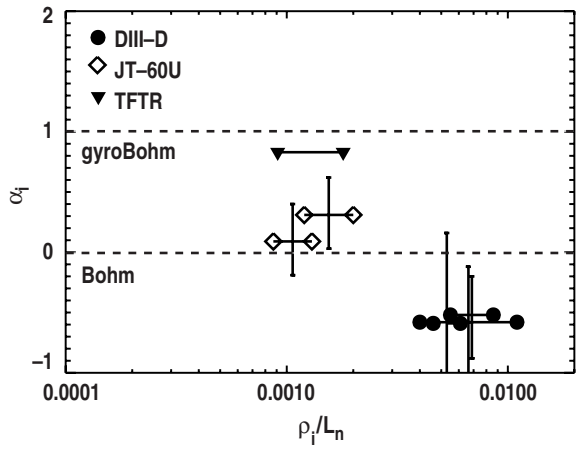

Figure 10. Plot of the L-mode ρ_*-scaling exponent for the ion heat diffusivity evaluated at the half-radius versus the ion gyroradius normalized to the density scale length. The machine from which the data were taken is denoted by the symbols given in the legend. The breadth of the scan is indicated by the horizontal length of the line.

To test this hypothesis, ρ_* scans were carried out in H-mode discharges with high q_{95} (flat density, but small L_q) and in L-mode discharges at low q_{95} (small L_n, but large L_q). In both cases, the electron scaling remained roughly as expected for gyroBohm scaling, while the ion ρ_* scaling in each case was roughly consistent with Bohm scaling [52]. Therefore, the ion ρ_* scaling is connected with both the density scale length and the poloidal magnetic field scale length. As the effective size of tokamaks (as measured by $\rho_{*,\mathrm{i}}$) increases, it would seem likely that the equilibrium scale lengths would scale with physical size. Therefore, if this view is correct, low q_{95} H-mode discharges should continue to scale according to gyroBohm scaling. It would be interesting to test whether low q_{95} L-mode discharges could be obtained with gyroBohm scaling in larger machines. Re-examination of the smallest ρ_*points in the high density TFTR ρ_* scan shows the heat flux begins to scale as expected for gyroBohm scaling (figure 13 of [23]). The accuracy of these data is too limited to draw a definite conclusion from that scan, but the indications are in the proper direction.

To summarize the experimental results, it appears that the measured electron ρ_* scaling in both stellarators and tokamaks under a variety of conditions is consistent with a gyroBohm model (figure 7(*a*)). The measured ion ρ_* scaling has significant variation, spanning nearly the entire range of α_ρ expected from theory (figure 7(*b*)). Experiments indicate a correlation of this variation with either the density scale length L_n or the magnetic shear scale length L_q. Using the limited data set where the published results allow a determination of L_n, the L-mode data indicate a trend in the direction of gyroBohm scaling for the ions when plotted against the ion gyroradius normalized to L_n (figure 10). The trend for the H-mode (not shown) is not clear, but there is a definite correlation between ρ_* and L_n in both the DIII-D and the JT-60U experiments that systematically reduces the range in ρ_*/L_n. The data are not available to test the trends with L_q, which may be more important for the H-mode data at low q_{95}. As discussed previously, the global ρ_* scaling can vary from the ion ρ_* scaling value to the electron ρ_* scaling value, depending on the fraction of the heat flux in each fluid. Therefore, studies of the global scalings need to be aware of the potential systematic error in the analysis, if equal electron and ion ρ_* scalings are assumed.

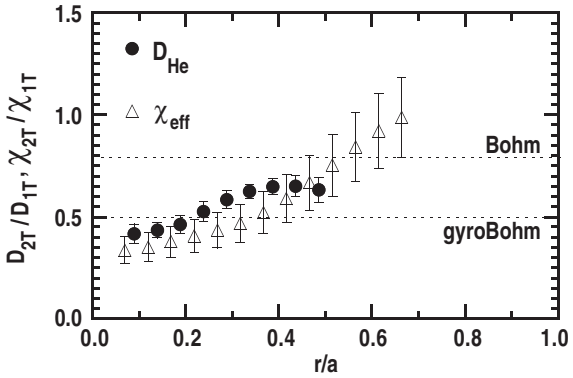

Figure 11. Ratio of the helium and single-fluid diffusivities for the ρ_* scan in DIII-D H-mode discharges. Reprinted from [53] by permission of the American Physical Society.

3.3.2. Particle transport. Dimensionless parameter scaling techniques have also been applied to particle transport. It is implicitly assumed that the same dimensionless parameter set relevant to energy transport is also valid for particle transport, since no identity experiments have been performed. The particle flux Γ is written as $\Gamma = -D\nabla n + nV$ and the particle continuity equation $(\partial n/\partial t) + \nabla \cdot \Gamma = S$ is assumed to hold in the plasma interior. Here D is a particle diffusivity and V is a convective velocity. All of the experiments discussed here measure the transient response to a perturbation in the region where the source $S = 0$. As will be evident, the species whose transport is directly measured depends on the available diagnostics. In a stationary case, only one parameter can be determined, but the time-evolving perturbation allows evaluation of both D and V.

The first experiments reported were measurements of the helium (He) transport in H-mode plasmas in DIII-D [53]. Knowledge of the helium transport is essential for prediction of the fusion gain in deuterium–tritium experiments with substantial fusion power. The charged byproduct of deuterium–tritium fusion reactions is an α particle—a He ion. Buildup of He 'ash' would substantially reduce the fusion output of such a plasma. The helium density is measured by direct spectroscopic observation of charge exchange excited states in the heating beam. The determination of D and V is limited to radii inside $\rho = 0.6$, due to the limited time resolution of the spectroscopic measurements. The helium particle diffusivity D_{He} is found to be very close in magnitude and radial dependence to the one-fluid thermal diffusivity (χ_{eff}). The ρ_* scalings are also similar, with the central scaling close to gyroBohm, drifting to between Bohm and gyroBohm in both cases near $\rho = 0.5$ (figure 11). The inferred convective velocity is inward and $|V_{\mathrm{He}}|$ decreases strongly with increasing ρ_*. This would imply peaking of the He density with smaller ρ_*. However, the electron density shows a similar peaking, leaving the concentration unchanged. This indicates no preferential accumulation of helium.

The next experiment employed the capability of the JET tokamak to operate with tritium to probe the transport of hydrogen ions [54]. Taking advantage of the large deuterium–tritium fusion cross-section and the unique 14 MeV neutron signature of the reactions, the time evolution of the tritium density was inferred from the neutron signature on a multi-chord collimated neutron camera. The D_{T} and V_{T} were inferred using the method described above. Both L-mode and H-mode ρ_* scans were reported. In L-mode, the diffusivity was found to be Bohm like and the data were consistent with $V_{\mathrm{T}} = 0$. For H-mode, the core ($\rho < 0.6$) and edge ($\rho > 0.6$) had distinct scalings. In the core, D_{T} had a gyroBohm scaling and again the data were consistent with V_{T} independent of ρ_*, as shown in figure 12. In the edge

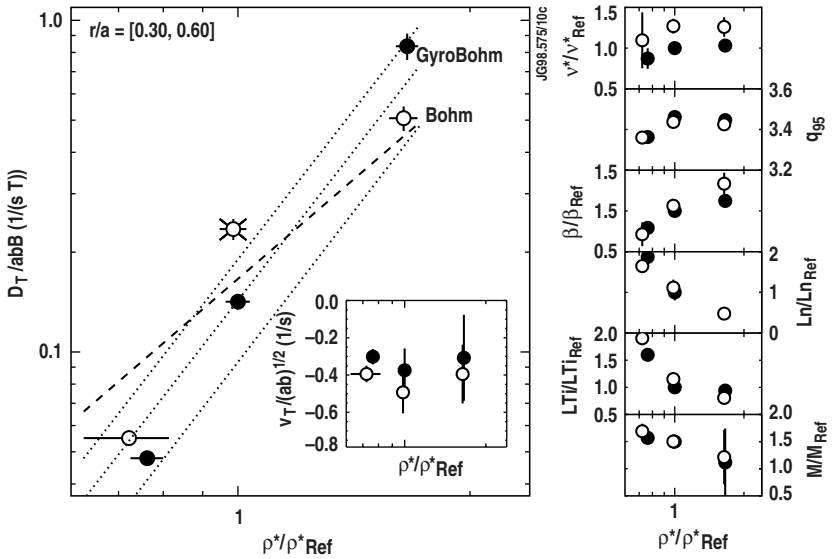

Figure 12. The left panel shows the normalized tritium diffusivity measured in JET plotted versus ρ_* normalized to the value in the reference discharge. The dotted lines indicate the expected variation for gyroBohm scaling with a 30% confidence interval. The dashed line shows the expected trend for Bohm scaling. The inset shows the normalized tritium convective velocity. The open and closed symbols denote two distinct scans with higher and lower collisionality, respectively. The right panel shows the quality of the match of selected dimensionless parameters: collisionality, q_{95}, β, density scale length, temperature scale length and Mach number (top to bottom). The density scale length appears to be poorly matched in both scans, which is a concern for particle transport analysis. Reprinted from [54] by permission.

region, D_{T} was more consistent with Bohm scaling, while the convective velocity is inward. The magnitude $|V_{\mathrm{T}}|$ decreased strongly with increasing ρ_* as reported for helium in DIII-D H-modes. Unfortunately, a comparison with the heat diffusivity was not reported; however, the scaling of D_{T} is similar to the ρ_* scaling of χ reported in other JET experiments [31, 43].

Recently, the particle transport experiments using trace tritium in ELMing H-mode plasmas on JET were repeated and found the ρ_* dependence of the particle diffusivity to be essentially as expected for gyroBohm scaling in the core regions [55, 56]. The dependence was closer to Bohm scaling in the outer third of the plasma radius. This is in agreement with the previous results and also with the energy transport scaling, which was not reported in the previous experiments. A best fit for the diffusivity and convection velocity was determined by simulating the neutron data using a 1.5D particle transport code. For $\rho < 0.4$, this gave a tritium transport scaling like $D/D_{\mathrm{Bohm}} \sim \rho_*^{1.22\pm0.62}$, whereas for $\rho = 0.65$–0.85 the result was $D/D_{\mathrm{Bohm}} \sim \rho_*^{-0.10\pm0.38}$. The ρ_* scaling of the convection term was not reported. (Note that the JET reports use the normalization D/B rather than D/D_{Bohm} as used here. The original normalization is equivalent to an additional ρ_*^2 in the scaling.)

Finally, measurements of the electron and helium transport were reported from an L-mode ρ_* scan on the DIII-D tokamak [57]. The helium transport was measured as discussed above, while the electron transport was inferred from time-dependent measurements by Thomson scattering of the response to deuterium gas puffs. Both D_{e} and D_{He} showed Bohm scaling over most of the measurement range, with D_{e} degrading to Goldston scaling and beyond in the plasma center. The energy transport scaling was also reported individually for electrons and ions. The electron heat diffusivity had clear gyroBohm scaling while the ions had Goldston

scaling over the outer half of the plasma as reported previously [38]. Contrary to the other results reported here, the inferred convective velocity for both electrons and helium increased strongly with ρ_*, although still directed inward as in the other cases.

The general observation from the particle transport scaling experiments is that the widely observed correlation of the magnitude of the particle diffusivities with the heat diffusivities is extended to agreement in the ρ_* scaling. In the case of the DIII-D analysis where the heat diffusivity could be separated into electron and ion channels, the particle diffusivities followed the ion channel scaling in both L-mode and H-mode. This correspondence may be a useful assumption for modeling particle transport in projections to burning plasmas, since the energy transport has been studied much more extensively than the particle transport.

3.3.3. Issues with the application of dimensionless parameter scaling. While the description of the experimental situation given above is self-consistent, concerns about the dimensionless parameter scaling approach (and specifically with respect to ρ_* scaling) have been raised and should be addressed here. The main concerns fall into three categories—the influence of hidden variables, multiple transport mechanisms and threshold behavior in the turbulence.

The concern about the influence of hidden variables stems partly from the inability of the dimensionless scaling approach to uniquely define the appropriate scaling parameters or even the number of important parameters. As discussed in the section on the conceptual basis, Buckingham's theorem gives the minimum number of dimensionless parameters required but cannot set a maximum. In addition, the theorem only determines the relationship of the dimensional quantities to each other; the phenomenon of interest can be any complicated functional of the dimensionless parameters. The present set of dimensionless parameters is chosen because they have both a physical significance and appear in theoretical formulations [11]. As discussed in the section on identity experiments, these variables have been shown to describe the plasma transport. This conclusion comes with the caveat that any other variables not considered are either well enough matched accidentally or are not important. An example of an inappropriate choice of variables was also given, showing the identity test can discriminate against some choices of dimensionless parameters.

Nevertheless, the experimental measurements of the variation of the ion ρ_* scaling and the discussion of a possible resolution by normalizing ρ_i to L_n rather than to a suggest that the concern about hidden variables must be taken seriously. One candidate for a hidden variable based on theoretical considerations is the shear in the bulk $\boldsymbol{E} \times \boldsymbol{B}$ rotation velocity, where the radial electric field and the toroidal magnetic field are the important quantities. The standard theoretical model [58] is to reduce the transport calculated in the absence of rotation by a linear, no-threshold factor $1 - |\gamma_E|/\gamma_{max}$, where γ_{max} is the maximum linear growth rate and γ_E is the spatial gradient of the $\boldsymbol{E} \times \boldsymbol{B}$ velocity. If this factor is the correct one to describe transport, then it cannot be held constant in a conventional ρ_* scan at fixed Mach number. The diamagnetic part of γ_E scales like ρ_* while the bulk rotation parts are independent of ρ_* at fixed Mach number. If the intrinsic transport is independent of Mach number, as expected for $M \ll 1$, then in principle the bulk rotation could be adjusted to give fixed $|\gamma_E|/\gamma_{max}$.

Comparison of ρ_* scans for co-NBI and counter-NBI at similar dimensionless parameters are consistent with the picture that $|\gamma_E|/\gamma_{max}$ rather than M is the appropriate dimensionless parameter [48]. The counter-NBI ρ_* scan has an ion ρ_* scaling between Bohm and gyroBohm, while the ion ρ_* scaling in co-NBI is stronger than gyroBohm. The helium particle diffusivity is also observed to change in a manner similar to that of χ_i. Simulations using the GLF23 model with and without $\boldsymbol{E} \times \boldsymbol{B}$ shear effects can explain that observed change in scaling by a mismatch in $|\gamma_E|/\gamma_{max}$. In principle, this question can be settled experimentally by performing ρ_* scans with either M or $|\gamma_E|/\gamma_{max}$ fixed. It may also be possible to do identity experiments between

machines, taking care to match M or $|\gamma_E|/\gamma_{max}$ in a regime where $|\gamma_E|/\gamma_{max}$ is predicted to be important.

A key finding of the DIII-D study is that $\boldsymbol{E} \times \boldsymbol{B}$ shear does not affect the electron heat transport. This is consistent with the observation reported above that the ρ_* scaling of the electron heat diffusivity is always close to gyroBohm scaling. However, if $\boldsymbol{E} \times \boldsymbol{B}$ shear (or any other mechanism correlated with L_n or L_q that acts as a long-wavelength cutoff of the turbulence) is responsible for the variation of the ρ_* scaling of the ion heat diffusivity, then the electron heat transport is dominated by something at shorter wavelengths that is unaffected by this cutoff.

The issue of the existence of multiple transport mechanisms has several facets. The simplest case to deal with is the situation where there is no threshold behavior. The stationary energy balance equation can be integrated to give

$$\chi(\rho) = \frac{-P(\rho)}{H\rho n(\mathrm{d}T/d\rho)}, \tag{3.4}$$

where the heat flux is assumed to have the form $q = -n\chi(\mathrm{d}T/\mathrm{d}\rho)$. The power deposited within the normalized radius ρ is $P(\rho)$, $H\rho$ is a geometric factor accounting for non-circular cross-section, n is the local density, and $\mathrm{d}T/\mathrm{d}\rho$ is the local temperature gradient. (A single fluid is assumed for illustration.) In a perfect ρ_* scan, the variations in n and T can be cast in terms of the toroidal field B. Therefore,

$$\frac{\chi_H}{\chi_L} = \frac{P_H/P_L}{(B_H/B_L)^2}, \tag{3.5}$$

where the labels 'H' and 'L' refer to the 'high' and 'low' toroidal field cases. Assume that χ is now a linear combination of two processes with different ρ_* scalings:

$$\chi = \chi_B(A\rho_*^a + D\rho_*^d). \tag{3.6}$$

Putting equation (3.6) into equation (3.5):

$$\left(\frac{B_H}{B_L}\right)^{-1/3}\left(\frac{A\rho_{*,H}^a + D\rho_{*,H}^d}{A\rho_{*,L}^a + D\rho_{*,L}^d}\right) = \frac{P_H/P_L}{(B_H/B_L)^2}. \tag{3.7}$$

Without loss of generality, it can be assumed that $a \leqslant d$. Equation (3.7) can then be rearranged to give

$$\left(\frac{B_H}{B_L}\right)^{(5-2a)/3}\left[\frac{1+(D/A)\rho_{*,H}^{d-a}}{1+(D/A)\rho_{*,L}^{d-a}}\right] \equiv \left(\frac{B_H}{B_L}\right)^{(5-2a)/3} C_M = \frac{P_H}{P_L}. \tag{3.8}$$

By definition, $C_M \leqslant 1$. If $a = d$, then $C_M = 1$, and there is no effect of multiple transport mechanisms. Solving equation (3.8) for a:

$$a = \frac{5}{2} - \frac{\ln(P_H/C_M P_L)^3}{\ln(B_H/B_L)^2}. \tag{3.9}$$

Clearly, $C_M < 1$ leads to an increase in a, with upper limit being d in the case $D/A \gg \rho_{*,L}^{a-d}$. As one might expect, the result of a perfect scan with such a mixed model would be an answer close to the dominant scaling (if there is one) with a correction in the direction of the other scaling.

However, equation (3.8) tells us that the power deposition profile must vary in a precisely prescribed manner to allow the temperature profiles to match. This being unlikely, the signature of multiple transport models would be the inability to match the temperature profile shapes for centrally heated discharges. To go beyond this qualitative statement, a specified model and ρ_* scan would be required. The quality of temperature match in the ρ_* scaling experiments has

some variation, but is in general quite good. (See [41] for examples.) One possible indication of this sort of problem would be that the global energy confinement ρ_* scaling and the local transport ρ_* scaling are substantially different. This is not a unique indicator, since there are other possible causes of this behavior as will be discussed below.

A variation on the problem of multiple transport mechanisms is when the edge boundary condition scales differently from the core transport. The most obvious case of this is when the power required at the lower end of an H-mode ρ_* scan approaches the power required to maintain H-mode. Analysis of the H-mode power threshold database [59] indicated a different ρ_* scaling for the power threshold from the gyroBohm scaling found for H-mode energy transport, but similar to the Goldston-like ρ_* scaling found for the ion energy transport in L mode (see section 3.3.1 for the ion energy transport ρ_* scaling results). Given these two distinct scalings, the power required to maintain fixed β in a ρ_* scan will eventually become less than the power to keep the discharge in H mode as ρ_* is reduced. Experiments in JET [49] explored this regime and found that the global ρ_* scaling indeed follows the ρ_* scaling of the H-mode power threshold rather than reflecting the core transport scaling. The implications of this for extrapolating present dimensionless scaling results to future experiments such as ITER are discussed in [50].

The question of the effects of threshold behavior in the transport mechanisms was raised in the interpretation of one of the original experiments [51]. The issue could be particularly important if the increase in transport above the threshold is very strong. The situation where the increase in transport is so strong that large increases in input power do not increase the temperature gradient would lead to so-called 'stiff' profiles. For the ρ_* scaling experiments, the concern is that the measured scaling could take on almost any value, since large changes in input power (and therefore χ or τ_E) would result in similar temperature profiles. Most models that have such threshold behavior take the form [60]

$$\chi = \chi_0 + \lambda T^{\alpha} \left(\frac{|\nabla T|}{T} - k \right)^{\beta} H \left(\frac{|\nabla T|}{T} - k \right), \tag{3.10}$$

where the threshold occurs when the temperature scale length drops below $1/k$. If the plasma transport actually follows this form, then the ρ_* scans maintain the same relative position to the critical scale length $1/k$ as long as k is not a function of ρ_*. The effect of the leading terms having different ρ_* scalings has already been discussed in the preceding paragraph. In general, the threshold condition should be cast in terms of dimensionless parameters; if it is independent of ρ_*, then there is no effect on a ρ_* scan of the threshold.

The effect of global constraints, such as adiabatic invariants [61], can be discussed in the same manner. If the constraint, like the canonical toroidal angular momentum in [61], can be cast in terms of dimensionless variables, then the impact of the ρ_* scan is determined by the dependence on ρ_*. For the case cited, the density and temperature profiles are fixed by the q profile, which must be matched in a ρ_* scan. Therefore, the results of the ρ_* scan should not be changed by the global constraint.

3.3.4. Extending dimensionless parameter scaling to turbulence measurements. Experiments have begun which take the dimensionless parameter scaling approach down to the fundamental fluctuation level. The idea behind these experiments is to look for the dimensionless parameter scaling of the spatial and temporal correlations of the turbulence itself, in order to compare both with theoretical expectation and empirical transport results. In DIII-D [62], a ρ_* scan was performed in L-mode. One goal of the fluctuation measurements was to try to find the mechanism responsible for breaking the expected gyroBohm scaling. The local one-fluid transport and the global energy confinement both exhibited ρ_* scaling close to Bohm scaling.

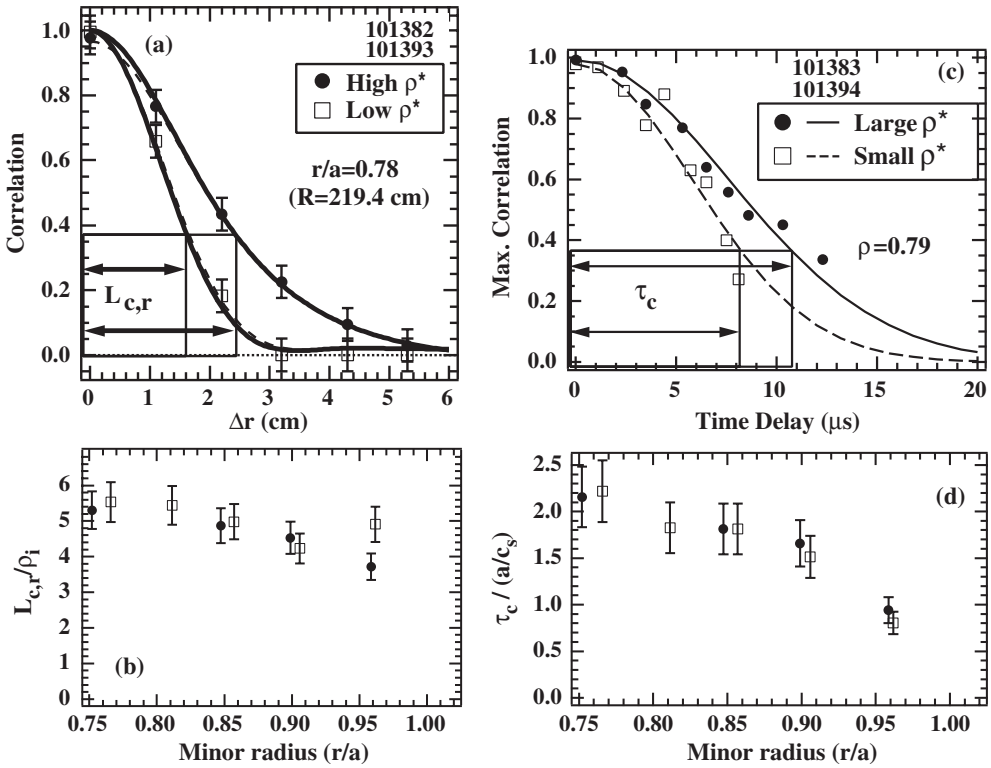

Figure 13. (*a*) Radial correlation function at $r/a = 0.78$ for the two discharges in the DIII-D L-mode ρ_* scan showing a shorter radial correlation length $L_{c,r}$ in the low ρ_* discharge, and (*b*) the ratio of the radial correlation length profile to the ion gyroradius showing $L_{c,r} \sim 5\,\rho_i$. (*c*) Temporal correlation function of turbulence at $r/a = 0.79$ showing an increase in decorrelation time from $\tau_c \approx 8$ to $\tau_c \approx 11\mu$s as ρ_* is increased. (*d*) Profiles of τ_c normalized to a/c_s showing a match between the two conditions, indicating a gyroBohm-like scaling. Reprinted from [62] by permission.

However, the underlying fluctuations still manifested correlation lengths proportional to ρ_i and decorrelation times proportional to a/c_s as expected from gyroBohm theories (figure 13). Unfortunately, the signal-to-noise of the fluctuation measurements at that time limited these scaling studies to fluctuations in the outer 25% of the plasma. Simple mixing length transport estimates gave scalings close to gyroBohm (figure 8 of [62]), except very near the separatrix where the quality of the match of the dimensionless parameters is likely not very good. The mechanism responsible for the local and global confinement varying from the gyroBohm scaling observed in the turbulence data has not yet been identified.

Similar analysis has been carried out in helium plasmas heated only by ohmic heating in Tore Supra [63]. The k spectrum and decorrelation times were measured using scattering of laser light. In this case, the global energy confinement scaling was nearly gyroBohm. (The density at the low magnetic field was too large, yielding some mismatch in the other dimensionless parameters. A weak increase in global energy confinement time with density would give a perfect gyroBohm scaling, if this mismatch were corrected.) The variation of the k spectrum of the measured density fluctuations agreed with the expected variation from gyroBohm scaling, as did the variation of correlation times. As in the DIII-D experiment, the behavior of the density fluctuations with variations in the plasma

parameters agrees with the gyroBohm scaling of the equations that are expected to describe the turbulence.

Pursuit of such fluctuation measurements is very difficult in hot plasmas. Smaller devices [64, 65], in which probe arrays can be inserted, may be the means of solving these problems. The key to understanding turbulent transport at this level is not just the density fluctuations, as measured on DIII-D and Tore Supra, but also the fluctuations of the electric potential for particle transport, and both potential and temperature fluctuations for heat transport. Preliminary results from TJ-K [64, 66] indicate that the correlation lengths over a range of k values scale with ρ_s as expected from gyroBohm scaling. At the lowest k values, which are difficult to measure, this may not be true, suggesting an area for further study.

3.4. Dependence on β

Determining the β scaling of heat and particle transport helps to differentiate between the various instabilities proposed as underlying the turbulence that causes the transport, especially between those that are primarily electrostatic or primarily electromagnetic. Physics arguments suggest that transport should be independent of β at low β, where the turbulent transport is expected to be a consequence of electrostatic microinstabilities, and should increase with β as the ideal ballooning stability limit is approached. However, the interpretation of the physics responsible for the β scaling of transport is only straightforward when the ion gyroradius is chosen as the size scaling parameter [10]. This can be demonstrated using the simple example of a plasma with purely electrostatic fluctuations, in which case the local thermal diffusivity scales as $\chi \propto \chi_B \rho_* \beta^0$. An alternative length parameter, such as the skin depth, $\delta = \sqrt{m_e c^2 \varepsilon_0 / e^2 n_e}$), could be chosen in place of ρ_i. If δ/a is used in place of ρ_* as the non-dimensional size parameter, then the local thermal diffusivity is recast in the form $\chi \propto \chi_B (\delta/a)\sqrt{\beta/2}\sqrt{m_i/m_e}$. Thus, using δ as the size scaling parameter, the diffusion coefficient can appear to depend upon β even for models in which β is neglected. For this reason, ρ_* appears to be a judicious choice for the non-dimensional size parameter since it makes the physics responsible for β scaling more transparent.

Most models of drift wave turbulence in which fluctuating $\boldsymbol{E} \times \boldsymbol{B}$ transport is the dominant mechanism show little enhancement or even a reduction in transport with increasing β up to some fraction (typically 50%) of the ideal ballooning stability limit [67–69]. This β scaling can usually be explained by the stabilizing influence of β (and magnetic well depth) on the ITG mode [70–72]. On the other hand, electromagnetic effects on turbulent transport, like magnetic flutter, generally have a strong increase with β. Magnetic island theories and models of resistive fluid turbulence can also predict strong increases in transport with β [73]. Thus, if a strong β scaling is experimentally measured, then electromagnetic effects are probably essential to the turbulent transport process. Probing for electromagnetic effects near the ideal ballooning stability limit (β_{crit}) generally requires the utilization of H-mode plasmas, while the electrostatic limit is best obtained with low β L-mode plasmas[7]. It should be noted that, theoretically, the relevant dimensionless parameter is β/β_{crit}, where β_{crit} is the ideal ballooning stability limit. However, since q, κ and R/a as well as the current and pressure scale lengths are to be kept fixed in these experiments, one can speak interchangeably about β, β_N or β/β_{crit} scaling of transport.

The β scaling of heat transport has been studied in H-mode plasmas on the JET and DIII-D tokamaks, both of which found only a weak β dependence. To scan β in fixed magnetic

[7] Most fusion devices are optimized for a high ideal ballooning limit to allow high pressure, which maximizes the fusion power. The power to reach high pressure in L mode normally exceeds the threshold power to obtain H-mode confinement.

geometry by varying the magnetic field strength while keeping ρ_*, ν_C and q fixed, the plasma density, temperature and current needed to be scaled as $n \propto B^4$, $T \propto B^2$ and $I \propto B$. This results in β varying as B^4 and the Bohm diffusion coefficient varying as B. Hence, relatively small variations of B and I are required. The initial set of β scaling experiments on DIII-D [74–76] and JET [77] varied β by about a factor of 2 using a two-point scan. Both the JET and the DIII-D experiments used co-NBI for plasma heating, but since the toroidal Mach numbers were fairly well matched, the effects of rotational shear suppression of turbulence should not have affected the measured β scaling result. For DIII-D, $\beta_{th,N}$ was varied from 0.8 to 1.7, and over this range the thermal energy confinement time had almost no β dependence, $B\tau_{th} \propto \beta^{0.03\pm0.11}$. In regard to local heat transport, the ion thermal diffusivity had a strong decrease with β, $\chi_i \propto \chi_B \beta^{-1.1\pm0.06}$, while the electron thermal diffusivity had a much weaker dependence, $\chi_e \propto \chi_B \beta^{0.1\pm0.04}$. The difference between the observed β scalings of the ion and the electron thermal transport is consistent with gyrokinetic transport calculations showing that the decrease in the electrostatic component of the transport with increasing β is stronger in the ion channel while the electron channel is more sensitive to the increase in the electromagnetic component of the transport with increasing β [78]. These calculations neglected the effects of β on the equilibrium, which are expected to reduce transport with increasing β. Similar experiments in H-mode plasmas on JET scanned $\beta_{th,N}$ from 1.2 to 2.2 and also found the thermal energy confinement time to have a small dependence on β, $B\tau_{th} \propto \beta^{-0.05}$. No uncertainties were quoted, and only the global scaling was given for this scan. These experimental results confirmed an earlier analysis of the JET H-mode database that found no apparent variation of the normalized energy confinement time with β, although a weak variation could not be ruled out [79, 80].

These initial β scaling experiments in H-mode plasmas on JET and DIII-D had several weaknesses that motivated additional experiments. One issue was that the large β variation pushed the end points of the scan towards extreme regimes. As a result, the measured β dependence for a two-point scan may not have given a result indicative of the β dependence for intermediate points. Therefore, to ensure that the apparent β scaling was not corrupted by having confinement for the high β case degraded by MHD activity, a more detailed scan at high β values was needed. Another issue was that each pair of discharges from the initial JET and DIII-D β scans were comprised one Type III and one Type I ELMing H-mode plasma, meaning that β and ELM type were correlated. This could affect the result if a lower confinement in Type III ELMing H-mode plasmas caused a β scan across ELM types to not observe a β dependence that was present for Type I ELMing H-mode plasmas. A related edge effect is the variation in the height of the H-mode pedestal. On DIII-D, the edge pedestal β value was not fixed but rather varied in tandem with the core β value (as desired since the plasma profile scale lengths should remain constant according to Connor–Taylor invariance). However, it was not clear if this was just a coincidence owing to the change in ELM type. Since the H-mode pedestal height plays an important role in the overall plasma confinement, the initial β scaling experiments on DIII-D and JET could not be certain whether the measured weak dependence would be different in plasmas with Type I ELMs exclusively.

To address the above concerns regarding the two-point β scans on DIII-D and JET, new experiments were done on both tokamaks to cover a wider range of β_N with more points in each scan as well as a significant β scan with Type I ELMs only. A multi-point scan would show if the β scaling near either the low β or high β endpoints was not representative of the whole. On DIII-D, a four-point scan was executed with β_N varying from 1.0 to 2.8, corresponding to β being varied from 30% to 85% of the ideal ballooning mode stability limit [81]. The radial profiles of the thermal component of β are shown in figure 14 for this DIII-D experiment. The β_{th} value of the H-mode edge pedestal did not remain fixed, but

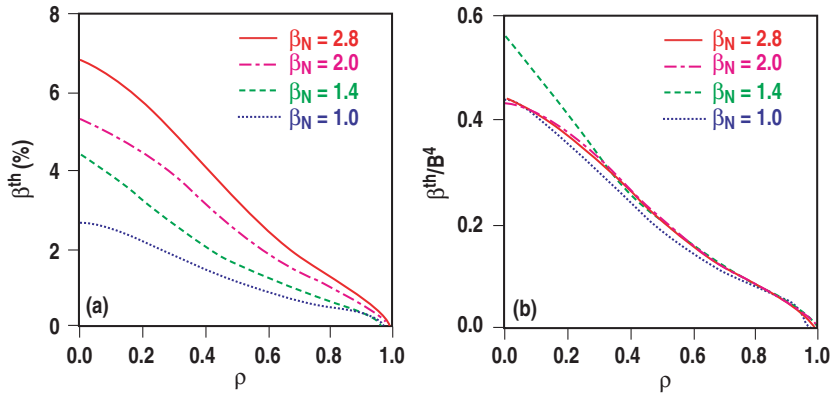

Figure 14. (*a*) Radial profiles of the thermal β from a DIII-D H-mode β scan. (*b*) The same profiles scaled by B^4 to illustrate the similarity of the profile shapes from the core to the pedestal region. Reprinted with permission from [81], Copyright 2004, American Institute of Physics.

varied in concert with the core β_{th} value, even in the presence of Type I ELMs. Therefore, the height of the H-mode pedestal does not saturate due to stability limits along this trajectory in dimensionless parameters. Figure 15 shows that the dimensionless parameters other than β were kept nearly constant during this H-mode β scan. The lowest β case had Type III ELMs while the three higher β cases all had Type I ELMs. The normalized thermal confinement times had a very weak dependence on β over the entire scan, $B\tau_{th} \propto \beta^{-0.01\pm0.09}$. Figure 16 shows the radial profiles of the effective (or one-fluid) thermal diffusivities normalized to the Bohm diffusion coefficient χ_{eff}/χ_B (or more simply χ_{eff}/B) for the four-point β scan, showing that the normalized χ_{eff} profiles were essentially the same for the three higher β discharges with Type I ELMs. While the lowest β discharge with Type III ELMs had a systematically larger value of normalized χ_{eff} than the other cases, it was still within the indicated uncertainties. On JET, recent experiments using three β scans with different values of ρ_* and q showed that the weak β scaling of heat transport was a generic feature of JET plasmas [82]. For a three-point scan that extended from $\beta_N = 0.72$ to $\beta_N = 2.03$, the normalized energy confinement time changed little, $B\tau_{th} \propto \beta^{-0.01\pm0.11}$, and also confirmed that the H-mode results were independent of the type of ELM.

Summarizing the studies in ELMing H-mode plasmas, the six different published β scans from DIII-D and JET consistently found a near zero dependence of the normalized energy confinement time on β. This is shown in figure 17, where the results from each H-mode β scan on DIII-D and JET has been fit to the form $B\tau_{th} \propto \beta^{-\alpha_\beta}$, where α_β is taken to be a constant for each scan. (Although useful for summarizing the experimental results, this form is somewhat questionable for β scaling, since only the case $\alpha_\beta = 0$ can recover the correct electrostatic limit as $\beta \to 0$). Figure 17 shows that the measured β scaling exponents are tightly clustered around zero for all of the H-mode plasmas studied to date, and is much weaker than the inferred β scaling from the IPB98$(y, 2)$ relation [20]. This negligible β dependence of heat transport supports the conclusion that the dominant transport mechanisms are primarily electrostatic, such as $\boldsymbol{E} \times \boldsymbol{B}$ transport, rather than primarily electromagnetic mechanisms such as magnetic flutter transport or magnetic island transport. As β was increased in a given scan, the edge pedestal β rose along with the β of the core, despite the transition to a different ELM type and a change in the ELM frequency. Hence, for the range of β covered, the height of the edge pedestal does not show any saturation during a β scan. Considering only the portion of the β scans confined to the Type I ELM regime, a two-point scan on JET found an

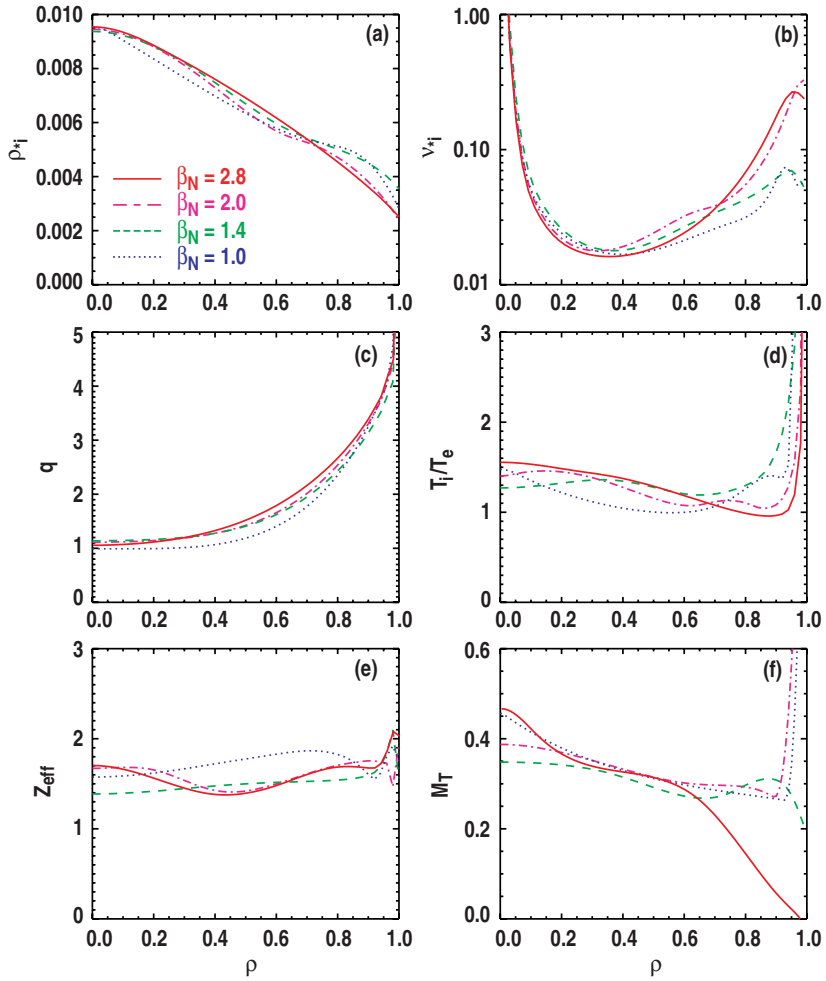

Figure 15. Radial profiles of (*a*) relative ion gyroradius, (*b*) ion collisionality, (*c*) safety factor, (*d*) ratio of ion to electron temperature, (*e*) effective ion charge and (*f*) toroidal Mach number from a DIII-D H-mode β scan. Reprinted with permission from [81], Copyright 2004, American Institute of Physics.

increase in confinement time with β ($\alpha_\beta = -0.43 \pm 0.95$), but with significant uncertainties. On DIII-D, a three-point scan in the Type I ELM regime showed the opposite tendency, with $\alpha_\beta = 0.10 \pm 0.10$, indicating a slight increase in transport with β. Therefore, the experimental results from the Type I ELM regime on JET and DIII-D are also consistent with heat transport being independent of β.

The β scaling of particle transport has also been studied. The normalized helium particle transport was found to decrease with increasing β on DIII-D in H-mode plasmas [81]. The impurity helium particle diffusivities were determined from the measured evolution of the helium density profile subsequent to a small helium gas puff. For a two-point scan over the range $1.0 \leqslant \beta_N \leqslant 2.0$, the helium particle transport inside $\rho = 0.4$ was measured to have a strong decrease with β that scaled like $D_{He}/\chi_B \propto \beta^{-1.67\pm0.16}$. The inward convective velocity for the helium ions also decreased with increasing β, but not as much as the diffusivity. Therefore, the helium density profile would tend to become more peaked with increasing

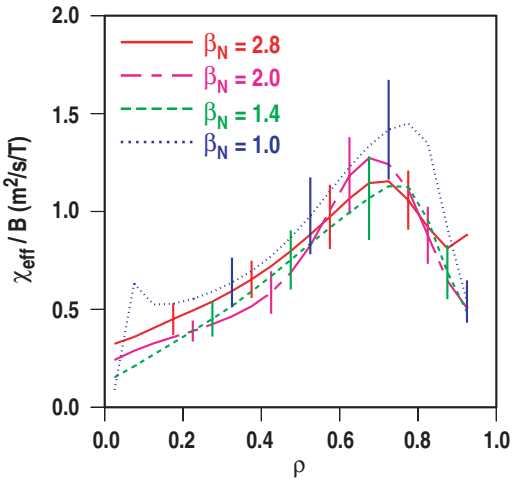

Figure 16. Radial profiles of the effective thermal diffusivity, normalized to the scaling of the Bohm diffusion coefficient, for the DIII-D H-mode β scan shown in figures 14 and 15. Reprinted with permission from [81], Copyright 2004, American Institute of Physics.

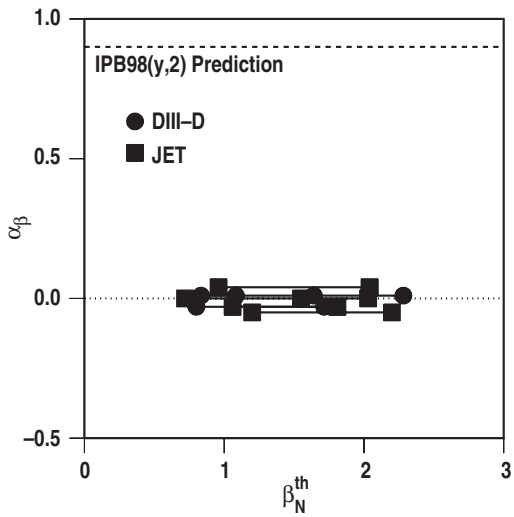

Figure 17. Scaling of thermal energy confinement with β for H-mode experiments. The machine from which the data are taken is denoted by the symbols in the legend. The symbols show the β value of the experimental points and the extent of the scans. Recall that the sign convention chosen implies a reduction in confinement for positive values of α_β.

β assuming a fixed helium source. Since fusion power in deuterium–tritium plasmas (and therefore the helium source) increases faster than linear with β (at fixed B), this scaling is of some concern for helium ash accumulation in burning plasmas. However, the ELMs in this two-point β scan change from Type III (at the lower β) to Type I (at the higher β), which introduces a systematic difference with unknown effects.

The measured β dependence of heat transport in L-mode experiments has not yielded a picture as consistent as in H-mode plasmas, but most of the results still indicate a weak overall

dependence. The first L-mode β scaling experiment was on TFTR [83], where a five-point scan varied $\beta_{\mathrm{th,N}}$ from 0.20 to 0.96. From the end points of the scan, it was concluded that a strong decrease in confinement with β was observed, $B\tau \propto \beta^{-0.5}$. However, it was noted that the apparent β degradation of transport was confined to the lower half of the β scan, and that the upper half of the β scan actually witnessed little β dependence of heat transport. This reported behavior on TFTR seems odd since it is in the wrong direction to reconcile with the electrostatic limit at zero β. The apparent strong β scaling of the energy confinement time at low β may have been actually due to the poor match in the dimensionless parameters, as seen in figure 4 of [83]. In particular, the match between the ohmic discharge and the beam-heated discharges was not good, especially in $T_{\mathrm{i}}/T_{\mathrm{e}}$. The dimensionless parameters were best matched for the upper half of the β scan on TFTR ($0.51 \leqslant \beta_{\mathrm{N}} \leqslant 0.96$). By itself, this scan gave a measured scaling like $B\tau \propto \beta^{-0.27}$, which was decidedly weaker than for the end points of the scan.

Experiments on DIII-D measured a β scaling of heat transport in L-mode plasmas that was close to zero [74–76], and thus was a weaker dependence than reported for TFTR. Comparing ohmically and rf heated discharges, the thermal energy confinement time on DIII-D was found to scale like $B\tau \propto \beta^{-0.05\pm0.10}$ over the range $0.26 \leqslant \beta_{\mathrm{N}} \leqslant 0.49$. The DIII-D experiments were the only ones in this area to report results from a local heat transport analysis, which showed that both the ion and electron thermal diffusivities had nearly zero β dependence. Further investigations of L-mode plasmas on DIII-D showed that the weak β scaling was not related to the specific auxiliary heating method or the fact that the rf heated plasmas were limited to low β values. Experiments with NBI heating, utilizing an inside wall limiter discharge to maintain an L-mode edge up to $\beta_{\mathrm{th,N}} = 1.53$, also found a weaker β scaling of energy confinement than reported for TFTR (figure 10 from [76]).

Two other β scaling experiments on toroidal machines bear mentioning. These took a different experimental approach by varying several dimensionless parameters simultaneously. On the ATF torsatron, a weak increase of the energy confinement time with β, $B\tau \propto \beta^{0.3}$, was reported for plasmas with an L-mode edge [84]. These experiments modulated β at fixed ν_{C} and fixed magnetic configuration by varying the density in proportion to the ECH power modulation, but ρ_* was also allowed to vary. The modulation period of 0.08 s was long in comparison with the energy and particle confinement times. Since ρ_* was not kept fixed during the β scan, gyroBohm-like scaling of the energy confinement time had to be assumed in order to determine the β scaling, but this assumption was in accord with experimental results on stellarators. It was reported that this β scaling worked equally well for low-density ECH plasmas and high-density NBI plasmas on ATF. The measured β dependence was consistent with previous magnetic configuration scans, where it was found that as the size of the magnetic well region expanded, the confinement improved. It was theoretically predicted that the magnetic well region should broaden with increasing β [85,86], which gives a plausible explanation for the increase in confinement with β observed in the ATF studies. It should also be noted that regression analysis of energy confinement in LHD found almost no dependence on β [87].

Finally, L-mode experiments in limiter plasmas on Tore Supra using rf heating gave a strikingly different result than the other experiments discussed in this section [88,89]. In these Tore Supra experiments, β was varied but not at fixed ν_C; thus, the data were analyzed assuming a weak ν_{C} scaling that was deduced from density scans at fixed β (the ν_{C} scans are discussed more fully in the following section). A regression analysis of this limited scan found a strong decrease in the global energy confinement time with β, $B\tau \propto \beta^{-1.3\pm0.2}$. For ohmically heated plasmas, a strong increase of the energy confinement time with β was reported, the opposite of the L-mode results. From this, it was concluded that the turbulence that causes transport

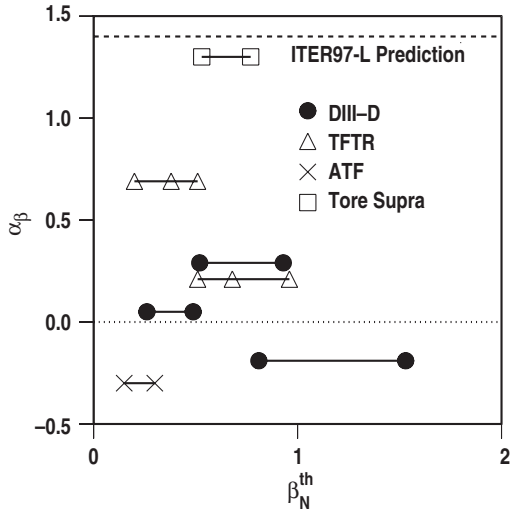

Figure 18. Scaling of thermal energy confinement with β for L-mode experiments. The machine from which the data are taken is denoted by the symbols in the legend. The symbols show the β value of the experimental points and the extent of the scans.

is electromagnetic in nature. The validity of this experiment on Tore Supra is more difficult to assess than for other tokamaks since (a) multiple dimensionless parameters were varied simultaneously, (b) the β scaling results depend upon the ν_C scaling results, which in turn depend upon the ρ_* scaling results and (c) no profile matches and very limited information on the plasma parameters were published. Certainly the experimental uncertainties were much higher in this experiment than for the experiments on TFTR and DIII-D.

The β scaling exponents of the thermal energy confinement times (i.e. $B\tau_{th} \propto \beta^{-\alpha_\beta}$) are summarized in figure 18 for L-mode plasmas on the various devices. The upper half of the β scan in TFTR was in good agreement with the weak β dependence of the energy confinement time measured in DIII-D for both rf and NBI heating. The strikingly different result from Tore Supra is evident, and it would be good to repeat this β scaling experiment using the standard approach to determine whether the turbulence regime on Tore Supra is more dominated by electromagnetic fluctuations than for other tokamaks. Figure 18 shows that the measured dependence of the energy confinement time on ATF increased more with β than in the tokamak experiments. This may be due to the different magnetic configuration of ATF. All of the measured β scalings are weaker than the inferred β scaling from the ITER97-L relation [21]. While the β scaling exponents for L-mode plasmas shown in figure 18 have a larger scatter than for H-mode plasmas (figure 17), most of the β scaling exponents are confined to the range $-0.3 \leqslant \alpha_\beta \leqslant 0.3$. This weak β dependence supports theories of turbulence transport where magnetic flutter transport is not dominant over fluctuating $\boldsymbol{E} \times \boldsymbol{B}$ transport.

3.5. Dependence on collisionality

Conventional drift wave models of turbulent transport can be classified by their predicted dependence on collisionality ν_* [11, 79], which is the collision frequency normalized to the bounce time of a thermal particle trapped in a magnetic well. The term collisionless refers to the regime where particles oscillate in the well many times on average before experiencing a

significant collision. In the collisional regime, the particles do not sample the full magnetic geometry on average before a collision. The transition region between these two limits is called the plateau regime. The collisionless ion temperature gradient (ITG) mode and collisionless trapped electron mode (TEM) are expected to exhibit little dependence of the thermal diffusivity on collisionality [67]. However, recent nonlinear simulations show that turbulent transport can increase with ion-ion collision frequency, even in regimes where the dynamics of the underlying instabilities are collisionless, because of the neoclassical damping of zonal flows that regulate the turbulence [90, 91]. For the (edge) resistive ballooning mode, the thermal diffusivity is expected to increase with collisionality [92], while the thermal diffusivities for the dissipative trapped-electron and dissipative trapped-ion modes (TIM) are expected to decrease with increasing collisionality [11]. Thus, determining the collisionality scaling of heat transport experimentally should discriminate among various proposed theories of turbulent transport from drift waves.

Since the safety factor is to be held fixed during the scans of the collisionality, it is not possible to distinguish between the scaling of heat transport with different normalizations of the collision frequency, such as the collision frequency normalized to the thermal transit time ($\nu_C \propto na/T^2$) used in the previous sections or the collision frequency normalized to the bounce frequency ($\nu_* \propto naq/T^2$). The quantity ν_C was identified as the scaling parameter to be used, primarily because it is more practical to match and it maintains orthogonality of the dimensionless parameters. The quantity ν_* is important theoretically in that it distinguishes where trapped particles play a role, as discussed above. Since the two quantities are inseparable with respect to the scans discussed here, the results will be given in terms of ν_*. The term 'collisionality' will be used to describe either normalized collision frequency, although it technically refers only to ν_*.

To scan ν_* at fixed geometry by varying the magnetic field strength while keeping ρ_*, β and q fixed, the plasma density, temperature and current needed to be scaled as $n \propto B^0$, $T \propto B^2$ and $I \propto B$. This results in the collisionality varying as $\nu_* \propto B^{-4}$ and the Bohm diffusion coefficient varying as $\chi_B \propto B$. Since a large range in heating power is generally not needed to keep ρ_* and β constant, it is relatively straightforward to scan ν_* by an order of magnitude. This large scan in ν_* reduces the sensitivity of the measured confinement scaling to imperfections in keeping the other dimensionless parameters fixed. Since the ratio of the plasma density to the Greenwald density limit [29, 93] varies during a ν_* scan like $n/n_{GW} \propto B^{-1}$, it is clear that this ratio cannot be kept fixed during a ν_* scan, unless plasmas of different physical size are compared. The collisionality could also be scanned by varying Z_{eff} at fixed electron density and temperature, but this method is not used generally. Variation in Z_{eff} would also change the primary ion dilution, which is another dimensionless parameter that can influence drift wave stability [94–96].

For L-mode plasmas in the banana regime ($\nu_* < 1$), experiments on TFTR found the power flow normalized to Bohm diffusion to be independent of collisionality [23, 83]. A sequence of four discharges with primarily NBI heating varied B by a factor of 2.5 while attempting to hold the other dimensionless parameters constant. This should have changed the collisionality by a factor of 38, but in reality ν_* spanned less than a factor of 5 owing to systematic variations in ρ_*, β, T_i/T_e and Z_{eff}. As a result, a range of ν_* scalings can be inferred from the TFTR experiment depending upon the assumed scaling of heat transport on the other dimensionless quantities. If the radial power flows were normalized to electrostatic Bohm-like transport, then the TFTR results were best fit by $\chi \propto \chi_B \nu_*^0$, although error bars do not exclude a weak exponent of ν_* within ± 0.25. With the same assumption of Bohm scaling, the thermal energy confinement time was best fit by $B\tau_{th} \propto \rho_*^{-2}\nu_*^{-0.1}$. This assumes that the factor of 2 variation in Z_{eff} had no effect on heat transport other than through the ν_* dependence. Making

different assumptions about the ρ_* and $Z_{\rm eff}$ scalings of heat transport can alter the exponent of ν_* by ≈0.2.

In similar L-mode experiments on DIII-D, essentially no collisionality dependence of heat transport was measured [74, 75, 97]. These experiments with combined NBI and fast wave heating scanned ν_* by up to a factor of 8 in two steps with the other dimensionless parameters (ρ_*, β, $T_{\rm i}/T_{\rm e}$, q, ...) held constant, although the effective ion charge varied from $Z_{\rm eff} \approx 1.3$ to $Z_{\rm eff} \approx 1.9$. A local transport analysis found that the ν_* scaling of the effective thermal diffusivity was weak over the entire range studied, $\chi_{\rm eff} \propto \chi_{\rm B}\nu_*^{-0.08\pm0.10}$, and did not vary with radius. The ν_* dependences of the ion and electron fluids were the same to within the experimental uncertainties. The thermal confinement time was also almost independent of collisionality, $B\tau_{\rm th} \propto \nu_*^{0.02\pm0.03}$. With such a large scan in ν_* (factor of 8), imperfect matches of the other dimensionless parameters will not skew the inferred exponent of ν_* by a large amount. The systematic error due to the 50% mismatch in $Z_{\rm eff}$ is estimated here to change the ν_* exponent by no more than 0.1. The lack of ν_* scaling, even in the collisional plasma edge, indicates that the dissipative trapped-particle modes and resistive ballooning mode were not significant at any radii for these L-mode plasmas.

The collisionality scaling of electron heat transport measured on Tore Supra was similar to the TFTR and DIII-D results [88, 89]. Using central electron heating with fast waves and lower hybrid waves, ν_* and ρ_* were scanned simultaneously in L-mode plasmas at fixed β and q. The inferred ν_* scaling of $\chi_{\rm e}$ was only slightly dependent on what is taken for the ρ_* scaling, with the results from a local transport analysis falling within the range $\chi_{\rm e} \propto \chi_{\rm B}\nu_*^{0.3\pm0.2}$. The scaling of the energy confinement time with collisionality was consistent with the local transport analysis, $\tau/\tau_{\rm B} \propto \nu_*^{-0.1\pm0.2}$, where a ρ_* scaling that was intermediate between Bohm and gyroBohm scaling was also inferred. A much stronger ν_* scaling was reported for ohmic plasmas.

A weak collisionality scaling of the energy confinement time was also measured on the ATF torsatron for plasmas with an L-mode edge [84]. These experiments modulated ν_* at fixed β by varying the density out of phase with the ECH power modulation. However, ρ_* was also allowed to vary. The modulation period of 0.08 s was long in comparison with the energy and particle confinement times. Scaling of the energy confinement time was assumed to be gyroBohm (in accord with experimental results on stellarators) to factor out the ρ_* variation, resulting in a collisionality scaling of the energy confinement time as $\tau/\tau_{\rm B} \propto \rho_*^{-1}\nu_*^{-0.18}$. This ν_* scaling was also reported to be in agreement with the general ATF confinement database, including NBI heated plasmas. It should also be noted that regression analysis of energy confinement in LHD did not find any significant ν_* dependence for an inward shifted configuration that minimized neoclassical transport [87].

For L-mode plasmas approaching the plateau regime, collisionality scans in RTP found a strong decrease in electron heat transport on ν_* [98]. These experiments used central ECH with power deposition inside the $q = 1$ surface, which limited the variation in B to ≈10%. While holding ρ_*, β and q fixed, as shown in figure 19, this limited the ν_* scan to about a factor of 1.5. A local transport analysis found that the (dominant) electron heat transport scaled as $\chi_{\rm e}/\chi_{\rm B} \propto \nu_*^{-0.5\pm0.2}$ in the region $0.35 \leqslant \rho \leqslant 0.65$, as seen in figure 20. A larger factor of 4 scan in ν_* was also studied on RTP by keeping B (and thus the ECH deposition location) fixed and allowing ρ_* to vary slightly (β and q were still held constant). Assuming the scaling of heat transport to be gyroBohm for the electron fluid, the best fit to the electron heat transport gave $\chi_{\rm e}/\chi_{\rm B} \propto \nu_*^{-0.3\pm0.1}$ in the region around the mid-radius. Both of these scans were repeated at different $I_{\rm p}$ and n values with similar results.

Finally, on Alcator C-Mod a strong decrease in the energy confinement time with ν_* was measured in L-mode plasmas in the plateau regime [99]. Comparing plasmas with fast wave

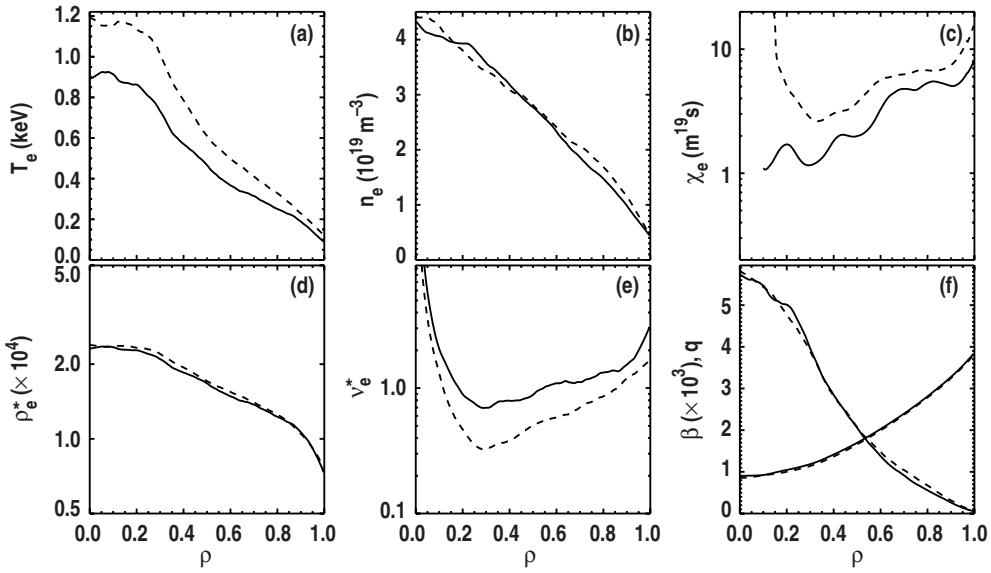

Figure 19. Profiles of the (*a*) electron temperature, (*b*) electron density, (*c*) electron heat diffusivity, (*d*) normalized electron gyroradius, (*e*) normalized electron collision frequency and (*f*) β and safety factor for an L-mode collisionality scan for the RTP tokamak. Reprinted from [98] by permission.

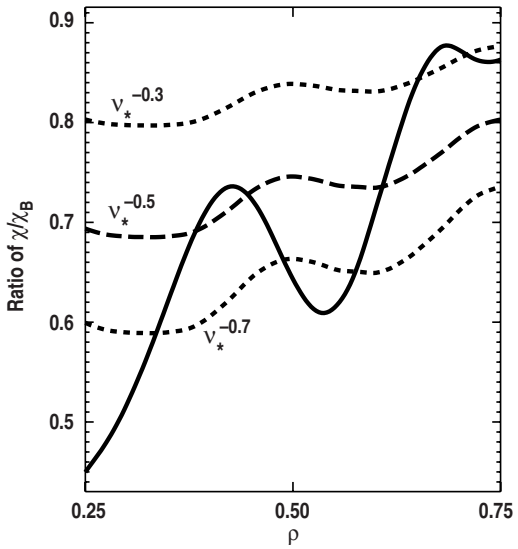

Figure 20. Ratio of the heat diffusivities normalized to χ_B for the L-mode ν_* scan from the RTP tokamak. The expected ratio for three values of the scaling exponent are shown. Reprinted from [98] by permission.

and ohmic heating, ν_* was varied by more than an order of magnitude at constant ρ_*, β and q. Regression analysis of a small set of discharges yielded a collisionality scaling of the energy confinement time as $B\tau \propto \nu_*^{-0.4\pm0.1}$. An unintended factor of 1.5 change in Z_{eff} occurred during the scan in ν_*. This systematic variation could alter the exponent of ν_* by no more than

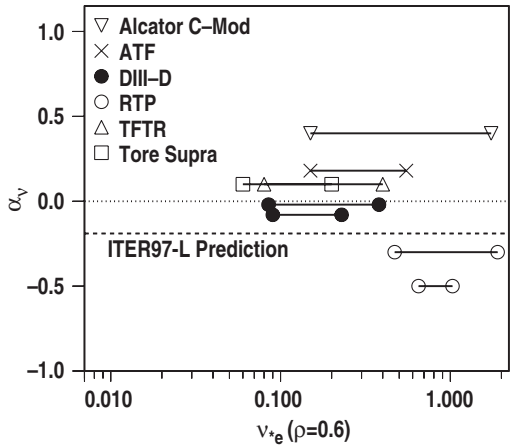

Figure 21. Scaling of energy confinement with ν_* for L-mode experiments. The machine from which the data are taken is denoted by the symbols in the legend. The symbols show the collisionality at the experimental points and the extent of the scans.

0.1, which is comparable to the uncertainty arising from the measurements. A local transport analysis of the best-matched pair found a ν_* scaling of the effective thermal diffusivity that was consistent with the global scaling, $\chi_{\rm eff} \propto \chi_{\rm B}\nu_*^{0.5\pm0.4}$. The ν_* dependences of the ion and electron fluids were the same to within the experimental uncertainties.

Summarizing the studies in L-mode plasmas, the normalized energy confinement time was found to have only a weak collisionality scaling in the banana regime on both tokamaks and stellarators. This is shown in figure 21, where the results from each L-mode ν_* scan have been fit to the form $B\tau_{\rm th} \propto \nu_*^{-\alpha_\nu}$, where α_ν is taken to be a constant for each scan. (Since energy confinement times were not reported for RTP, the scaling of the electron thermal diffusivity is plotted instead.) The collisionality scalings measured on TFTR, DIII-D, Tore Supra and ATF for $\nu_* \ll 1$ are similar and lie in the narrow range $-0.1 \leqslant \alpha_\nu \leqslant 0.2$. These measured ν_* scalings are weaker than, or have the opposite sign of, the inferred dependence of the ITER97-L scaling relation for L-mode plasmas. The absence of a ν_* dependence of heat transport is expected for the collisionless ITG mode and collisionless TEM. A less-consistent collisionality scaling was measured in plasmas approaching the plateau regime ($\nu_* \sim 1$) on Alcator C-Mod and RTP, where α_ν varied between -0.5 and 0.4. While it is of some concern that experiments on Alcator C-Mod [99] and RTP [98] using essentially the same experimental method found the opposite ν_* scalings, the fact that $T_{\rm e} \approx T_{\rm i}$ in the former experiments and $T_{\rm e} \gg T_{\rm i}$ in the latter may provide an important clue to resolving this discrepancy.

For H-mode plasmas, experiments on various tokamaks found a moderate increase in heat transport with collisionality that increased in strength with larger ν_*. The lowest collisionality H-mode plasmas with Type I ELMs were studied in JET, with ν_* close to the expected ITER value ($\nu_*/\nu_*^{\rm ITER} = 1.3$–$3.4$) [77]. For NBI heated plasmas, the normalized thermal energy confinement time was observed to decrease weakly with increasing ν_* at fixed ρ_*, β and q. A two-point scan measured a dependence like $B\tau_{\rm th} \propto \nu_*^{-0.27}$. More recent experiments on JET measured the ν_* scaling of energy and particle transport in more collisional H-mode plasmas [44, 55, 56]. A four-point scan found a slightly stronger collisionality dependence to the normalized thermal energy confinement time $B\tau_{\rm th} \propto \nu_*^{-0.35\pm0.04}$. Using trace tritium injection, the local particle transport was measured by following the 14 MeV fusion neutron evolution with adequate space and time resolution. In a factor of 1.8 scan in ν_*, the local

particle transport was found to have a scaling like $D/D_{\rm Bohm} \propto \nu_*^{-0.51\pm0.17}$ in the inner part of the plasma and $D/D_{\rm Bohm} \propto \nu_*^{-0.40\pm0.15}$ in the outer region.

In DIII-D, a factor of 8 scan in ν_* with the other dimensionless parameters held constant measured a similar increase in heat transport with collisionality in H-mode plasmas [74,75,97]. Interestingly, this ν_* scaling became stronger as the plasma became more collisional in these NBI heated plasmas, with the ν_*dependence of the normalized thermal energy confinement time changing from $B\tau_{\rm th} \propto \nu_*^{-0.35\pm0.04}$ at the lower collisionality end to $B\tau_{\rm th} \propto \nu_*^{-0.56\pm0.06}$ at the higher collisionality end. A local transport analysis confirmed that the effective thermal diffusivity had a moderate ν_* dependence, $\chi_{\rm eff}/\chi_{\rm B} \propto \nu_*^{0.34\pm0.10}$, over the factor of 8 scan. A two-fluid transport analysis was not possible for these H-mode plasmas owing to the strong coupling between the ion and electron fluids. A portion of the measured ν_* scaling of heat transport could be attributed to neoclassical transport, especially in the regions of the plasma where the measured diffusivity approached the ion neoclassical value. It is interesting to note that cross-machine studies between H-mode plasmas in DIII-D and JET that varied ν_* while keeping fixed $n/n_{\rm GW}$ found the same ν_* scaling of the normalized thermal energy confinement time as was found for single machine studies in which $n/n_{\rm GW}$ varied along with ν_* [30]. This result shows that $n/n_{\rm GW}$ has no direct influence on heat transport.

In JT-60U, a similar dependence as JET and DIII-D of the confinement time on the normalized collision frequency was measured in ELMing H-mode plasmas [47]. In high triangularity plasmas, ν_* was scanned by a factor of 1.8 in two steps at constant β in NBI heated plasmas. The gyroradius was not kept constant but varied systematically by ≈10% during the ν_* scan. Utilizing the ρ_* scaling of energy confinement measured in similar high triangularity plasmas in JT-60U, the normalized thermal energy confinement time was found to have a scaling like $\tau_{\rm th}/\tau_{\rm B} \propto \nu_*^{-0.32}$. The systematic error due to the mismatch in ρ_* changes the exponent of ν_* by only 0.06 as the ρ_* scaling is varied from $\alpha_\rho = 0.5$ to $\alpha_\rho = 1.0$. Although a local heat transport analysis was not reported, the electron and ion channels appear to have nearly the same ν_* dependences. The electron and ion heat flows were well separated because the equipartition energy flow was much smaller than the conductive heat flow.

Experiments using ECH in COMPASS-D found a weak dependence of the H-mode confinement time on collisionality, with a value close to the results from NBI heating in larger tokamaks [100,101]. The volume-averaged ν_* was varied by a factor of 5 by comparing ohmically heated and ECH ELMing H-mode plasmas, although the match in q, ρ_* and β was not exact owing to the proximity of the L–H threshold and the uncontrolled heating power in ohmic plasmas. The normalized energy confinement time was measured to decrease weakly with increasing ν_*, $\tau/\tau_{\rm B} \propto \langle\nu_*\rangle^{-0.2}$. The value of the exponent of ν_* could change by 0.1 depending upon the assumed scalings of confinement with the other dimensionless parameters.

The highest collisionality H-mode plasmas were studied in Alcator C-Mod, where the heat transport was found to have a strong dependence on the normalized collision frequency [46,99]. These plasmas with ICRH and $T_{\rm i} \sim T_{\rm e}$ did not have Type I ELMs but rather were in the EDA regime. For a factor of 5 scan in ν_*, the energy confinement time scaled as $B\tau \propto \nu_*^{-1.0\pm0.2}$. A local transport analysis found that the effective thermal diffusivity had the same dependence, $\chi_{\rm eff}/\chi_{\rm B} \propto \nu_*^{1.0\pm0.4}$. However, somewhat weaker ν_* dependences can be inferred by considering the imperfections in keeping the other dimensionless parameters fixed during the ν_* scan (evident since ν_* should have changed by a factor of 16 in an ideal experiment). For example, correcting for the ρ_* mismatch gives a scaling like $B\tau \propto \rho^{-3}\nu_*^{-0.8}$. Correcting for mismatches in $Z_{\rm eff}$ and β can further reduce the dependence to $B\tau \propto \nu_*^{-0.5}$, which is consistent with the ν_* scaling deduced from a C-Mod H-mode dataset. These systematic errors in matching probably dominate the uncertainties, so results in the range $B\tau \propto \nu_*^{-0.75\pm0.25}$ can all be in agreement with the C-Mod measurements.

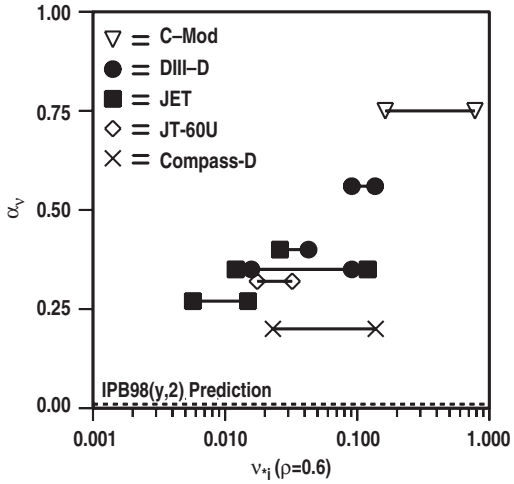

Figure 22. Scaling of energy confinement with ν_* for H-mode experiments. The machine from which the data are taken is denoted by the symbols in the legend. The symbols show the collisionality at the experimental points and the extent of the scans. Lines with different symbols indicate a coordinated scan between machine. The Alcator C-Mod and COMPASS-D data are plotted against volume-averaged collisionality rather than the local value at $\rho = 0.6$.

Summarizing ν_* scans in H-mode plasmas, the normalized energy confinement decreases with increasing ν_*, especially in high collisionality plasmas. Figure 22 shows the results of fitting the ν_* scan from each H-mode experiment to the form $B\tau_{\rm th} \propto \nu_*^{-\alpha_\nu}$. Every tokamak measured decreasing confinement with ν_* with a much stronger decrease than that inferred from the ν_* scaling in the IPB98$(y, 2)$ scaling relation. Figure 22 also shows that the measured value of α_ν increased as the collisionality increased (the exception being COMPASS-D). The measured ν_* scalings for H-mode plasmas fall between $\alpha_\nu = 0$, the dependence expected for collisionless ITG mode and collisionless TEM, and $\alpha_\nu = 1$, the dependence predicted for the resistive ballooning mode. However, the resistive ballooning mode should be applicable only in the region close to the plasma boundary. The reduction in transport with increasing collisionality predicted for the dissipative TEM and dissipative TIM was not observed in these experiments. The decrease in confinement with increasing ν_* in H-mode plasmas may be possibly explained by the collisional damping of the zonal flows that regulate turbulence by reducing the radial correlation length of the microturbulence [102]. The zonal flows are damped by collisions, so increased collisionality should correlate with increased heat transport, as observed in recent gyrokinetic simulations [90]. In this picture, the stronger ν_* scaling for H-mode, compared with L-mode, plasmas could be a consequence of H-mode plasmas having temperature gradients that are closer to marginal stability. Another possible explanation of the trend with increasing collisionality is the strong collisionality dependence of neoclassical transport (the diffusivity is roughly linear in ν_*) being manifest in H-mode experiments, where the measured diffusivity might be near the ion neoclassical value.

3.6. Dependence on safety factor and elongation

Determination of the scaling of heat transport with safety factor (q) and elongation (κ) experimentally helps to validate theory-based models of turbulent transport. The q and κ dependences need to be considered together, because changing the plasma cross-section usually

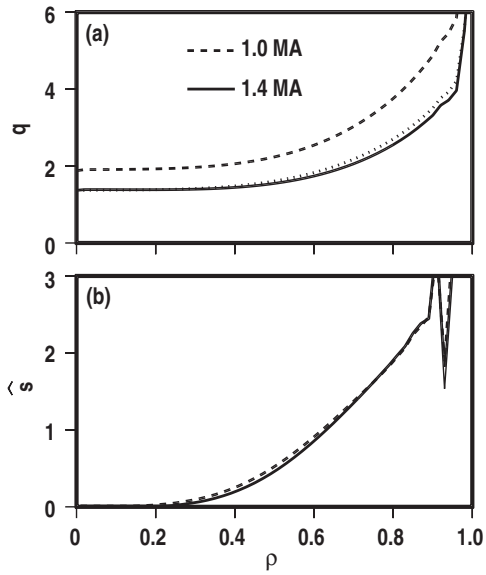

Figure 23. Radial profiles of (*a*) safety factor and (*b*) magnetic shear for the H-mode q scan from the DIII-D tokamak. The dotted line in (*a*) represents the q profile from the 1.0 MA profile scale to 1.4 MA. Reprinted with permission from [25], Copyright 1998, American Institute of Physics.

alters the q profile. Drift wave models of turbulent transport generally predict a q dependence in the range $\chi/\chi_B \propto q^{1-2}$ [73]. For example, the ITG mode and TEM exhibit an approximately linear increase in transport with q, owing to a downshift of the maximum contribution to the transport to longer perpendicular wavelengths as well as a change in the turbulence growth rates [67]. Models of the resistive ballooning mode, which is predicted to be important only in the plasma edge, have a robust q scaling like $\chi/\chi_B \propto q^2$ [103]. The dependence of heat transport on the magnetic shear is expected to be more complicated and non-monotonic. Nonlinear simulations show that transport has a relative maximum for values of magnetic shear around $\hat{s} \sim 0.5$, shifting to larger $\hat{s}$ with finite Shafranov shift. Transport is predicted to decrease as the magnetic shear either increases (strong positive shear) or decreases (weak or negative shear) away from this value [104].

Experiments in DIII-D have determined separately the dependence of the heat transport on safety factor and magnetic shear. A strong scaling of heat transport with safety factor at fixed elongation was measured in H-mode plasmas in DIII-D [25, 105]. As seen in figure 23, q was varied by a factor of 1.4 while holding $\hat{s}$ fixed; the plasma density and temperature were also held fixed which kept ρ_*, β, and ν_C fixed. (Note that the use of ν_C rather than ν_* as the normalized collision frequency greatly simplifies the execution of a q-scaling experiment, because ν_C is independent of q.) The energy confinement time was found to vary like $B\tau_{th} \propto q^{-2.42\pm0.31}$. A local transport analysis found a similar strong q dependence of the heat transport across the entire plasma radius, with the effective thermal diffusivity scaling like $\chi_{eff}/\chi_B \propto q^{2.3\pm0.6}$ as shown in figure 24. A two-fluid transport analysis showed that the strong q scaling occurred in both the electron and ion channels, with the electrons having a weaker q dependence than the ions for $\rho > 0.4$. This experiment also studied the dependence of the thermal diffusivities on magnetic shear in H-mode plasmas by varying q_{95} at fixed $q(0)$ with the other dimensionless parameters kept constant. This combined $\hat{s}$ and q scan resulted in a weaker scaling of the energy confinement time with the edge safety factor, $B\tau_{th} \propto q_{95}^{-1.43\pm0.23}$. This

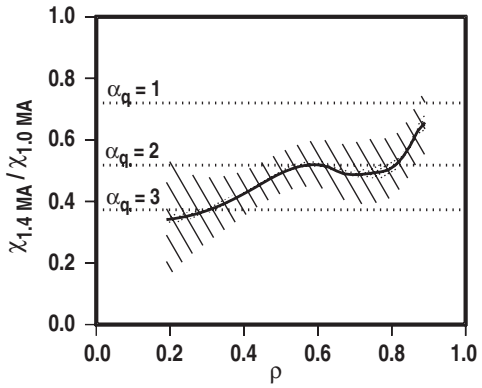

Figure 24. Radio of effective thermal diffusivities for the H-mode q scaling discharges from the DIII-D tokamak. The lined shading indicates the standard deviation of the random error, while the dotted shading indicates the potential effect of systematic error. Reprinted with permission from [25], Copyright 1998, American Institute of Physics.

scaling was attributed to the smaller variation in the volume-averaged q profiles, rather than a decrease in transport with $\hat{s}$. In fact, after correcting for the q scaling of heat transport, a local transport analysis found that the effective thermal diffusivity increased with $\hat{s}$ in the (central) low shear region of the plasma, as expected in the weak and negative shear regimes [104].

A significantly weaker scaling of heat transport with safety factor at fixed elongation was measured in L-mode plasmas in DIII-D [106]. This experiment varied q by a multiplicative factor of 1.8 across its entire profile while keeping $\hat{s}$ and other dimensionless parameters nearly unchanged. A weaker than linear dependence of the energy confinement time on q was measured, $B\tau_{\rm th} \propto q^{-0.8\pm0.1}$. The scaling of the effective thermal diffusivity was nearly the same, $\chi_{\rm eff}/\chi_{\rm B} \propto q^{0.84\pm0.15}$, with the ion fluid having a stronger q dependence than the electron fluid in the outer half of the plasma.

The safety factor can also be varied by changing the plasma cross-section, and elongation scans at both constant q and constant I were studied in DIII-D to resolve any ambiguity between the κ scaling and q scaling of heat transport. The effects of changing the plasma elongation were isolated by keeping the minor radius, as well as the other dimensionless parameters mapped to the minor radius, constant. The initial analysis of these experiments showed strong and opposing dependences of heat transport on q and κ [107]. For H-mode plasmas, a scan in κ from 1.7 to 2.0 at fixed q found that the effective thermal diffusivity was reduced with increasing κ, $\chi_{\rm eff}/\chi_{\rm B} \propto \kappa^{-1.8}$. In strong contrast, the effective thermal diffusivity increased with κ at fixed I, $\chi_{\rm eff}/\chi_{\rm B} \propto \kappa^{1.5}$. However, these apparently disparate results can be reconciled by taking into account the q dependence of heat transport for the fixed I case, resulting in a unified transport scaling like $\chi_{\rm eff}/\chi_{\rm B} \propto q^{2.5}\kappa^{-1.8}$ (no attempt has been made to correct for any $\hat{s}$ dependence). Similar analysis of the dependences of the thermal confinement time yielded the unified scaling $B\tau_{\rm th} \propto q_{95}^{-1.4\pm0.6}\kappa^{2.2\pm0.6}$. (Note that the relation $\tau \propto \kappa a^2/\chi$ should be used when comparing the scaling of the global confinement and the local diffusivity to account approximately for the geometric effect on the confinement time at fixed diffusivity.) Figure 25 shows that the q scaling exponents for H-mode plasmas, found by fitting the thermal energy confinement times to the form $B\tau_{\rm th} \propto q^{-\alpha_q}$, are the same regardless of whether q was varied by changing κ at fixed I or by changing I at fixed κ. This figure also shows that the measured q scaling is much weaker than the inferred q scaling from the IPB98(y, 2) relation.

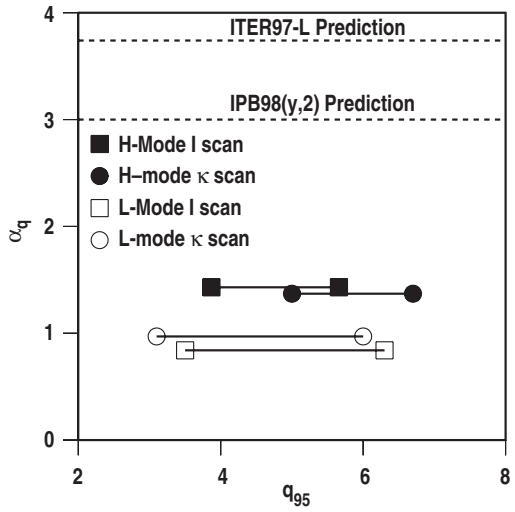

Figure 25. Scaling of the thermal energy confinement with q for L-mode and H-mode experiments in the DIII-D tokamak. The symbols show the type of scan as denoted in the legend and the extent of scans.

In figure 26, it is seen that the experimental κ scaling of the energy confinement time is much weaker than the inferred κ scaling from the IPB98(y, 2) relation.

A similar set of experiments in L-mode plasmas in DIII-D found a weaker κ and q dependence of heat transport than for H-mode plasmas. A scan in κ from 1.2 to 1.8 found that the effective thermal diffusivity decreased with larger κ at fixed q ($\chi_{\rm eff}/\chi_{\rm B} \propto \kappa^{-0.6}$) but increased with larger κ at fixed I ($\chi_{\rm eff}/\chi_{\rm B} \propto \kappa^{1.4}$). The difference between the two cases could be reconciled if the heat transport scaled like $\chi_{\rm eff}/\chi_{\rm B} \propto q^{1.5}\kappa^{-0.6}$. The global scaling of the thermal energy confinement time followed the scaling of the effective thermal diffusivity, offset by an additional factor of κ to account for the increase in cross-section area with elongation, $B\tau_{\rm th} \propto q_{95}^{-1.0\pm0.2}\kappa^{1.6\pm0.2}$. It is noted that the q scaling exponents for L-mode plasmas derived from I scans at fixed κ and the κ scans at fixed I are in agreement, as seen in figure 25. Thus, these experiments indicate that the true influence of cross-section shape can be seen only with κ scans holding q fixed. The κ scaling of the energy confinement time is weaker in L-mode plasmas than in H-mode plasmas, as seen in figure 26. Figures 25 and 26 also show that the measured q and κ scalings of L-mode energy confinement are much weaker than the inferred scalings from the ITER97-L relation.

Turbulence measurements during the L-mode q scan also indicated that the radial correlation lengths of density fluctuations scaled with the ion toroidal gyroradius rather than the ion poloidal gyroradius [108]. The ρ_* scaling experiments discussed previously (section 3.3.4) showed that the radial correlation lengths of density fluctuations scaled approximately linearly with ρ_* [62], but since the toroidal and poloidal ion gyroradii were perfectly correlated, there remained some ambiguity as to the physical process. In the q scaling experiment, measured turbulence characteristics obtained from a heterodyne correlation reflectometer showed that the radial correlation length of density fluctuations was relatively insensitive to the poloidal ion gyroradius, indicating that in the previous ρ_* scaling studies the radial correlation length must have been varying with the toroidal ion gyroradius. This experimental result agreed with numerical simulations by the gyrokinetic particle-in-cell code UCAN [109] that also showed no dependence of the radial correlation length on the poloidal ion gyroradius.

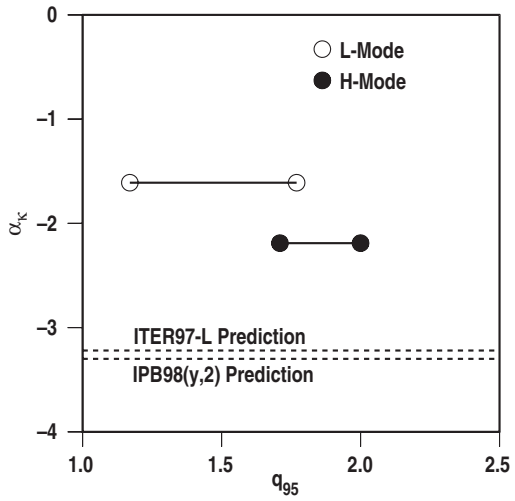

Figure 26. Scaling of the thermal energy confinement with κ for L-mode and H-mode experiments in the DIII-D tokamak. The symbols show the type of scan as denoted in the legend and the extent of scans.

The transport and turbulence measurements in q scaling experiments for H-mode and L-mode plasmas in DIII-D appear to support models of drift wave turbulent transport that are based on gyrokinetic and gyroLandau-fluid simulations. The simulated q scaling of the effective thermal diffusivity by the gyroLandau-fluid GLF23 transport model [67] was in good agreement with the experimental value as long as the effects of $\boldsymbol{E}\times\boldsymbol{B}$ shear and Shafranov shift stabilization were included [106]. For these DIII-D experiments, the effect of $\boldsymbol{E}\times\boldsymbol{B}$ shear was to strengthen the apparent q scaling of heat transport. The weaker q scaling for L-mode, compared with H-mode, could be a consequence of an increase in the critical temperature gradient with lower q, since H-mode plasmas have temperature gradients that are closer to marginal stability. The strong scaling of energy transport with κ observed in H-mode plasmas appear to be more consistent with the *ad hoc* geometry corrections in the Multi-Mode model [110] than with the weaker scalings found in general geometry drift wave calculations [111, 112].

3.7. Dependence on A and Z

The mass dependences of energy and particle transport are of fundamental interest for both developing an understanding of turbulent transport and accurately projecting confinement for future burning plasma experiments. These experiments, such as ITER, will likely use a mixture of deuterium and tritium, while present-day experiments normally use a single isotope of hydrogen or helium. In addition, next-step devices may desire low activation operation in helium or hydrogen plasmas, so it is important to know the effect of the ion charge state on heat transport in addition to the mass dependence. While many experiments have measured the mass scaling of confinement at constant external heating power, mainly using hydrogen or deuterium but occasionally helium-4 as well, relatively few experiments have taken a Connor–Taylor scale invariance approach and held the relevant dimensionless parameters fixed while varying the ion mass normalized to the proton mass A and the ion charge normalized to the proton charge Z.

The clearest measurements of the mass-scaling exponent α_A were made in ELMing H-mode plasmas in JET, where the thermal diffusivities were compared for different isotopes of hydrogen at fixed ρ_{*i}, β and ν_C [113, 114]. This requires that the magnetic field, density and

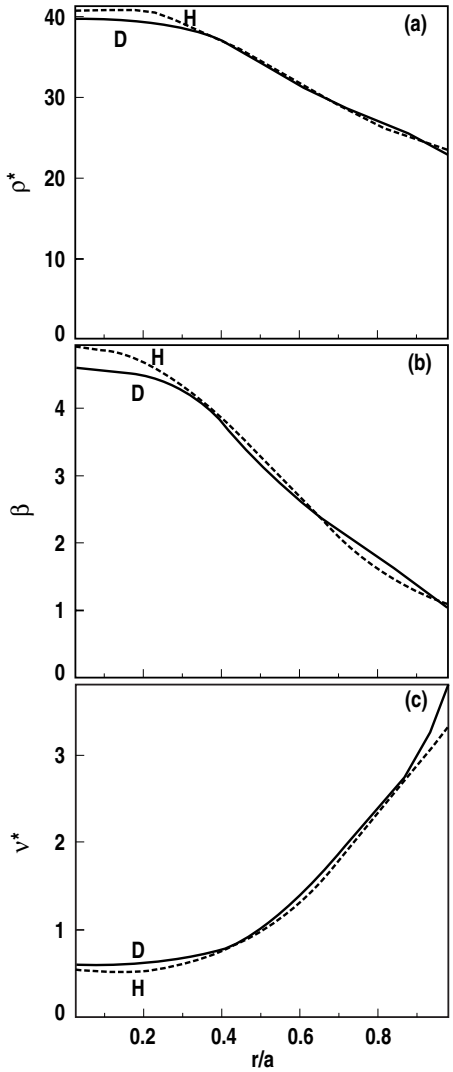

Figure 27. Matches of the dimensionless parameters (*a*) ρ_*, (*b*) β and (*c*) ν_* versus normalized radius for the scan of A in H-mode plasmas from the JET tokamak. Reprinted from [114] by permission of the Institute of Physics.

temperature scale with isotope mass like $B \propto A^{3/4}$, $n \propto A$ and $T \propto A^{1/2}$. To match $\rho_{*\mathrm{i}}$, β, and in the edge region between H and D plasmas, as seen in figure 27, it was found that strong gas puffing was needed for the plasmas with higher isotope mass. The normalized ELM frequencies and normalized thermal energy confinement times were nearly the same for the H and D plasmas, giving a weak mass scaling like $\Omega\tau \propto A^{0.14}$ for the best-matched cases. Figure 28 shows that the radial profiles of the normalized effective thermal diffusivities were also similar for the H and D plasmas; no mass dependence was observed for $\rho > 0.6$, with a maximum dependence like $A\chi_{\mathrm{eff}}/B \propto A^{-0.55\pm0.5}$ around $\rho = 0.45$. This result converts to a weak decrease of the energy confinement time with increasing mass at fixed heating power, which seems consistent with the whole of the JET H-mode database [115].

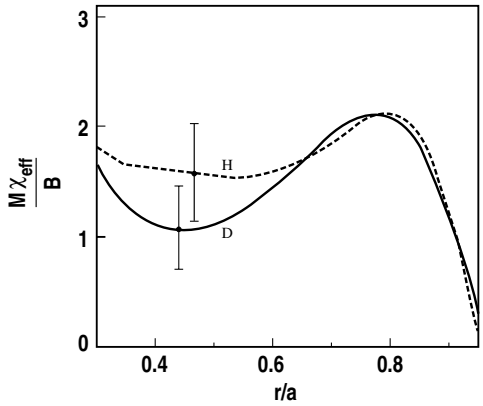

Figure 28. Ratio of the effective heat diffusivities versus normalized radius for the A scan in H-mode plasmas from the JET tokamak. Note that the M in the vertical axis label is the ion mass, not the Mach number as used in this paper. Reprinted from [114] by permission of the Institute of Physics.

Other experiments in ELMing H-mode plasmas in JET compared D and T at the same I, B, n and P, but since the temperatures did not change this was equivalent to a $\rho_{*\mathrm{i}}$ scan at fixed β and ν_{C} [115, 116]. The measured energy confinement time between D and T did not change in this experiment, which implies that heat transport has a mass dependence that cancels out the change in $\rho_{*\mathrm{i}}$ as A was increased. Analysis of pairs of H, D and T plasmas in JET gave a mass scaling of the thermal energy confinement like $\Omega\tau \propto \rho_{*\mathrm{i}}^{-2.88} A^{0.53\pm0.30}$. However, a local transport analysis gave the opposite dependence for the ion thermal diffusivity, $\chi_{\mathrm{i}} \propto \chi_{\mathrm{B}} \rho_{*\mathrm{i}} A^{0.23\pm0.4}$. It was reported that the mass scaling of χ_{eff} was weaker, but still positive, which would be in better agreement with the global confinement dependence.

For plasmas with L-mode edge, the scaling of heat transport with hydrogenic isotope mass was extensively studied in TFTR [117]. These experiments kept the plasma temperature and density fixed, resulting in a combined A and $\rho_{*\mathrm{i}}$ scan at constant β and ν_{C}. However, if Bohm-like scaling prevailed in these L-mode edge plasmas, then the change in $\rho_{*\mathrm{i}}$ with A should not have affected the measured transport dependence. Experimentally in TFTR, the ion thermal diffusivity scaled like $\chi_{\mathrm{i}} \propto A^{-1.8}$ at fixed local parameters in supershots. This was in agreement with scaling results of the energy confinement time at fixed heating power. A comparison of D and D–T plasmas in supershots in TFTR found that the energy confinement time scaled like $\Omega_{\mathrm{ci}}\tau \propto A^{1.0}$ when the NBI power was adjusted to keep the density and temperature profiles fixed [118]. A similar experiment in L-mode plasmas in TFTR found an even stronger scaling of the energy confinement time with ion mass at fixed temperature and density, $\Omega_{\mathrm{ci}}\tau \propto A^{1.2}$ [119].

Summarizing the mass-scaling experiments, strikingly different dependences were measured in L-mode and H-mode plasmas. Figure 29 shows the measured mass-scaling exponent (α_{A}) for the JET and TFTR experiments, defined by $\Omega\tau \propto \rho_{*\mathrm{i}}^{-(2+\alpha_\rho)} A^{-\alpha_{\mathrm{A}}}$. Here α_ρ is chosen to be 1 for H-mode plasmas and 0 for L-mode plasmas. All of the measured mass dependences for H-mode plasmas in JET are weaker than the inferred dependence from the IPB98(y, 2) scaling relation, while for L-mode plasmas in TFTR, the measured mass scaling is stronger than the inferred mass scaling from the ITER97-L scaling relation. The main explanation that has been put forth by the theoretical community to explain the improvement of confinement with mass is the effect of the different isotopes on the shear flow and the resultant modification of the ITG driven turbulence [119]. In this case, the stronger mass

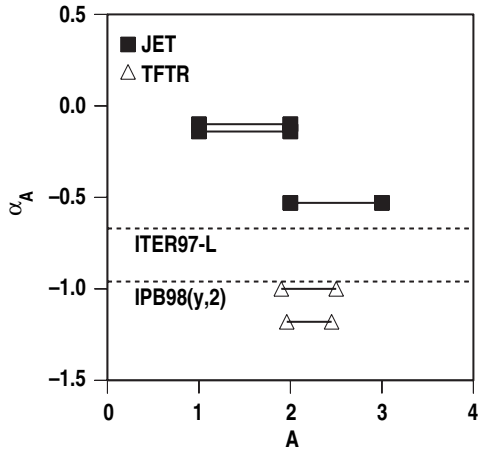

Figure 29. Scaling of the thermal energy confinement with A for L-mode experiments from the TFTR tokamak and H-mode experiments from the JET tokamak. The symbols show the machine as denoted in the legend and the extent over which A was varied in each scan. Fractional values correspond to mixtures of isotopes.

scaling of transport in TFTR may be due to the stronger shear flow stabilization of supershot plasmas.

The effect of the ion charge state on energy confinement was studied in ELMing H-mode plasmas in JET by comparing mass fueling with helium-4 and deuterium [120]. Since the ion mass also varied along with charge state, the mass scaling from the IPB98$(y, 2)$ scaling relation was utilized to isolate the charge dependence of heat transport. The best fit to the thermal energy confinement times in helium-4 Type I ELMing H-modes and the deuterium reference discharges gave $\Omega_{ci}\tau_{th} \propto \rho_{*i}^{-2.70}\nu_*^{-0.01}A^{0.96}Z^{-3.54\pm0.38}$. (Note that this formula corrects for a factor of Z^{-2} left out in [120]). It should be remembered that JET experiments with hydrogen and deuterium at matched ρ_{*i}, β and ν_* found a much weaker isotope mass scaling than IPB98$(y, 2)$, which might reduce the magnitude of α_Z by as much as 1 unit.

The effect of primary ion dilution on electron heat transport was studied in RTP for ohmic and ECH plasmas [121]. Using helium and neon as fill gases, Z_{eff} was varied from ≈1.5 to ≈9 while keeping n_e and T_e nearly constant. Since the ion charge state of the primary ion (deuterium) was not changed, this constituted a combined Z_{eff} and ν_* scan (ρ_{*i} and χ_B are taken to be independent of Z_{eff}). For ohmic plasmas in the plateau regime, the electron heat transport was found to scale as $\chi_e \propto n_e^{-0.55\pm0.14}Z_{eff}^{0.23\pm0.03}$. The Z_{eff} scaling of χ_e for ECH plasmas in the banana regime was reported to be slightly weaker than this. In [121], this was interpreted as constituting a ν_* scaling of transport like $\chi_e \propto n_e^{-1.2}\nu_*^{0.4}$, but this is the opposite dependence as found from ν_* scans at constant Z_{eff} in RTP [98]. These disparate results from RTP can be reconciled if Z_{eff} and ν_* are both regarded as important dimensionless parameters, allowing the electron heat transport for ohmic plasmas in [121] to be written as $\chi_e/\chi_B \propto \nu_*^{-0.55\pm0.14}Z_{eff}^{0.78\pm0.17}$. The local transport dependences were consistent with the dependences of the global confinement time, $B\tau \propto \nu_*^{0.42\pm0.10}Z_{eff}^{-0.60\pm0.12}$. Thus, the effects of primary ion dilution on transport appear to be weaker than the effect of the primary ion charge state. This is also a nice example of how apparently inconsistent results obtained using a combination of engineering and dimensionless parameters are reconciled when a full dimensionless parameter scaling approach to the analysis is applied.

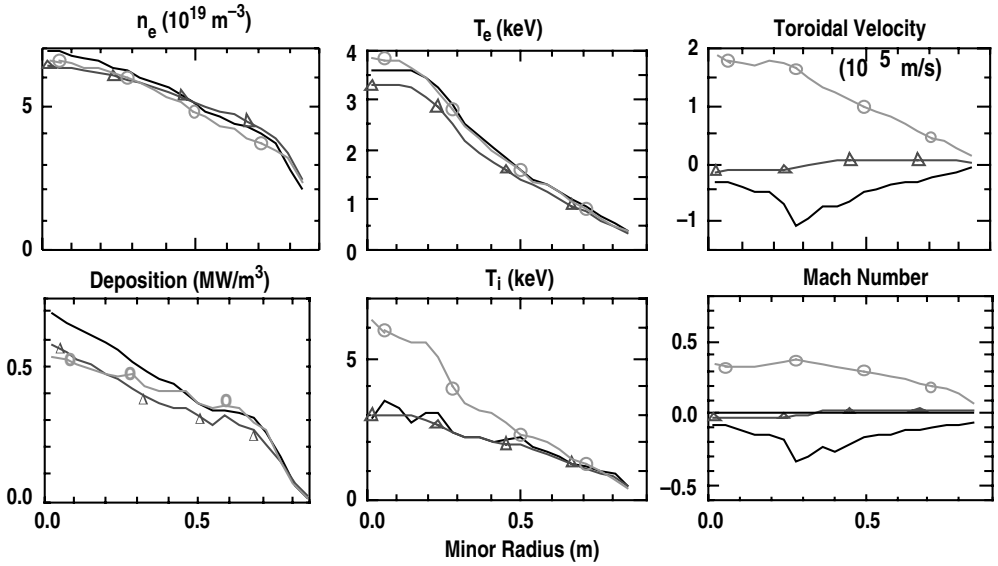

Figure 30. Comparison of kinetic profiles for the TFTR Mach number scan at $B = 4.75$ T. The top row shows the electron density, electron temperature and toroidal velocity versus minor radius. The bottom row shows the NBI power deposition, ion temperature and Mach number versus minor radius. Reprinted from [122] by permission.

3.8. Other dependences

The plasma rotation, expressed as a Mach number (the ratio of the toroidal rotation velocity to the ion sound wave speed), is also expected to affect transport rates, primarily through flow shear stabilization [58, 104]. This could act as a hidden parameter in dimensionless parameter scaling experiments that use only uni-directional beam injection. Such an effect was previously discussed in section 3.3.3 with regard to ρ_* scaling experiments in DIII-D using NBI [48]. For plasmas with a small pressure gradient contribution to E_r, the normalized rotational shearing rate is expected to scale as $|MB_p/B|$. In an interesting experiment in TFTR, M was varied in sawtoothing L-mode plasmas to determine the effect on the energy confinement time [122]. The plasma toroidal velocity was varied by changing the net torque applied to the plasma from a combination of neutral beams injecting either coincident with or counter to the plasma current direction. The plasma profiles, and thus the dimensionless parameters, were kept constant for a scan at higher B (figure 30) while M was varied from +0.3 to −0.3. (Positive value refers to rotation in the plasma current direction.) The exception was the core ion temperature (figure 30), which was highest for the pure co-NBI plasma. Not surprisingly, kinetic analysis showed that ion energy confinement was affected the most by rotation. The energy confinement time was measured to be smallest for moderate values of negative rotation, and increased confinement was observed for both strong positive and strong negative rotation (figure 31). The variation of the energy confinement time at lower B is even more pronounced (figure 31). The symmetry of the dependence about the minimum is in agreement with simple models of flow shear stabilization that suggest that the effects of rotation should depend only on the magnitude of M, but the offset of the minimum from zero torque is not explained by this model.

Scaling of transport with the ratio of ion temperature to electron temperature can also help differentiate between the various theories of turbulent transport. This scaling is also

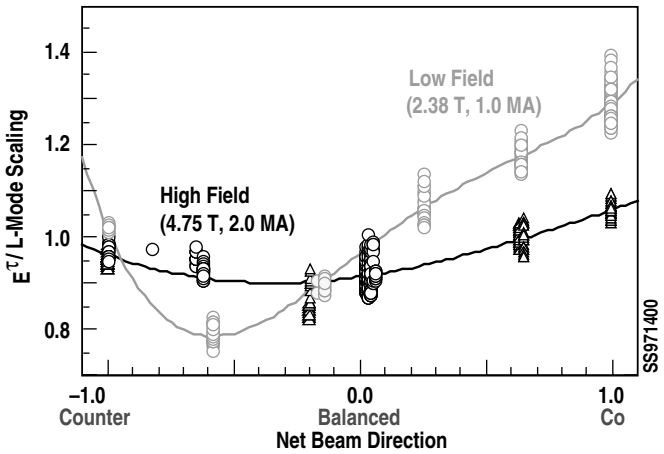

Figure 31. Variation of the normalized energy confinement time in TFTR with the mixture of the NBI direction from pure counter-injection to pure co-injection. Scans from two different values of magnetic field at fixed q are shown. The L-mode confinement scaling used to normalize the energy confinement time is not specified in the paper. Reprinted from [122] by permission.

important because if transport has a strong dependence on T_i/T_e, then projection of the transport results from hot-ion plasmas, which generally have good confinement, to future burning plasma devices with $T_e \geqslant T_i$ may lead to optimistic predictions. Experiments in DIII-D measured the T_i/T_e dependence of heat and particle transport in ELMing H-mode plasmas with nearly equal electron and ion temperatures and T_i profiles close to the predicted marginal stability point for the ITG mode [105, 123]. A systematic series of experiments showed that increasing T_i/T_e reduced the electron and ion thermal diffusivities and the helium particle diffusivity regardless of which temperature was being varied. Figure 32 shows a 20% scan in the temperature ratio at fixed β using combined rf and NBI heating to determine if transport was dependent upon how the plasma stored energy was divided between the electron and ion fluids. The thermal energy confinement time increased strongly with increasing ion to electron temperature as $B\tau_{th} \propto (\langle T_i \rangle / \langle T_e \rangle)^{2.1\pm0.2}$. Local transport analysis showed that the heat transport and helium particle transport had similar dependences on T_i/T_e, as seen in figure 33. Additional experiments that varied T_e and T_i separately found similar results, demonstrating a strong coupling between the ion and electron fluids through the transport coefficients (rather than through collisions). Simulations of this experiment using the GLF23 transport model showed that the sensitivity of heat transport to changes in T_i/T_e is consistent with the scaling of the ITG mode near the threshold arising from the T_i/T_e dependence of the critical ion temperature gradient.

3.9. Summary and discussion

While a definitive description of energy transport in magnetic fusion plasmas remains in the future, the results reviewed here do provide significant constraints and guidance to the quest for such a description. The correlations among the variables for the various scans discussed in this section, including the size scalings for intermachine scans, are given in table 4. The summary figures (figures 5, 9, 17, 18, 21, 22, 25, 26 and 29) in the previous sections illustrate the results of these various types of scans, and the discussion of those figures will not be repeated here. This section attempts to mark out the constraints that follow from the experiments discussed above.

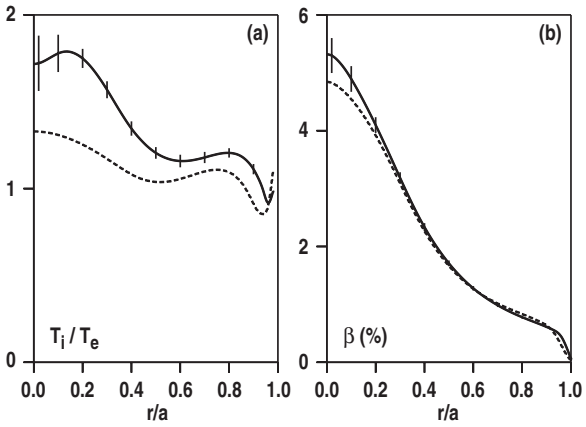

Figure 32. Ratio of (*a*) the ion and electron temperatures and (*b*) thermal β versus normalized radius for an H-mode T_i/T_e scan at fixed β from the DIII-D tokamak. Reprinted from [123] by permission of the American Physical Society.

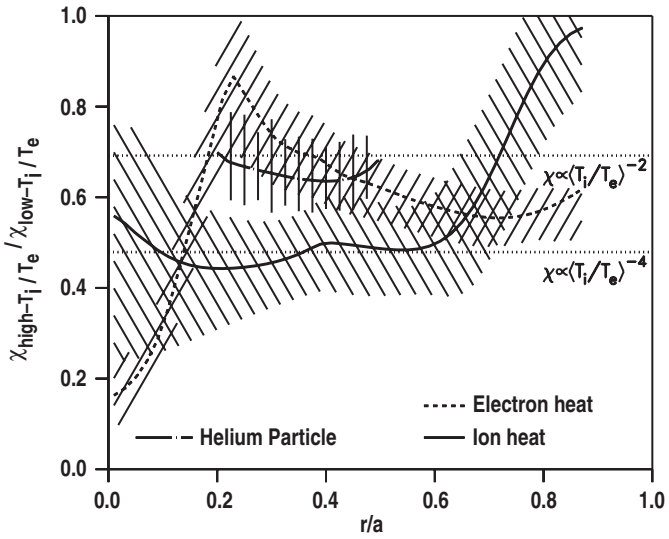

Figure 33. Ratio of electron and ion thermal diffusivities and helium particle diffusivity versus normalized radius for an H-mode T_i/T_e scan at fixed β from the DIII-D tokamak. Reprinted from [123] by permission of the American Physical Society.

The first key result is that the experiments clearly demonstrate the ability to apply dimensionless scaling principles to magnetic fusion plasmas. In many experiments, but particularly in the identity experiments (section 3.2), it is possible to make matches of the profiles of dimensionless parameters with only central heating. This indicates that the correct parameters to describe transport have been identified, and counter-examples illustrating a lack of match have been seen when other parameter sets are chosen.

The robust result of gyroBohm scaling in the electron channel (figure 9(*a*)) across a variety of magnetic configurations, confinement regimes and heating schemes would seem to validate the basic picture of turbulence from microinstabilities causing transport across good magnetic

Table 4. Required correlations of the dimensional variables to perform the scans listed in the first column. For the identity scan, only one parameter is necessary; the minor radius a is used. For the other scans, two parameters are used, either B, I or $\omega_{\rm tor}$ as listed in the table. The cross-section, aspect ratio and ion mass are assumed to be fixed.

Scan	I	n	T	$\omega_{\rm tor}$	B	τ_E	χ
Identity	$a^{-1/4}$	a^{-2}	$a^{-1/2}$	$a^{-5/4}$	$a^{-5/4}$	$a^{5/4}$	$a^{3/4}$
ρ_*	Ba	$B^{4/3}a^{-1/3}$	$B^{2/3}a^{1/3}$	$B^{1/3}a^{-5/6}$	—	$B^{-1}\rho_*^{\alpha_\rho}$	$Ba^2\rho_*^{\alpha_\rho}$
β	Ba	B^4a^3	B^2a^2	B	—	$B^{-1}\beta^{\alpha_\beta}$	$Ba^2\beta^{\alpha_\beta}$
$\nu_{\rm C}$	Ba	a^{-2}	B^2a^2	B	—	$B^{-1}\nu_{\rm C}^{\alpha_\nu}$	$Ba^2\nu_{\rm C}^{\alpha_\nu}$
q	—	a^{-2}	$a^{-1/2}$	$a^{-5/4}$	$a^{-5/4}$	$a^{5/4}q^{\alpha_q}$	$a^{3/4}q^{\alpha_q}$
M	$a^{-1/4}$	a^{-2}	$a^{-1/2}$	—	$a^{-5/4}$	$a^{5/4}M^{\alpha_{\rm M}}$	$a^{3/4}M^{\alpha_{\rm M}}$

surfaces. If there were significant regions of magnetic stochasticity, the electrons should be more sensitive to this than the ions, resulting in a much different ρ_* scaling. In addition, direct measurements of the scaling of the turbulence characteristics indicate a gyroBohm scaling (figure 13), further corroborating the micro-instability model.

Other measured scalings support the basic drift wave turbulence model of transport. The lack of β scaling, especially in H-mode plasmas (figure 17), also validates the standard picture that transport arises from the fluctuating $\boldsymbol{E} \times \boldsymbol{B}$ motions of plasma due to electrostatic waves. The increase in transport with increasing collisionality (figure 22) is qualitatively consistent with collisional damping of zonal flows, which are predicted to limit the growth of turbulence. The variation in the ion ρ_* damping in DIII-D between co-current and counter-current NBI experiments was shown by modeling to be consistent with the mismatch of the bulk $\boldsymbol{E} \times \boldsymbol{B}$ shear, a turbulence suppression mechanism related to the zonal flows. The ion heat diffusivity is dependent on the electron temperature and vice versa in H-mode plasmas, as expected for ITG-mode turbulence.

The sum of the evidence discussed above strongly supports the present standard paradigm of heat transport dominated by ITG-mode turbulence including the influence of zonal flows and bulk $\boldsymbol{E} \times \boldsymbol{B}$ shear on the turbulence. The picture is most consistent in H-mode plasmas, but the same trends appear in L-mode plasmas, albeit with more variation.

However, there are some notable discrepancies between the data presented and the standard theoretical picture. The most obvious is the variation of the ion ρ_* scaling in contrast to the lack of variation in the electron ρ_* scaling. In the DIII-D H-mode experiments, the variation in the ion ρ_* scaling was consistent with modeling of the effects of a mismatch in the bulk $\boldsymbol{E} \times \boldsymbol{B}$ shear. However, the electron transport scaling did not change. This difference in the ion and electron ρ_* scaling is not described by the theories that invoke bulk $\boldsymbol{E} \times \boldsymbol{B}$ shear (e.g. [124]) or other mechanisms (e.g. [125–127]) to break the gyroBohm scaling intrinsic in the basic equations. The different scaling in the two fluids would imply that either another mode that is insensitive to $\boldsymbol{E} \times \boldsymbol{B}$ shear effects dominates the electron transport or the two species are sensitive to different wavelengths of the ITG turbulence. The two-mode explanation is inconsistent with the theoretical predictions of strong electron heat transport from ITG-mode turbulence. The explanation invoking sensitivity to different wavelengths for the electron and ion heat transport conflicts with the standard modeling form used to account for the effects of $\boldsymbol{E} \times \boldsymbol{B}$ shear. The effects are modeled as a linear, no-threshold reduction of the turbulence by the ratio of the $\boldsymbol{E} \times \boldsymbol{B}$ shearing rate to the maximum linear growth rate. This implicitly assumes the effects of $\boldsymbol{E} \times \boldsymbol{B}$ shear are independent of wavelength, at least over the wavelengths of unstable ITG modes. The ρ_* scaling paradox could be reconciled with the model of different wavelength sensitivity if the ion transport were dominated by the longest wavelength modes and the change in ion ρ_*

scaling were due to changes in the long wavelength cutoff. This could also be consistent with the observations that bulk $\boldsymbol{E} \times \boldsymbol{B}$ shear, density scale length, and magnetic shear all have been correlated with the variation in the ion ρ_* scaling. Any of these three could be invoked to limit the longest wavelength in the turbulence spectrum.

Related to these speculations about wavelength are the observed differences in the q and κ scalings in L-mode and H-mode plasmas. Since both of these quantities are made of ratios of quantities with the same units, dimensional analysis gives no insight into how they relate to the other dimensionless parameters, except that ρ_* β and ν_C must be held constant to measure the variation of transport with q or κ. The measured scalings in L-mode plasmas are consistently weaker than those in H-mode plasmas (figures 25 and 26). If a single type of turbulence were governing both L-mode and H-mode plasmas, a similar dependence on the magnetic geometry might be expected. It is expected that drift waves such as the ITG mode know about the magnetic geometry through the magnetic well and the magnetic shear, just as ideal ballooning modes do. However, inclusion of this effect in calculations of the maximum linear growth rate gives much weaker dependence on geometry than measured in L-mode plasmas. Perhaps this is where the expected β effect is hiding—the increased β in the H-mode plasmas may cause stronger coupling to the stable electromagnetic modes (and their magnetic geometry dependence) without increasing the magnetic flutter transport. Another possibility is that the parallel correlation lengths are limited to the bad curvature region by some unexplained mechanism, whereas the ideal ballooning calculations have long parallel correlation lengths extending through the good curvature region, perhaps even multiple times. Because the drift modes are nearly resonant on the local magnetic field lines, restrictions on the parallel correlation length would translate directly into constraints on the perpendicular wavelengths.

In addition to the scalings themselves, extrapolation of the early H-mode ρ_* scans to ITER showed the importance of boundary conditions to the dimensionless scaling exercises. The projections indicated that the energy confinement in ITER would be so good that no stationary operating point was possible (the self-heating power was larger than the projected loss power). However, it was quickly noticed that the ρ_* scaling of the L–H transition was stronger than the transport loss power scaling. This meant that the power to maintain the plasma in H-mode was larger than that to maintain the scaled stored energy. Subsequent experiments showed that ρ_* scans that ran into the L–H threshold found global energy confinement scalings consistent with the scaling of the L–H threshold rather than the intrinsic transport scaling. Therefore, maintaining the boundary conditions under which the results were obtained is a necessary condition for a valid extrapolation. Determination of the L–H transition power scaling with dimensionless parameters will be discussed more in section 5.1.

Particle transport studies are not nearly as well developed as energy transport studies. There is a general correlation between the inferred ρ_* scaling of the particle diffusivity and that of the ion heat diffusivity. Both hydrogenic and helium transport studies show strong increases in the inward convection with decreasing ρ_* (toward burning plasma conditions). In the case of the helium measurements, there was no preferential accumulation as ρ_* decreased. This is a positive result for deuterium–tritium fusion, where the byproduct is a central source of helium. The results indicate helium 'ash' from the fusion burn will not build up under the conditions studied. The increasing V/D ratio for helium with increasing β is of concern, since increases in β are seen as the primary means to enhance the fusion power output in a given device. Accumulation of helium ash in higher β discharges would lessen or even counteract the anticipated increase in fusion power at higher β. Theoretical work in particle transport is still developing due to the difficulty of handling calculations of the non-adiabatic electron response that contains the information about particle transport.

4. Application of dimensionless parameter scaling to global confinement databases

The techniques of dimensionless parameter scaling discussed in previous sections can also play a useful role in analyzing and interpreting the information contained in the global energy confinement databases. The databases contain information described by measured quantities, such as density or magnetic field strength, or quantities derived from measurements, such as energy confinement time. The database variables correspond to the quantities $\{Q_i\}$ that appear in equation (2.1). These dimensional variables can be transformed into averaged versions of the dimensionless parameters that have been found to describe the local energy transport. Typically, one quantity of interest is chosen as the dependent variable, and the rest are treated as independent variables. Then, regression analysis is used to infer how the dependent variable is correlated with the independent variables. (An alternative analysis employing Bayesian statistics will also be discussed. A discussion of the merits and applications of both analysis techniques can be found in [128].) An unconstrained fit to the database provides a quantitative relation for the dependences on the dimensional variables, which can then be cast in terms of dimensionless parameters for comparison with the single parameter scans. In addition, the resulting unconstrained fit should be 'dimensionally correct'; in other words, having no remaining dimensional dependence if the correct dimensionless variables are used and the database is well conditioned. This dimensional constraint and the individual parameter scan results can also be imposed as fitting constraints on the dataset to see how well the dimensionless parameter scaling concepts describe a larger variety of data. In the following sections, examples of the application of dimensionless parameters to database analysis will be given, with particular attention given to the tokamak confinement databases compiled for the ITER project design activities.

4.1. Database analysis in terms of dimensionless parameters

Comparison of experiments with different plasma parameters using dimensional parameter scaling has a long history in magnetic fusion studies (see, for example, [129]). Concerted efforts to compile and analyze multi-experiment databases in order to study the scaling of the energy confinement in tokamaks commenced in the early 1980s. A notable early contribution in this area was made by Goldston [130], who used the experimental data from the early tokamaks to derive an empirical scaling expression for the global energy confinement time. The relationship of the confinement time τ_E (s) inferred from the database of deuterium plasmas to the dimensional variables plasma current I (MA), major radius R (m), minor radius a (m), elongation κ and heating power P (MW) was

$$\tau_{E,\mathrm{Goldston}} = 6.4 \times 10^{-5} I R^{1.75} a^{-0.37} \kappa^{0.5} / P^{0.5}. \tag{4.1}$$

This surprisingly simple power-law scaling was quite successful in predicting the L-mode behavior of the larger experiments DIII-D, JET, JT-60 and TFTR that came into operation in the late 1980s.

Following this early work, a formal international structure was set up under the auspices of the ITER project to assemble the confinement data from tokamak experiments throughout the world, with the goal of providing guidance in the design of ITER. Starting in 1989, the original L-mode database used by Goldston [130] was upgraded to include data from the newer tokamaks DIII-D, JET, JT-60 and TFTR. A new L-mode scaling ITER89-P [131] was derived. This expression has been used extensively as a standard for comparison of measured confinement times. It has the form

$$\tau_{E,\mathrm{ITER89-P}} = 0.038 I^{0.85} B^{0.2} n^{0.1} R^{1.5} \varepsilon^{0.3} \kappa^{0.5} A^{0.5} P^{-0.5}, \tag{4.2}$$

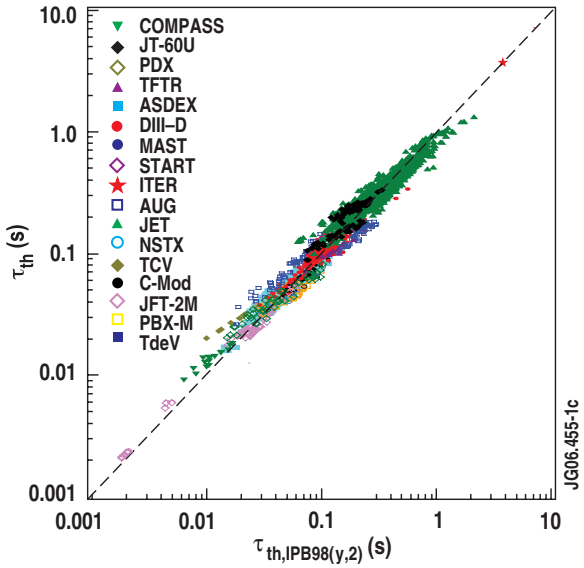

Figure 34. Plot of the measured H-mode thermal energy confinement time versus that predicted by the IPB98(y, 2) scaling expression. The symbols indicate data from different tokamaks as noted in the legend.

where ε is the inverse aspect ratio ($\varepsilon \equiv a/R$), B is the toroidal magnetic field in T, and n is the line-averaged density in 10^{19} m^3. However, the anticipated operating regime for ITER is not L-mode, but ELMing H-mode. Therefore, an H-mode database was formed [132] containing both ELM-free and ELMing H-mode data. A full description of the H-mode database and its variables can be found in [133, 134] and a description of the L-mode database in [21].

Both the L-mode and H-mode databases have been routinely updated. The current recommended expressions to be used for the scaling of energy confinement time with selected dimensional variables are ITER97-L [21] for the Lmode and IPB98(y) and IPB98(y, 2) [20] for the H-mode. Unlike the Goldston and ITER89-P expressions, both of these scaling expressions pertain to the thermal energy confinement time ($\tau_{\rm th}$) rather than the global energy confinement time (τ_E), which includes the energy content in fast ions from auxiliary heating. The IPB98(y, 2) scaling expression, which is now a standard H-mode energy confinement benchmark, has the form:

$$\tau_{\rm th,IPB98(y,2)} = 0.0562 I^{0.93} B^{0.15} P^{-0.69} n^{0.41} A^{0.19} R^{1.97} \varepsilon^{0.58} \kappa_{\rm a}^{0.78}. \tag{4.3}$$

The prediction of the IPB98(y, 2) is plotted in figure 34 against the measured confinement times in the international H-mode database (DB3). Note that the present experimental data spans three orders of magnitude in confinement time. The L-mode scaling ITER97-L has the form

$$\tau_{\rm th,ITER97\text{-}L} = 0.023 I^{0.96} B^{0.03} P^{-0.73} n^{0.40} A^{0.20} R^{1.83} \varepsilon^{-0.06} \kappa^{0.64}. \tag{4.4}$$

In order to apply dimensional analysis to these scaling relations, a method for transforming the dimensional variables into the chosen dimensionless parameters must be specified. The set $\{\rho_*, \beta, \nu_{\rm C}\}$ that was found in section 3.2 to describe the plasma behavior in identity experiments will be used here. The database contains no information on the plasma rotation, so the Mach number is omitted from the dimensionless parameter set; it can be considered a hidden variable in the database analysis. It is also assumed that radiation and charge exchange losses are

ignorable[8], as discussed in section 3.1. The current will be related to the magnetic field through q. The other variables in the scaling relations are already dimensionless ratios. The first application of the dimensionless parameters is to check whether the scalings are dimensionally correct. This is sometimes described as the scaling satisfying the Kadomtsev constraint or the high-β constraint. However, it is simply a relationship among the dimensionless parameters such that no explicit size dependence remains when the scaling relation derived using dimensional variables is recast in dimensionless form. Assuming a power-law form for the scaling relation in both dimensional and dimensionless parameters, the exponent on the 'leftover' length scaling α_{L} in the dimensionless relation is

$$4\alpha_{\mathrm{L}} + 5 = [4\alpha_{\mathrm{R}} + 4\alpha_{\mathrm{a}} - 8\alpha_{\mathrm{n}} - \alpha_{\mathrm{I}} + 2\alpha_{\mathrm{P}} - 5\alpha_{\mathrm{B}}]/[1 + \alpha_{\mathrm{P}}], \tag{4.5}$$

where the α's are the exponents of the dimensional variables in the scaling relation. Evaluating α_{L} for the scaling relations given above, the Goldston scaling (equation (4.1)) gives $\alpha_{\mathrm{L,Goldston}} = 0.51$, the ITER89-P scaling (equation (4.2)) gives $\alpha_{\mathrm{L,ITER89P}} = -0.08$, the IPB98$(y, 2)$ (equation (4.3)) gives $\alpha_{\mathrm{L,IPB98(y,2)}} = -0.01$ and the ITER97-L scaling (equation (4.4)) gives $\alpha_{\mathrm{L,ITER97\text{-}L}} = 0.19$. The L-mode scalings are not quite dimensionally correct, with the ITER89-P scaling being the best. The H-mode scaling is remarkably close to being dimensionally correct. Several conditions can contribute to the scaling not being dimensionally correct. If the physics governing the energy confinement is not described by the dimensionless variables chosen, then there is no reason to expect a dimensionally correct scaling relation. Given the success of the identity experiments (section 3.2), this is unlikely; however, it is important to take seriously the caveat about rotation (and by implication $\boldsymbol{E} \times \boldsymbol{B}$ shear) being a hidden parameter in the dataset. Another possible cause for the scaling to deviate from the dimensionally correct form is that the dataset is poorly conditioned, i.e. it is not sufficiently populated across all the variables or significant correlations exist. For the L-mode database, the quantity and variety of data seem to be good; however, the boundaries of the set will have correlations in the variables, such as the L–H threshold, the ohmic heating at low power and the density limit. Similar issues could be raised with the H-mode dataset with the addition of the β limit at high power. Methods to look for these effects will be discussed in the next section.

Beyond checking for dimensional correctness, the scaling relations can be completely transformed into the dimensionless variables. The transformations between the dimensional and dimensionless variables are listed in table 5. From this table, it is clear that using power as the variable to describe temperature introduces some significant complications, due to the appearance of $(1 + \alpha_{\mathrm{P}})$ in the demoninator of the conversion factors from dimensional to dimensionless variables. Since α_{P} is typically between -0.5 and -1.0, the values of the dimensionless exponents are somewhat sensitive to α_{P}. This point will be discussed further toward the end of this section. Using the transformations in table 5, the IPB98$(y, 2)$ scaling takes the form:

$$\Omega_{\mathrm{i}}\tau_{\mathrm{th,IPB98(y,2)}} \sim \rho_*^{-2.69}\beta^{-0.90}\nu_{\mathrm{C}}^{0.08}A^{0.96}q^{-3.0}\varepsilon^{0.73}\kappa^{3.29}R^{-0.01}. \tag{4.6}$$

The ITER89-P L-mode scaling takes the form

$$\Omega_{\mathrm{i}}\tau_{\mathrm{E,ITER89-P}} \sim \rho_*^{-2.05}\beta^{-0.53}\nu_{\mathrm{C}}^{-0.23}A^{1.03}q^{-1.7}\varepsilon^{-0.05}\kappa^{1.20}R^{-0.08}. \tag{4.7}$$

The ITER97-L scaling is not nearly as dimensionally correct; however, the transformations can still be applied. The transformed scaling takes the form

$$\Omega_{\mathrm{i}}\tau_{\mathrm{th,ITER97-L}} \sim \rho_*^{-1.85}\beta^{-1.41}\nu_{\mathrm{C}}^{0.21}A^{0.67}q^{-3.56}\varepsilon^{-0.37}\kappa^{2.58}R^{0.19}. \tag{4.8}$$

[8] In using these scaling relations to project to ITER, which could have significant bremsstrahlung or synchrotron radiation, the calculated radiation losses can be added to the estimates here of the diffusive losses to estimate the true energy confinement time.

Table 5. Tables of transformations between scaling laws in dimensional and dimensionless variables.

$\tau_E \propto I^{\alpha_I} B^{\alpha_B} P^{\alpha_P} n^{\alpha_n} a^{\alpha_a} R^{\alpha_{R,E}} \kappa^{\alpha_{\kappa,E}} A^{\alpha_{A,E}}$

$\Omega_i \tau_E \propto \rho_*^{\alpha_\rho} \beta^{\alpha_\beta} \nu_C^{\alpha_\nu} q^{\alpha_q} R^{\alpha_{R,D}} \varepsilon^{\alpha_\varepsilon} \kappa^{\alpha_{\kappa,D}} A^{\alpha_{A,D}}$

Dimensional to dimensionless:

$\alpha_\rho = [-\frac{3}{2}\alpha_I - \frac{3}{2}\alpha_B - 3\alpha_P - 2\alpha_n]/[1 + \alpha_P] - \frac{3}{2}$

$\alpha_\beta = [\frac{1}{4}\alpha_I + \frac{1}{4}\alpha_B + \frac{3}{2}\alpha_P + \alpha_n]/[1 + \alpha_P] + \frac{1}{4}$

$\alpha_\nu = [-\frac{1}{4}\alpha_I - \frac{1}{4}\alpha_B - \frac{1}{2}\alpha_P]/[1 + \alpha_P] - \frac{1}{4}$

$\alpha_q = [-\alpha_I]/[1 + \alpha_P]$

$\alpha_{R,D} = [-\frac{1}{4}\alpha_I - \frac{5}{4}\alpha_B + \frac{1}{2}\alpha_P - 2\alpha_n + \alpha_a + \alpha_{R,E}]/[1 + \alpha_P] - \frac{5}{4}$

$\alpha_\varepsilon = [\frac{1}{2}\alpha_I - \frac{3}{2}\alpha_B - \alpha_P - 2\alpha_n + \alpha_a]/[1 + \alpha_P] - \frac{3}{2}$

$\alpha_{\kappa,D} = [\alpha_I + \alpha_P + \alpha_{\kappa,E}]/[1 + \alpha_P]$

$\alpha_{A,D} = [\frac{3}{4}\alpha_I + \frac{3}{4}\alpha_B + \frac{3}{2}\alpha_P + \alpha_n + \alpha_{A,E}]/[1 + \alpha_P] - \frac{1}{4}$

Dimensionless to dimensional:

$\alpha_I = -\alpha_q/[1 - \frac{1}{2}\alpha_\rho - \alpha_\beta + 2\alpha_\nu]$

$\alpha_B = [-\alpha_\rho - 2\alpha_\beta + \alpha_q - 1]/[1 - \frac{1}{2}\alpha_\rho - \alpha_\beta + 2\alpha_\nu]$

$\alpha_P = [\frac{1}{2}\alpha_\rho + \alpha_\beta - 2\alpha_\nu]/[1 - \frac{1}{2}\alpha_\rho - \alpha_\beta + 2\alpha_\nu]$

$\alpha_n = [-\frac{1}{2}\alpha_\rho + 3\alpha_\nu]/[1 - \frac{1}{2}\alpha_\rho - \alpha_\beta + 2\alpha_\nu]$

$\alpha_a = [-2\alpha_\rho - 2\alpha_\beta + 4\alpha_\nu + 2\alpha_q + \alpha_\varepsilon]/[1 - \frac{1}{2}\alpha_\rho - \alpha_\beta + 2\alpha_\nu]$

$\alpha_{R,E} = [-\frac{1}{2}\alpha_\rho - \alpha_\beta + 3\alpha_\nu - \alpha_q + \alpha_{R,D} - \alpha_\varepsilon]/[1 - \frac{1}{2}\alpha_\rho - \alpha_\beta + 2\alpha_\nu]$

$\alpha_{\kappa,E} = [-\frac{1}{2}\alpha_\rho - \alpha_\beta + 2\alpha_\nu + \alpha_q + \alpha_{\kappa,D}]/[1 - \frac{1}{2}\alpha_\rho - \alpha_\beta + 2\alpha_\nu]$

$\alpha_{A,E} = [\frac{1}{2}\alpha_\rho + \alpha_{A,D} + 1]/[1 - \frac{1}{2}\alpha_\rho - \alpha_\beta + 2\alpha_\nu]$

There are distinct differences between the H-mode and L-mode scalings and between the two L-mode scalings. Some of the difference between the L-mode scalings may be due to the physical difference in the quantity that is being scaled; the ITER89-P scaling looks at global energy confinement time, while the ITER97-L scaling pertains to the thermal energy confinement time. The H-mode scaling expression is quite close to gyroBohm scaling, which has the form $B\tau_E \propto \rho_*^{-3}$, while the L-mode scalings are close to Bohm scaling ($B\tau_E \sim \rho_*^{-2}$). It is also important to note that the exponents of the dimensionless parameters in the scalings change significantly with this transformation because of the dependence of the dimensional variables on the dimensionless parameters used in the regression. Therefore, some care must be exercised when discussing mass scaling or κ scaling to understand the method by which the scaling was obtained.

With the scaling relations now transformed to dimensionless variables, it is interesting to compare the results of the dedicated single-parameter scans reported in section 3 with the results of the regression analysis on a larger dataset. As noted above, the IPB98(y, 2) H-mode scaling (equation (4.6)) is close to gyroBohm scaling. This agrees with the H-mode experiments shown in figure 5. The discussion in section 3.3 pointed out that the deviation from gyroBohm scaling occurred in the ion scaling in experiments with higher q_{95} or smaller L_n, although the cause was not definitely established. The majority of the H-mode database is at $q_{95} < 4$, but a significant amount of data exists at higher q_{95}. In spite of this, the results of the regression analysis of the H-mode global confinement database and the H-mode ρ_* scans are in qualitative agreement. The same conclusion holds for the comparison between the L-mode ρ_* scans and the L-mode global confinement database analysis. There is a wide variety of ρ_* scalings obtained in the L-mode ρ_* scans, but the results center roughly around the expectation for Bohm scaling. Both the ITER89-P scaling (equation (4.7)) and the ITER97-L scaling (equation (4.8)) are close to Bohm scaling, as noted above.

The scaling of confinement with β shows the largest discrepancy between the single-parameter scans and the database analysis. This discrepancy also has the most significant implications for predictions of fusion performance, since the fusion power produced scales faster than linear with pressure and a strong negative β scaling implies a strong degradation of confinement with increased power. The H-mode β scaling results (figure 17) tightly cluster around β^0, while the IPB98(y, 2) scaling (equation (4.6)) indicates a degradation of confinement nearly linear with β. The β scaling results in L-mode experiments (figure 18) have some variation, but most reliable results lie near β^0 (see section 3.4 for a detailed discussion of these results). The L-mode global scalings show a significant degradation with β, especially the ITER97-L scaling (equation (4.8)). Since the β scaling has such large implications for the optimization of tokamak fusion performance [135], work done to understand the source of this discrepancy for the H-mode comparison will be discussed below, following the completion of the comparison of the single-parameter scans with the database analysis.

The scaling of confinement with collisionality is weak in both the experimental scans and all of the scalings; however, the effect of the collisionality scaling should not be neglected, due to the large variation possible in tokamaks. Note that the choice of normalization of the collision frequency is important here. The quantity ν_C was used here in the transformation of the engineering parameters to dimensionless parameters. A different q scaling would be obtained if ν_* were used. As discussed in section 3.5, the two definitions are equivalent in that context and in the comparison below, since q was held fixed in those experiments. Because of the operational limit on the density that can be obtained in tokamaks [29], fusion energy systems are expected to operate with low collisionality. The H-mode collisionality scaling results (figure 22) have a trend that may approach the IPB98(y, 2) scaling as the collisionality is reduced; however, the experimental results from the dedicated collisionality scans are still well above the scaling determined from the fit to the database. The L-mode single-parameter scan data (figure 21) show some variation with the bulk of the data between the ITER89-P and the ITER97-L collisionality scalings.

The scaling of confinement with q from the single-parameter scans and the database analysis are in significant disagreement for both L-mode and H-mode data. DIII-D has data from variations in q by two distinct methods (changes in current and in shape). The q scaling obtained by these two methods (discussed in detail in section 3.6) is in good agreement in both L-mode and H-mode experiments, as shown in figure 25. This agreement gives some confidence in the results. Both the ITER97-L (equation (4.8)) and the IPB98(y, 2) scalings (equation (4.6)) have very strong q scalings. However, looking at table 5, it is clear that the power degradation has a very strong influence on the value inferred for the q scaling. As discussed above, the power degradation obtained from the database analysis is suspect; therefore, to a greater extent than the other dimensionless variables, the q scaling exponent is also suspect. This assertion is borne out by the fact that the weaker β scaling (or equivalently weaker power degradation) in the ITER89-P scaling (equation (4.7)) is reflected in the weaker q scaling inferred. However, the q dependence of the ITER89-P scaling is still stronger than that measured in the DIII-D experiments, consistent with the β scaling being closer to β^0. Similar comments apply to the comparison between the κ scaling found in the experiments and the database analysis.

Strong conclusions from the comparison of the mass scaling between experiments and database analysis cannot be drawn due to the difficulties in mounting a dimensionless parameter scaling experiment (section 3.7) and the limited data in the dataset with different hydrogen isotopes. Comparing the results in figure 29 with the scalings (equations (4.6)–(4.8)), the L-mode data from TFTR show a stronger mass dependence than the ITER97-L scaling, but

are close to the ITER89-P scaling. The JET H-mode data indicate a weaker mass dependence than the IPB98(y, 2) scaling.

The results from the individual dimensionless parameter scaling experiments can also be transformed back into the dimensional variables included in the confinement database. As an example, the dimensionless parameter scalings determined in the DIII-D experiments will be used, since scalings for q and κ are only available from that experiment. Using the transformations given in table 5, the dimensional variable scalings are determined completely by the combined ρ_*, β, ν and q scalings through a straightforward algebraic manipulation [25, 75, 105, 106]. The H-mode dimensionless parameter scaling results can be summarized as

$$\Omega_i \tau_{th} \propto \rho_*^{-3.15\pm0.2} \beta^{-0.01\pm0.10} \nu_C^{-0.35\pm0.04} q_{95}^{-1.43\pm0.23} \kappa^{2.2\pm0.6}, \tag{4.9}$$

where the ν_C dependence from low collisionality (more reactor relevant) plasmas is utilized. Converting this into a confinement scaling in dimensional parameters gives

$$\tau_{th} \propto I^{0.76\pm0.14} B^{0.39\pm0.17} n^{0.28\pm0.07} P^{-0.47\pm0.05} L^{2.14\pm0.21} \kappa^{0.88\pm0.16}, \tag{4.10}$$

where L represents the physical size scaling needed to make the scaling relation dimensionally correct. Thus, it can be seen that the dimensionless parameter scaling approach yields a definitive prediction for the size scaling of confinement, even from experiments on a single machine. Comparison with the benchmark IPB98(y, 2) H-mode scaling (equation (4.3)) indicates reasonable agreement. However, transformation of variables in this direction compresses the most significant discrepancy (the different P scaling) because the large errors in the power-scaling exponent come from the error in the ρ_* scaling, not the β scaling. Using P as the dependent variable and W as one of the independent variables in the regression analysis would resolve some of the technical difficulties found in the regression analysis [136] and reduce the sensitivity to the power-scaling exponent in the transformation of variables between dimensionless and dimensional variables.

The same exercise for the results of the L-mode experiments is not as straightforward, due to the observed difference between the ion and electron ρ_* scalings. However, for the typical case of approximately equal ion and electron heat conduction, Bohm-like scaling of the energy confinement time is assumed here, with a 10% uncertainty assigned. The L-mode results from DIII-D can be summarized as

$$\Omega_i \tau_{th} \propto \rho_*^{-2\pm0.2} \beta^{-0.05\pm0.10} \nu_C^{0.2\pm0.03} q^{-0.8\pm0.1} \kappa^{1.6\pm0.2}. \tag{4.11}$$

Converting this to dimensional parameters gives

$$\tau_{th} \propto I^{0.40\pm0.08} B^{0.12\pm0.15} n^{0.51\pm0.04} P^{-0.52\pm0.04} L^{2.13\pm0.17} \kappa^{0.77\pm0.09}. \tag{4.12}$$

Comparison with the benchmark ITER97-L scaling for L-mode energy confinement (equation (4.4)) shows significant differences, especially in the current and power scalings. The power degradation inferred from the dimensionless parameter scaling experiments is much weaker due to the weak β dependence found there. The additional discrepancy in the I dependence is less straightforward to explain; the q scaling of heat transport in the DIII-D L-mode experiments would need to be more than two times stronger than that shown in figure 25 to bring the scaling derived from the dimensionless parameter scans into agreement with the scaling derived from the database analysis. This difference may be due to changes in a hidden parameter not included in the database, such as the flow shear stabilization of turbulence. For plasmas with a small pressure gradient contribution to E_r, the normalized rotational shearing rate is expected to scale as $|M/q|$. In the multi-machine confinement database, M is likely to be inversely proportional to q for current scans in discharges heating with uni-directional NBI power. The manifestation of this correlation would be a strengthening of the apparent

q scaling of the confinement scaling relation compared with q scaling experiments in DIII-D where M was kept fixed.

As discussed above, the largest discrepancy (and the one with the most significant consequences for optimization of tokamak fusion energy production) between the dedicated single-parameter scans from the dimensionless parameter scaling experiments and the database analysis transformed into the same dimensionless variables is in the inferred scaling with β. The condition of a recent version of the H-mode confinement database (DB3v12) was examined in detail [137] using principal component analysis to quantify the condition of the database. It was found that the standard deviation of the weakest principal component (the direction of least variation in the database) is very similar to that of the measurement of errors in that direction, and hence simple regression analysis may have a non-negligible bias in this direction. Interestingly, the form of this weakest principal component in terms of the dimensionless variables is $\beta^{0.5}\nu_{\mathrm{C}}^{-0.3}q_{\mathrm{cyl}}^{-1}$. Given this form, multiplication of the resulting confinement scaling by a factor that is this weakest principal component raised to a power can transform degradation of $B\tau_E$ with respect to β into degradation with respect to ν_{C} with minimal change in the fitting residuals. This would move both the β scaling and the ν_{C} scaling closer to the single-parameter scan results.

Further tests of the latest version of the H-mode confinement database indicated other potential problems with simple regression analysis related to the one discussed above [136]. The database was shown to have limited variation in ion mass (A) and cross-section shape (characterized by elongation κ or surface area). To avoid bias due to the insufficient population of the database in these directions, a selection of the database containing only deuterium data and κ in a narrow range was made. A selection was also made in the allowed range of the safety factor. Coupled with the limited range in κ, this has the effect of removing B as an independent variable. The predicted bias in this direction was not the same magnitude as that predicted when κ and A were included, so it is not obvious from purely statistical arguments that it should be removed. From the pragmatic perspective, this restriction is logical, because the goal of the exercise was to improve the projection of the confinement time to ITER plasmas with $q_{95} = 3$. The standard regression analysis assumes that the independent variables are known perfectly and only the dependent variable has uncertainty. This, of course, is not the case for any experimental data, but the analysis will work if the dependent variable has larger uncertainty than any of the independent variables. A more elaborate regression technique (errors-in-variables method) can properly treat cases where the independent variables have significant uncertainties. Both the restriction of the dataset and the errors-in-variables method were applied to the H-mode database. When applied independently, both analysis refinements lead to a reduction in the inferred β scaling. However, the analysis showed that the β scaling exponent was quite sensitive to the choice of the relative size of the stored energy and power uncertainties. This again seems to indicate the need for a better-conditioned database.

Fortunately, in projecting to the confinement expected for the baseline ITER scenario, only the ρ_* dependence is significant. Since the β values in the database are similar to those expected for ITER operation, the dependence of the confinement time on β does not affect the projection. However, for reactor designs that operate at high β such as compact ignition devices [135] or tight aspect ratio reactor designs [138] there is a significant difference in the projected confinement time and dependence of fusion gain on β. (See, for example, figures 13 and 14 in [81] or figure 3 in [136].) Use of the confinement scalings derived from the database analysis could yield optimizations or projections for these types of tokamak operation that are too pessimistic, due to the bias against high β operation.

A different approach to interpretation of energy confinement time data with dimensionless parameters has been used to determine scaling relations from a dataset from the Wendelstein

VII-AS stellarator [139–141]. The analysis described earlier in this section is simply a transformation of variables of the scaling relation derived by regression analysis from the physical fitting variables into dimensionless variables. This alternative approach used to analyze the stellarator data is very much in the spirit for introducing dimensionless parameters of the early Connor and Taylor work (section 2.2). The analysis employs a Bayesian statistical approach to find the most likely scaling for the dataset from a variety of physically motivated scalings. Neither a detailed exposition nor a detailed critique of the approach is within the scope of this review; rather, a flavor of this alternative approach and a few simple observations about the results are offered here. A description of how the Bayesian statistical approach applies to this analysis is given in [139].

In the initial work [139], scalings from six different physical models (four kinetic and two fluid models) were compared with the Wendelstein VII-AS data. These models all have simple power-law forms for the physical models. In this Bayesian approach, the first result is a probability that a hypothesis (here the dimensional relation implied by the physical model) is true, given the existing data. Out of the six models tested, the highest probability was that assigned to the collisionless high β model, indicating that this provided the best description of the dataset. The selection of this model as best describing the data is somewhat surprising, since the range of collisionality and β in the dataset would seem better described as collisional low β. It is interesting that this statistical approach does not automatically favor models with more free parameters. The conditional probability takes into account that the addition of another free parameter (here the addition of collisions) does not improve the description of the data. It was noted that the variation of the conditional probability was not large enough to infer definitively against the other kinetic models. For each of the models, the analysis also provides quantitative estimates for the power-law exponents for evaluation of the scaling relation.

In an extension of this analysis [140, 141], the choice of power-law dependence for the scaling relation is relaxed in favor of a more general series expansion in the dimensionless parameters. The conditional probability now has an additional parameter, the expansion order. With this change in basis, the conditional probability favored the collisional low β model, as might be expected from the parametric range in the dataset, with very high discrimination. Comparison of data from single-parameter scans in the dataset to the description of the data using this more general form shows a better reproduction of the trends than that given by standard regression analysis. However, the results obtained using this basis appear to be very sensitive to variations in the data near the ends of the parameter range in the dataset. This sensitivity leads to large increases in the confidence intervals outside the range of the existing dataset; therefore, the technique appears unsuitable for extrapolation in any direction. The strength of this method appears to be in the identification of the proper dimensional constraints. This may contribute indirectly to the more challenging question of how to extrapolate confinement data to a future device.

4.2. Use of the confinement databases for validation of the single-parameter experiments

Single-parameter dimensionless parameter scaling experiments and compilation of a multi-machine database are complementary approaches to understanding the processes that lead to energy transport in magnetic confinement devices and to predicting (or optimizing) the confinement in future experiments. In the previous section, the single-parameter scan results were used to validate the database analysis. In this section, some original work is presented that attempts to validate the dimensionless scaling work using the confinement databases. This work is by no means comprehensive; rather, in the spirit of a review, it is intended to demonstrate the potential of this method and will hopefully stimulate further work in this area.

Some initial steps along these lines have been published [135]. As discussed in section 3.3, the scaling of H-mode transport is consistent with the theoretical expectation of gyroBohm scaling. In section 3.4, the H-mode experiments consistently showed that the transport was independent of β, consistent with theories of electrostatic turbulence. Imposing these two robust scaling results in a regression analysis of the H-mode confinement database, along with the constraint that the inferred scaling must be dimensionally correct, results in an energy confinement scaling relation (called here DS03):

$$\tau_{\mathrm{th,DS03}} = 0.028 I^{0.83} B^{0.07} n^{0.49} P^{-0.55} R^{2.11} \varepsilon^{0.3} \kappa^{0.75} A^{0.14}. \tag{4.13}$$

Imposing the gyroBohm and electrostatic constraints results in only a small increase in the rms error in describing the database. Comparing to the IPB98(y, 2) scaling derived from an earlier version of the same database (equation (4.3)), the most significant differences are the weak power degradation and the slightly stronger size scaling in the DS03 scaling. This scaling gives a favorable projection for the fusion performance in future burning plasma devices, especially for high-β operation [81, 135].

One of the fundamental assumptions of the dimensionless scaling approach is that the smallest dimensionless parameter—the reciprocal of the number of particles in a Debye sphere (N_{D})—can be ignored (section 2.4). With the large variety of plasma parameters contained in the databases, the validity of this assumption can be tested. In figure 35, the ratio of the measured confinement times in the database to various scaling predictions is plotted against $(W/V)^{3/2}/n^2$, where V is the plasma volume. This quantity is a proxy for the average number of particles in a Debye sphere. The ratio of the measured confinement time to the confinement scaling is basically a method of plotting the residual trends that are not described by the scaling. The free fit (figure 35(a)) appears largely independent of N_{D}, while the IPB98(y, 2) fit (figure 35(b)) seems to introduce an upward trend with increasing N_{D}. The residuals from the DS03 fit appear to have little trend with N_{D}. A concrete interpretation is difficult to put forward without more extensive analysis, but these plots indicate that the assumption that N_{D} is ignorable is supported generally by the H-mode confinement database.

Another assumption made in the choice of the dimensionless variables for confinement used here is that atomic physics is unimportant. For the data in the H-mode database, bremsstrahlung is negligible as a power loss. Since the atomic physics would enter the power balance largely through line radiation and charge exchange losses, the physical dimension of the plasma compared with typical neutral penetration lengths would be important, if atomic physics played a significant role in the power losses. In figure 36, the fit residuals are plotted against the minor radius of the plasmas. The residuals appear to be largely independent of a for all three fits, consistent with the assumption that atomic physics is ignorable in the dimensionless analysis.

A similar dimensionless scaling relation for L-mode plasmas, imposing constraints from the dimensionless scaling experiments, has not been derived. However, the residual from the ITER97-L fit to the L-mode database can be displayed in the same manner as the H-mode fits discussed above. In figure 37, the residuals are plotted against the same proxy for N_{D} discussed above. There appears to be a correlation of the residuals with N_{D}, especially in the ASDEX and TFTR data. The fact that there is a trend is consistent with the observation in section 4.1 that the ITER97-L scaling is not dimensionally correct. As discussed above for H-mode plasmas, the trend with N_{D} can be the result of correlations in the database that affect the fit or could be a real physics issue. With a colder edge, L-mode plasmas could be more susceptible to atomic physics playing a significant role. To check this, the residuals are plotted against minor radius in figure 38. There is notable structure in this plot, with an apparent trend downward with increasing plasma size. This could indicate some influence of neutrals

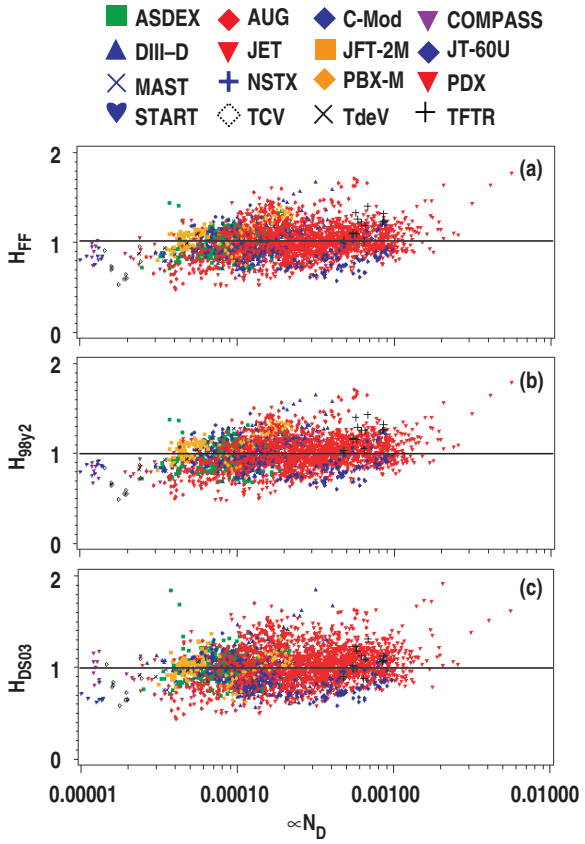

Figure 35. Plot of the ratio of the measured H-mode energy confinement time to the predicted energy confinement time versus a quantity proportional to the average number of particles in a Debye sphere (N_D) for three different scaling relations: (*a*) a free fit (equation (4) from [136]), (*b*) the IPB98(y, 2) scaling and (*c*) the DS03 scaling. The symbols indicate data from different tokamaks as noted in the legend.

in the smaller machines on the scaling. It would also be interesting, but beyond the scope of this review, to separate out the data by limiter and divertor L-mode operation, and by wall conditioning techniques.

As a final pair of examples, the residuals of the IPB98(y, 2) and DS03 fits to the H-mode database are plotted against β_N (figure 39) and ν_C (figure 40). (Here β_N is used rather than β to show where the data lie relative to the MHD limits. The definition of β_N and a discussion of its meaning are given in section 5.4.1.) There is an obvious trend in the IPB98(y, 2) residuals with β_N (figure 39(*a*)). For example, note the JFT-2M and PBX-M data in orange ranging from 0.8 at the lowest values of β_N to 1.3 at the highest values. This trend is in the direction such that confinement at high β is underestimated by the IPB98(y, 2) scaling relation. The DS03 residuals have a smaller global trend, indicating the scaling independent of β is consistent with the database (figure 39(*b*)). Plots of the individual machine data (not shown) bear out this difference in the trends of the residuals with β_N. This analysis is one of the strongest pieces of evidence that the strong β scaling implied by the IPB98(y, 2) fit is an artefact of the regression analysis and is not found directly in the data. The residuals from the IPB98(y, 2) fit have a slight downward trend with ν_C (figure 40(*a*)), consistent with the anti-correlation of

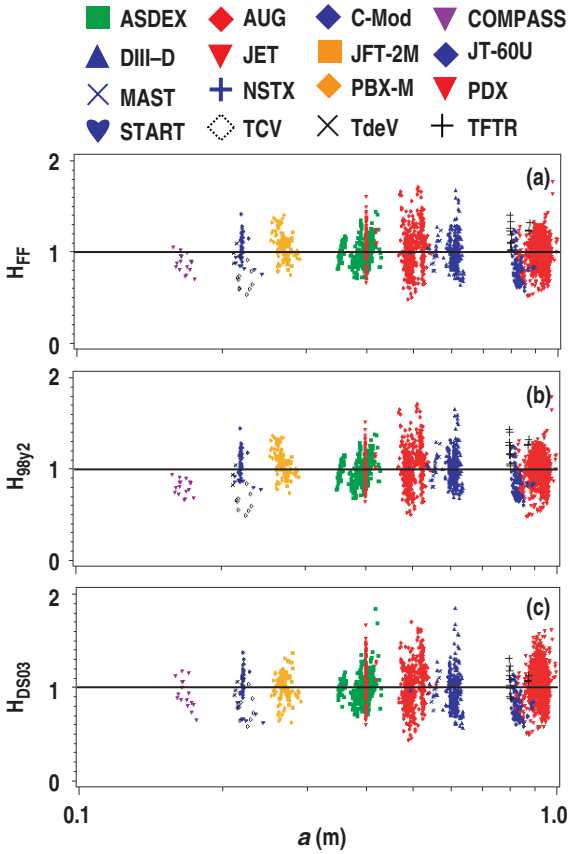

Figure 36. Plot of the ratio of the measured H-mode energy confinement time to the predicted energy confinement time versus minor radius (a) in m for three different scaling relations: (a) a free fit, (b) the IPB98(y, 2) scaling and (c) the DS03 scaling. The symbols indicate data from different tokamaks as noted in the legend.

ν_C and β in the smallest of the principal components, discussed in section 4.1. The DS03 fit (figure 40(b)), which was not constrained with respect to ν and has a weaker ν_C dependence than the IPB98(y, 2) fit, still has a slight residual trend. Both fits underestimate the data at low collisionality, but correlations with the appearance of hot-ion modes at low ν_C (corresponding to another neglected parameter, T_e/T_i), which have correspondingly better confinement, may explain this trend without implying an intrinsic ν_C scaling.

As stated in the introduction to this section, the purpose of these plots is to illustrate a new potential use for the confinement databases that has not been exploited up to now. Further studies, such as using the database to confirm the hypotheses about the breaking of the gyroBohm scaling with L_n or magnetic shear, could be carried out. The main conclusion of this work is that the combination of the results from the single-parameter scan experiments and the analysis of the databases is more powerful than the application of the two methods independently.

An even more ambitious analysis of JET transport data has been tried along these lines [142]. The basic philosophy was to attribute all of the variation in the thermal diffusivity inferred from power balance analysis (both the radial dependence within a single plasma and the parameter dependence from discharge to discharge) to power-law dependence on

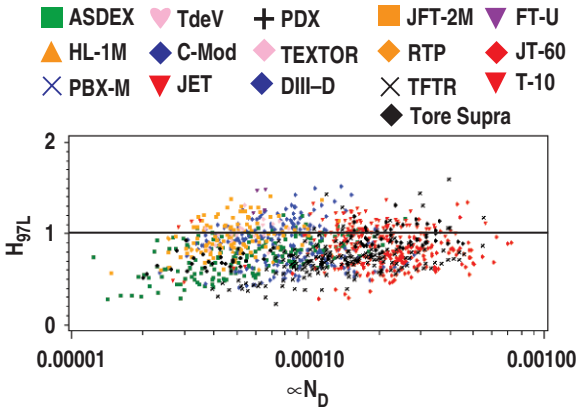

Figure 37. Plot of the ratio of the measured L-mode energy confinement time to the predicted energy confinement time from the ITER97-L scaling versus a quantity proportional to the average number of particles in a Debye sphere (N_D). The symbols indicate data from different tokamaks as noted in the legend.

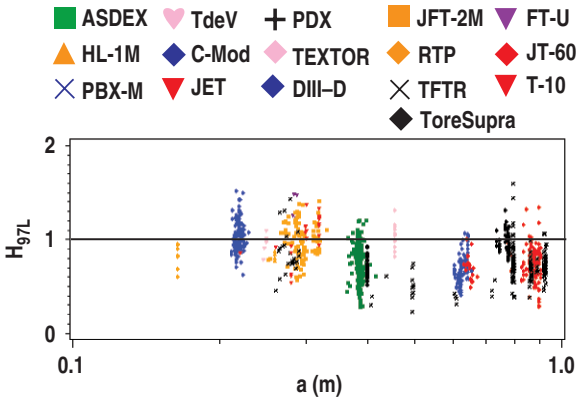

Figure 38. Plot of the ratio of the measured L-mode energy confinement time to the predicted energy confinement time from the ITER97-L scaling versus minor radius (a) in m. The symbols indicate data from different tokamaks as noted in the legend.

the dimensionless parameters. Analysis of the JET transport database found a favorable β dependence for the effective thermal diffusivity, $\chi_{\text{eff}} \propto \beta^{-0.57\pm0.05}$. The ν_C scaling derived from the database for the effective thermal diffusivity was $\chi_{\text{eff}} \propto \nu_C^{0.54\pm0.03}$, which is somewhat stronger than found in the single-parameter scans. It was suggested that the stronger mass dependence reported from the JET dataset may be due to the effect of the mass scaling of the H-mode power threshold. While these results are interesting, the omission of q in the scaling analysis seems to be a key issue, given the strong variation of q with radius and the strong scaling of H-mode transport with q (section 3.6). Even with the inclusion of q, there is no restriction from dimensional analysis on the dependence of transport on ratios of like quantities that have a strong radial dependence, such as the cross-sectional shape or the trapped-particle fraction. It would seem that a free function that is only dependent on radius and not the dimensionless variables would need to be included to account for these variations.

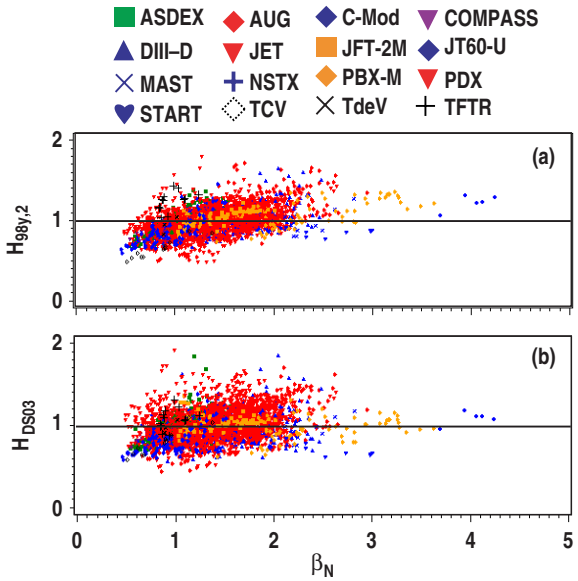

Figure 39. Plot of the ratio of the measured H-mode energy confinement time to the predicted energy confinement time versus normalized pressure (β_N) for two different scalings: (a) the IPB98(y, 2) scaling and (b) the DS03 scaling. The symbols indicate data from different tokamaks as noted in the legend.

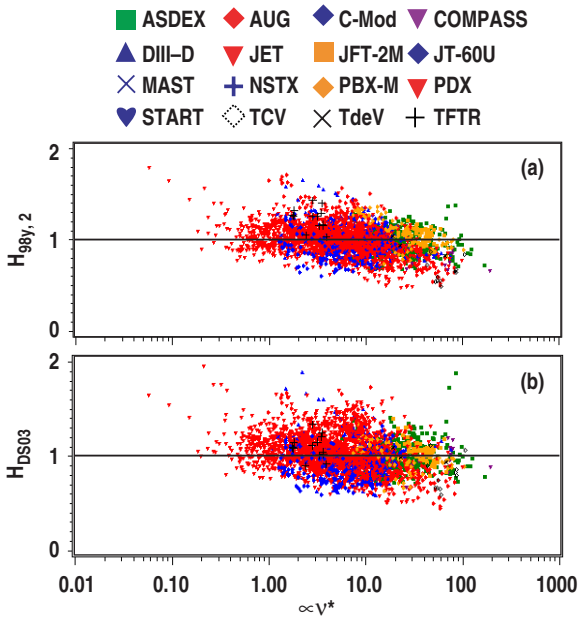

Figure 40. Plot of the ratio of the measured H-mode energy confinement time to the predicted energy confinement time versus a quantity proportional to the collisionality (ν_C) for two different scalings: (a) the IPB(y, 2) scaling and (b) the DS03 scaling. The symbols indicate data from different tokamaks as noted in the legend.

4.3. Summary and discussion

As discussed in the introduction to this section, the availability of large databases of global parameters related to energy transport provides an opportunity to check the validity of the two approaches to projecting the present data on confinement to future experiments—regression analysis of the database and scaling of dimensionless variables. The databases provide a significant validation of the key assumption of the dimensionless scaling approach—namely, that the dimensionless parameter related to the Debye length is ignorable compared with the other dimensionless parameters. The ρ_* scalings that arise from regression analysis of both the L-mode and H-mode databases are consistent with the trends seen in the dedicated ρ_* scaling experiments. This is very important, since the ρ_* scaling is the most critical for projections. However, the comparisons discussed here indicate that several significant discrepancies exist between the regression analysis of the databases and the dimensionless scalings inferred from single-parameter experiments. The most notable of these discrepancies are those in the inferred scalings with β in H mode (figures 17 and 39), with q in both L mode and H mode (figure 25), and with cross-section shape in L mode and H mode as characterized by κ (figure 26). These dependences are critical in the optimization of the design of a future tokamak, and the present information indicates the scaling relations should be used with great caution for this type of work. The first steps in generating scaling relations from the databases with constraints imposed by the dimensionless scaling experiments were discussed here. Further work along these lines could yield scaling relations that are more trustworthy for the design and optimization of future tokamaks.

5. Dimensionless parameter scaling applied to other areas

The success in applying dimensionless parameter scaling to energy and particle transport issues has encouraged applications in other areas of magnetic fusion studies. Significant questions, such as whether atomic physics is a crucial element in the transition between L-mode and H-mode confinement, are beginning to be addressed with the principles discussed in this paper. Four areas of plasma physics where dimensionless parameter scaling arguments are being applied are considered in this section—the L–H transition, H-mode edge pedestal behavior, divertor and scrape-off layer (SOL) physics and MHD phenomena. Another area that uses dimensionless parameters to interpret experimental results, non-inductive current drive [143], will not be reviewed here. Theoretical models of non-inductive current drive are generally tractable by analytic or numerical methods and correspond well to experimental observations; therefore, dimensional analysis is not expected to bring any additional insight to this area.

5.1. L–H threshold studies

The transition from L-mode behavior of the edge plasma to H-mode behavior is normally discussed in terms of a threshold controlled by the power flowing through the plasma boundary. In the energy confinement experiments discussed previously, the power was a free parameter. If the power in identity experiments scaled as expected from the dimensional analysis, then the variables chosen were deemed to properly describe the plasma behavior. When the scaling of a threshold phenomena under study has the power as the control variable, as is the case with the L–H threshold, the freedom to vary the input power as a means to make the dimensionless parameters match is lost. This makes the experimental determination of the dimensionless parameter scaling of such a threshold quite difficult. Efforts to determine the size scaling

of the L–H threshold power have focused more on experiments with similar dimensional parameters [144] or regression analysis of multi-experiment databases [20].

Analysis of the international database has indicated that the scaling of power threshold for the L–H transition in tokamaks can be described by the same plasma physics variables as the energy transport in the core plasma. Given this choice of variables, free fits to the database are nearly dimensionally correct [145]. If the power threshold depended strongly on neutral atom density or ripple losses of ions, it does not seem likely that good fits to the database using these variables could be obtained that are dimensionally correct.

Several authors have attempted to identify appropriate dimensionless scaling parameters, starting from theoretical models for the edge behavior. Models that assume the threshold is controlled by the edge radial electric field [146], velocity shear stabilization of drift and interchange turbulence [147] or electromagnetic effects on drift turbulence [148] all yield either a dimensionally correct threshold power scaling or at least a set of dimensionless parameters that should describe the variation of the threshold power. In principle, identity experiments with the various dimensionless parameter sets could be carried out to test these various theories.

Identity experiments of this type have been attempted between ASDEX-Upgrade and both JET and Alcator C-Mod [149]. The dimensionless variable set chosen for testing was ρ_*, β, ν_C and electron temperature T. (It was implicitly assumed that q was constant in all cases.) The latter is, of course, not a dimensionless variable. It could be made dimensionless by introducing atomic physics parameters [150] or equivalently and more directly by introducing the first ionization potential of the working gas E_0 as a dimensional parameter [151] and using the ratio T/E_0. Since E_0 has the same units as T, it only appears as a ratio of quantities with like units and will not affect the other dimensionless quantities (section 2.1). It is clear that all four of these parameters cannot be simultaneously matched when comparing two different experimental devices, unless the working gas is changed, which it was not in these experiments. The method adopted in the JET/ASDEX-Upgrade experiments was to compare the scaled electron temperature profiles just before an L–H transition (induced by a slowly increasing auxiliary power) with density and B scaled appropriately to match three of the four dimensionless parameters $\{\rho_*, \beta, \nu_C, T/E_0\}$ in turn. It was found that the scaled electron temperature profiles matched just prior to the L–H transition only when the density and B were scaled so as to match the set $\{\rho_*, \beta, \nu_C\}$ (figure 41). In other words the L–H transition was not observed to occur at a given threshold temperature. This was interpreted as evidence that the L–H transition is a plasma physics effect, not strongly influenced by atomic physics (neutral particle effects) at the boundary. While the ability to make a match between machines of these three parameters is compelling, the key question is how the threshold power scales when the match is made. The power scaling was not discussed for the JET/ASDEX-Upgrade experiments. In the case of energy confinement, the expected power scaling is derived from the relation $B\tau_E = \text{const.}$, which gives $Pa^{3/4} = \text{const.}$ for identity experiments (section 3.2). This is the method for determining the power scaling given for the various cases in [149]. (There appears to be an error in equation (2) of [149]—it should be $P \propto R^{3/2}$.) If the L–H threshold is governed by a transition at some boundary set by plasma physics parameters, with power as the control variable, then the scaling of the threshold power probably has the same scaling in a threshold identity match experiment as that found in a transport identity experiment. In any case, a heuristic formula for the threshold power scaling with size could be determined, but this was not done for the JET/ASDEX-Upgrade matches in [149]. However, in a previous report [152], the threshold powers for both machines are given for two cases. In the first case (for which the profile match is shown in [149, 152]), the threshold power is the same for both experiments, so the identity relation is not satisfied. In the second case (for which no profiles are shown for JET), the power scaling is close to $P \propto R^{-1}$, not far from the identity scaling. It

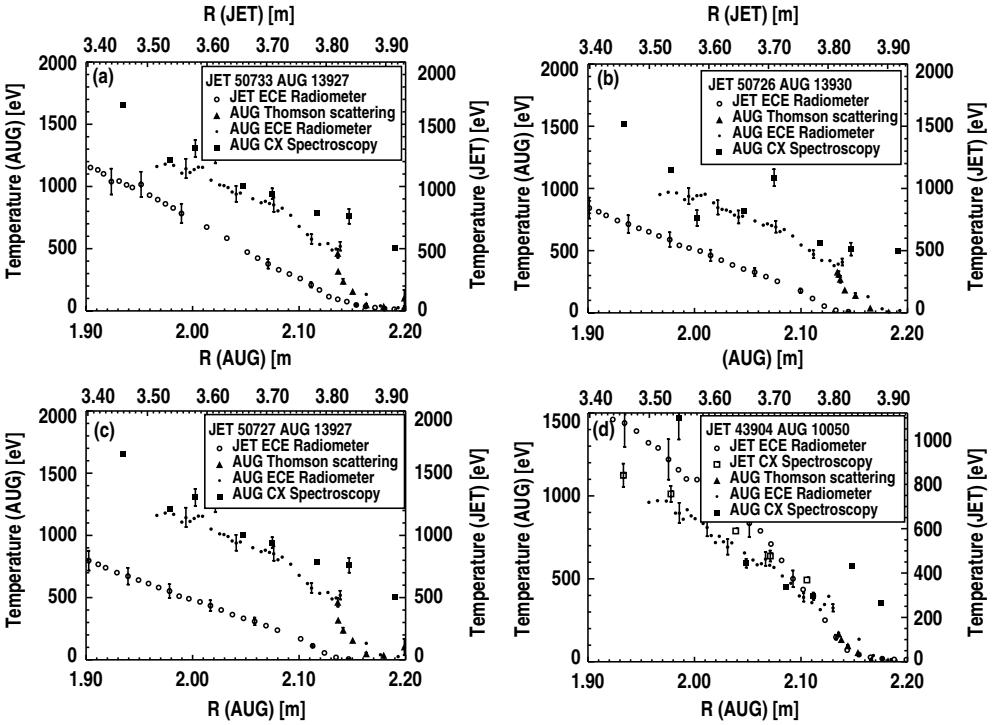

Figure 41. Edge electron and ion temperatures at the plasma edge just before the L–H transition in JET and ASDEX-Upgrade for conditions attempting to match different parameter sets (*a*) β, ν_C, T, (*b*) β, ρ_*, T, (*c*) ν_C, ρ_*, T (*d*) ρ_*, ν_C, β. Reprinted from [149] by permission.

is not clear whether these powers have been corrected for the time dependence of the heating or transient effects such as sawteeth that would alter the estimate of the power flow through the edge.

Attempts to obtain an identity match before the L–H transition in ASDEX-Upgrade and Alcator C-Mod were unsuccessful [149]. Only scaling using the set $\{\rho_*, \beta, \nu_C\}$ was attempted in this case. If the scaled density values matched, then the scaled electron temperature just before the L–H transition is much higher in ASDEX-Upgrade. The speculation was raised that neutral particle effects are more significant in Alcator C-Mod. However, this would need to be reconciled with the previous conclusions in the JET/ASDEX-Upgrade comparison.

The operational difficulty of obtaining an identity match for threshold phenomena should not be underestimated. In cases where the scaling of a threshold in power (such as the L–H threshold) or in β (such as MHD stability) is sought, a simple method is suggested here for the first time. In order to have a concrete example, the parameter set $\{\rho_*, \beta, \nu_C, q\}$ is chosen. To test this parameter set in an L–H threshold identity experiment between two devices, a β scan is recommended where both machines operate with the same ρ_*, ν_C and q. As described in the previous section on energy transport, a β scan entails a substantial change in power ($P \propto B^4$), while only requiring smaller changes in the other control parameters ($n \propto B, I \propto B$). Therefore, the scan, by definition, allows a scan of power (or β) with high resolution while maintaining the other parameters fixed. If the L–H threshold appears at the same β and the normalized powers match, then this set of parameters would be validated as sufficient to describe the variation of the L–H transition. In this specific case, the L–H

transition is known to be quite sensitive to the geometry of the plasma, so care must be taken to match this well. In addition to these considerations, it is probably important to match the ion parameters (especially if momentum effects are important) and to avoid the low-density regime where the threshold deviates from a simple density dependence [153].

5.2. H-mode pedestal studies

The formation of steep density and temperature gradients near the last closed flux surface of a magnetically confined plasma is the essence of an H-mode plasma. Predictions of the fusion performance of future devices such as ITER have a significant dependence on the height of the so-called pedestal [154]. This height is defined as the density or temperature value where there is a significant break in slope from the steep gradient region to the more gradual gradients in core plasma [155]. The edge is subject to repetitive instabilities known as edge localized modes or ELMs that relax the density gradient and in some cases the temperature gradient [156, 157]. The effect of ELMs on the current density is expected to correlate with the pressure gradient, since pressure-driven currents are expected to be the dominant contribution to the edge current. However, the core profiles appear largely unaffected by ELMs. A complete predictive model would describe the full dynamics of this cycle, but this does not yet exist. The present approach is to seek solutions for individual parts of the problem as an initial step to the more complete solution. The pedestal conditions between ELMs are a part of the cycle that has been investigated experimentally using dimensionless parameter scaling techniques.

A key question in modeling the pedestal is whether the pedestal height is determined by transport, stability or source profiles. The pressure gradient just outside the pedestal can be modeled by assuming that the linear stability to intermediate-n ideal MHD modes sets an upper limit [158, 159]. This model describes various dependences of the gradient, but the limit does not explain the width of the steep gradient region, nor does it explain the evolution of the quantities relevant to the stability. The density pedestal width has been modeled by taking into account the poloidal dependence of the flux expansion in real space and the penetration of neutrals with temperature at the edge ion temperature [160]. However, this model requires the density pedestal height as input. The main parameter of interest is the temperature pedestal height, but no model exists at present for this. Scaling studies of various pedestal phenomena have been attempted using both dimensional and dimensionless parameters [155,161–164] with no clear consensus. A review of these studies is beyond the scope of this work, but the multitude of scaling parameters used points back to the role of identity experiments in identifying the appropriate variables for scaling.

Two attempts have been made recently to perform identity experiments in the H-mode pedestal in tokamaks. The first was a test of the parameter set $\{\rho_*, \beta, \nu_C\}$ and fixed geometry between DIII-D and Alcator C-Mod [165]. It was possible to match the scaled parameters in the two machines from the top to the bottom of the steep gradient region that forms the pedestal (figure 42). When the edge parameters match, the characteristic instabilities of the H-mode, including the appearance of an enhanced D_α mode, were observed to scale appropriately in the two machines. The similarity of the instability phenomena is a clear indication that their behavior is governed by the chosen parameter set. The ability to match the profiles in the pedestal region would also seem to validate the hypothesis that the plasma physics parameters govern the gradient region. This would contradict models of the density pedestal that are sensitive to the neutral source distribution [160, 166]. However, as pointed out in [165], the density profile match could be consistent with the density pedestal models referenced above. This would require the neutral source in Alcator C-Mod to be from main chamber recycling while the neutral source in DIII-D would need to be primarily from the divertor. This difference

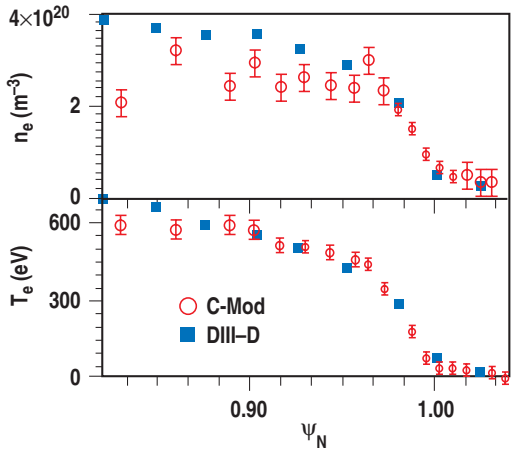

Figure 42. Time averaged profiles from Alcator C-Mod and DIII-D discharges with matched density pedestal height. DIII-D T_e and n_e are scaled as appropriate for an identity match to Alcator C-Mod parameters. Reprinted with permission from [165], Copyright 2003, American Institute of Physics.

in recycling location is consistent with reports from both machines [167, 168]. Subsequent attempts to match density pedestal profiles in DIII-D and JET have not been successful [169], perhaps due to both machines having similar neutral sources.

More recently, attempts have been made to match the same dimensionless parameter set in the pedestal region between JET and JT-60U [170]. A good match was not obtained to both density and temperature simultaneously. This is somewhat surprising since the machines are nearly the same size; therefore, the identity experiment in this case almost involves matching the dimensional parameters. The pedestal pressure is systematically lower in JT-60U, compared with JET (figure 43). It was not possible to match aspect ratio between the two machines, with the aspect ratio of the JET plasmas being 16% smaller than JT-60U plasmas. Since the pedestal pressure in JET is up to twice that in JT-60U, it seems unlikely that the relatively small difference in aspect ratio could be directly responsible for the difference in pedestal parameters. It was suggested that the difference in rotation at the edge could be responsible for the change in the pedestal height. In JET, the edge rotates in the direction of the plasma current, while in JT-60U the plasma rotates in the direction opposite to the plasma current, consistent with ripple loss of the NBI fast ions. If subsequent experiments with matched rotation yield a good identity match, this would be strong evidence for the role of the radial electric field in the determination of the pedestal height. (See section 3.3.3 for the relationship between rotation and E_r.) The mismatch could also be due to a change in the neutral source due to the lost ions in JT-60U. A detailed evaluation of the model [160] for the two machines would be interesting to assess whether this effect would have the trend observed in the measurements.

5.3. SOL and divertor

The various aspects of fusion plasmas discussed to this point pale in comparison with the divertor region in terms of complexity. The difference comes from the introduction of various excited atomic states of neutrals and partially stripped ions, which bring in all the details of atomic physics. In terms of dimensionless parameter scalings, this new regime requires the ratio of the density of each atomic state to some reference density such as the electron density.

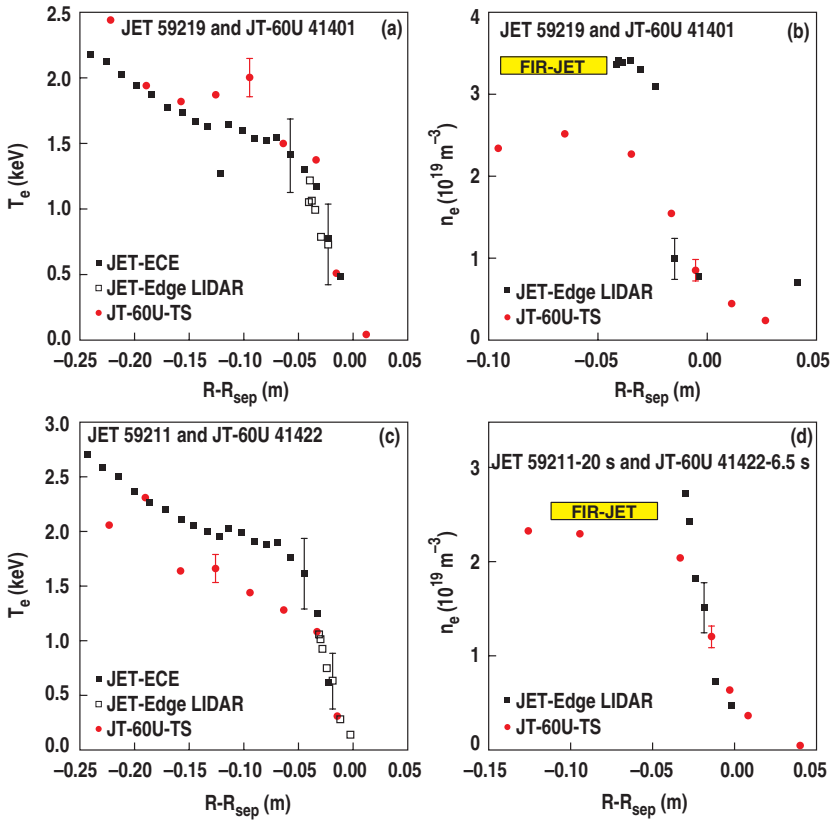

Figure 43. Comparison of edge T_e and n_e profiles for two pairs of plasma discharges: plots (*a*) and (*b*), JET/JT-60 pair with similar T_{ped} but different n_{ped}; plots (*c*) and (*d*), JET/JT-60U pair with similar n_{ped} but different T_{ped}. No simultaneous match of n_e and T_e was obtained. Reprinted from [170] by permission of the Institute of Physics.

In addition, the ratio of the excitation potential of each of these states (hc/λ) to the electron temperature is also required. As pointed out by Lackner [151], the only way to scale the entire SOL and divertor is to match the temperature exactly everywhere in the divertor, with some appropriate size scale factor. It is not possible to maintain fixed temperature while also maintaining the standard plasma physics variables $\{\rho_*, \beta, \nu_C\}$ and the geometry constant as the physical size is changed.

With this background, several authors have tried adding additional assumptions in order to arrive at some type of scaling relation. If finite β effects are neglected, then a similarity scaling of the divertor of P/R is obtained as the size is varied [151]. Subsequent authors have asserted that this scaling is subject to the additional constraint that only two-body excitation events are considered [171]. It is possible to include a more detailed description of neutral particle physics (while retaining a fluid plasma description) using the scale invariance approach, including the problems of detachment [172]. However, it seems unlikely that all of the dimensionless parameters identified (as many as 17 in [172], even with the impurity description reduced to a function of temperature only) can be controlled in an experiment. Relaxing the constraint that the divertor geometry should remain fixed, similarity scalings more readily satisfied over the size range between present-day tokamaks and ITER were obtained [173]. All of these attempts to apply dimensionless scalings to divertors tried to encompass the entire divertor. It

may be possible to isolate certain aspects of interest in divertor operation, such as heat flux or plasma flows, in order to reduce the number of dimensionless parameters required to describe the scaling of some piece of the divertor puzzle.

One such attempt isolates the scrape-off layer (SOL) width by assuming it is determined by transport perpendicular to B [174], Not surprisingly, the analysis follows the ideas in [10], beginning from various theoretical models and a consistency constraint on the dimensions. An impressive 24 models comprising 17 distinct theoretical approaches are tested in a least-squared error sense individually against COMPASS-D, Alcator C-Mod and JET data. The data from all three tokamaks were described best by models with significant electromagnetic components (collisionless skin depth or interchange mode). The next step would be to isolate the implied dimensionless parameters in these models and attempt an identity experiment to verify the sufficiency of these parameters to describe the SOL width. Similarly, the reduced descriptions in [151, 173] could be tested by identity experiments in existing machines.

5.4. MHD studies

The use of dimensionless parameters in theoretical MHD equilibrium and stability studies is quite extensive. The main dimensionless parameter of ideal MHD is the ratio of the kinetic pressure to the magnetic pressure, β. Instabilities are classified according to the free energy source that drives them—current-driven modes or kink modes, which can occur at $\beta = 0$, or pressure-driven modes, which require $\beta > 0$. The equilibria, of course, are characterized by many dimensionless numbers that are ratios of like quantities; for example, safety factor q, aspect ratio R/a, elongation κ, triangularity δ, etc.

When finite temperature effects are included, more modes that are liable to instability are supported by the equations, due to the effects of dissipation. Dissipation of current flow is characterized by a resistivity, while dissipation of mass flow is characterized by a viscosity. Two new dimensionless numbers appear—the Lundquist number S, which is defined as the ratio of the resistive diffusion time to the Alfvén time, and the magnetic Reynolds number R_m, which is defined as the ratio of the viscous diffusion time to the Alfvén time. Two new types of instabilities appear under the name 'resistive'. One involves a change in magnetic topology ('tearing' modes), while the other represents a modification of ideal modes to have a complex frequency ('resistive kink' or 'resistive ballooning'). Both types are unstable for parameters where ideal modes are stable. There has been considerable discussion in the literature about the set of dimensionless parameters that best describe the calculated instability threshold in the presence of finite resistivity and viscosity. The consensus [175–178] appears to favor the Hartmann number [$H \equiv (SR_\mathrm{m})^{1/2}$] over the magnetic Prandtl number ($P_\mathrm{m} = S/R_\mathrm{m}$) defined in analogy with fluid dynamics. While there is some debate over the need to retain viscous effects in fusion plasmas [179, 180], the set of parameters $\{S, H\}$ appears to classify compactly the stability of modes supported by the MHD equations with scalar resistivity and viscosity.

As pointed out by Connor [11], it is possible in some cases to take advantage of knowledge of the underlying equations using the scale invariance approach to obtain some information about combinations of dimensionless parameters, including ratios of like quantities, that appear naturally in the system of equations. The example of resistive MHD in the large-aspect ratio tokamak limit where $\beta \sim a/R \sim B_\mathrm{P}/B << 1$ yields the set of dimensionless parameters:

$$\tau/\tau_\mathrm{R} \propto F(\beta/\varepsilon, S, q), \tag{5.1}$$

whereas the complete set of equations would have β and ε appearing as separate dimensionless parameters. However, the reader may recall the rule of thumb introduced in the discussion of dimensional analysis (section 2.1) that N small dimensionless parameters of the same order

can be made into $N-1$ dimensionless parameters of O(1) and one small parameter. Applying this to the large-aspect ratio tokamak ordering parameters with B_p/B as the remaining small parameter yields directly $\beta(B/B_P)$ and aB/RB_P, which are closely related to the standard parameters β_N and q that characterize MHD stability. This example illustrates again that the dimensional analysis and scale invariance approaches are complementary methods capable of reaching the same conclusions.

When individual ions exceed the local Alfvén velocity v_A, Alfvén waves can be excited, analogous to Cherenkov emission of light. Under certain conditions, these waves are unstable and can modify the fast ion distribution in both velocity space and real space. In addition, a large fast ion population can support new modes that can also be unstable. This area is the focus of a great deal of theoretical and experimental research due to the key role played by fast ions in burning plasma experiments. With the addition of fast particles, dimensionless parameters describing their distribution function (relative density, trapped fraction, anisotropy, relative slope near the Alfvén velocity, etc) appear in the theory in addition to v/v_A. A complete description of which dimensionless parameters are important is beyond the scope of this section.

Given the emphasis on dimensionless parameters in MHD theory, it is somewhat surprising that there is little experimental verification of these concepts by direct experiment. This can be somewhat explained by two observations. First, the growth rates of both ideal and resistive modes in fusion plasmas are fast enough that it is difficult to observe the linear phase experimentally. Second, MHD stability (ideal and resistive) is sensitive to the details of the current density profile. Routine measurement of this quantity with sufficient precision is only recently available on some experiments. Given these difficulties, the focus of experiments has been on the stability boundary, with some success as discussed below.

5.4.1. Global mode stability. Calculations of MHD stability of tokamak plasmas to both kink modes [181] and ballooning modes [182] indicated the pressure limit could be characterized by a single dimensionless parameter $\beta_N = \beta/(I/aB)$. (Unfortunately, this 'dimensionless' parameter is not actually dimensionless in the conventional definition [183]. It can be made dimensionless as in [181] by dividing by μ_0, but this would also introduce an additional numerical factor from the conventional definition.) Large experience in tokamak operation has validated this parametrization [184]. The description of the stability boundary has been further improved by including the dependence of the boundary on spatial moments of the current distribution (such as internal inductance ℓ_i) [184] and pressure peaking [185]. This work is somewhat analogous to the use of the global energy confinement database to identify key dimensionless variables.

Direct dimensionless scaling experiments on MHD stability have been reported for a few areas. The most active area is that of tearing mode stability. In order to test the hypothesis that the onset of an $m = 2/n = 1$ tearing mode is a function of the standard set of plasma fluid dimensionless parameters $\{\rho_*, \beta, \nu_C\}$ in geometrically similar discharges, identity experiments were carried out between DIII-D and JET [186]. Matches were obtained at the 10% level, as illustrated in figure 44. The onset β values mapped in the control parameters n and B with appropriate scalings to compare the two experiments are shown in figure 45. The onset β values are similar in the region of control parameter space where there is near overlap. The variation in the onset β is of similar magnitude to the variation in the control parameters, such as the ion temperature. This comparison indicates that the dimensionless parameters chosen were adequate to describe the stability boundary. However, there is clearly still potential for carrying out a more definitive comparison.

One motivation for this comparison was to validate previous global database studies of the $m = 3/n = 2$ tearing mode onset [187] and similar studies of the $m = 2/n = 1$ onset [186].

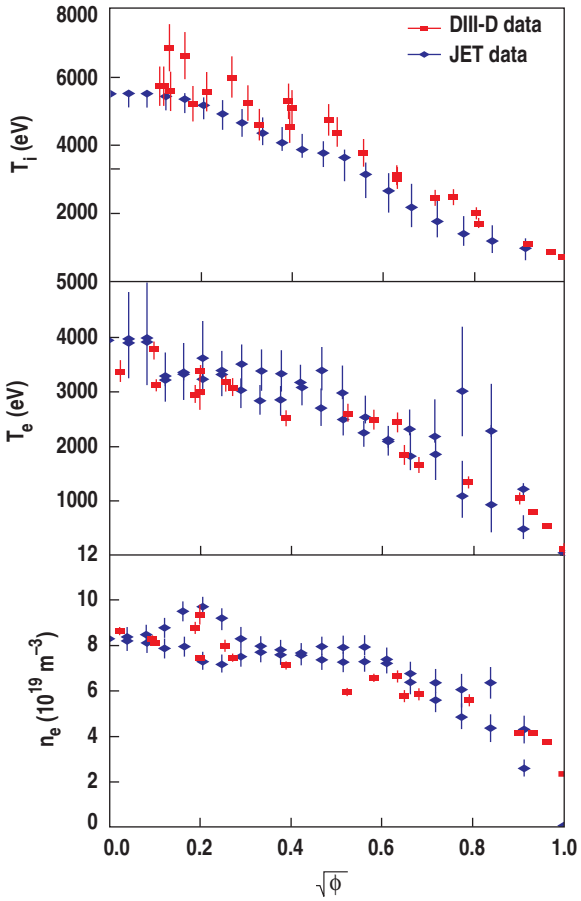

Figure 44. Comparison of ion temperature, electron temperature and density profiles from the JET and DIII-D tokamaks at the onset of an $m = 2/n = 1$ tearing mode. The radial variable used is the square root of normalized toroidal flux. The JET data are scaled to DIII-D size according to non-dimensional scalings (na^2 and $Ta^{0.5}$ constant). The density for the DIII-D case is slightly below that required for a non-dimensional match and correspondingly the ion temperature is slightly above. Reprinted from [186] by permission.

Similarly to the energy confinement work reported in section 4.1, data from multiple tokamaks have been gathered for the purpose of solidifying a projection of the onset β for the ITER burning plasma experiment. Dimensionless variables that were indicated by theory $\{\rho_*, \nu_C\}$ were used as regression variables to describe the onset β. The regression for the $m = 3/n = 2$ mode [187] indicated a strong dependence on ρ_* (approximately linear) with a weaker dependence on collisionality when the data from individual machines were fit. The combined database has a weaker ρ_* scaling and no obvious collisionality scaling. The linear ρ_* scaling persists in individual machine studies ([188] and references therein). The regression analysis for the $m = 2/n = 1$ mode onset also shows a linear ρ_* scaling [186]. If this scaling proves true, it could have significant implications for ITER or other burning plasma experiments, since ρ^* is reduced by a factor of 3–10 from present-day experiments. A drop of that magnitude in the β at which tearing modes appear would essentially guarantee the presence of tearing modes in any H-mode discharge.

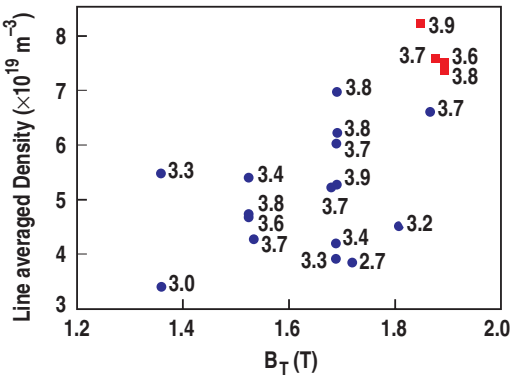

Figure 45. DIII-D data for the onset of $m = 2/n = 1$ tearing modes (closed circles) and JET cases scaled at constant ρ_*, ν_C and β_N to DIII-D dimensions (closed squares). The β_N is indicated for each case. Reprinted from [186] by permission.

Based on the experience gained in the energy confinement analysis in terms of dimensionless parameters, the methodology applied to the tearing mode analysis raises some significant concerns. The first concern is the condition of the database. Two pieces of evidence indicate that the databases may not be well conditioned. In [187], it is noted that the fit to the data of the three tokamaks combined is significantly different from the fits of the individual datasets. This could be a simple sampling issue, or it could indicate the influence of variables not included in the fit [189]. The second point is that the actual control variable dependences do not seem to describe the data. If the fit of the onset β for the $m = 2/n = 1$ mode found in [186] is transformed to the set $\{n, T, B, a\}$, then the dominant dependences are in B and a. Only weak dependences on n or T are obtained. The same is found for the $m = 3/n = 2$ fits in [188] and the individual tokamak fits in [187]. However, a plot of the $m = 3/n = 2$ data in [189] shows little dependence on a or B. This suggests that correlations in the database, originating either from operational or data selection correlations, are determining the relative exponents of ρ_* and ν_C. The commonly observed density dependence of the onset β is not recovered in the fit. Finally, the derived onset criterion does not predict the timing of the mode onset [189].

Another concern with the analysis is the use of the derived dimensionless parameters as the regression variables. As discussed in section 4.1, standard regression analysis assumes negligible errors in the regression variables compared with the fit variable. That is clearly not the case in this analysis. Either a complete regression including the regression variables errors or a fit in directly measured variables is recommended. In the case of fitting dimensional variables, the constraint of proper dimensions (section 4.1) can be applied to check the validity of the result and the condition of the database. As discussed in section 4.1, this is a necessary but not sufficient criterion on validity.

As with the L–H threshold, the design of a proper dimensionless parameter scaling experiment is not straightforward. The successful initial identity experiments for the $m = 2/n = 1$ mode onset [186] motivate exploring possibilities for a determination of the onset β scaling by direct dimensionless scaling experiments. Since the theory and experimental analysis suggest a strong ρ_* dependence, the onset envelope could be mapped by doing a sequence of ρ_* scans at fixed ν_C and increasing β. If a linear dependence of the onset β on ρ_* exists, then at some β the low ρ_* point in the scan will encounter a tearing mode. After finding that point, then the onset β at the high ρ_* value can be determined. By finding the extent by

which ρ_* can be varied at each β, the envelope of the onset β with ρ_* can be mapped. If there is no ρ_* dependence, the onset β should be the same at both ends of the scan. Since ρ_* can be scanned a factor of 1.5–2 in most divertor tokamaks, a fairly accurate determination of the ρ_* dependence of the threshold should be possible.

Identity experiments have also been carried out in the study of locked modes [190]. Locked modes are tearing modes that arise at very low pressure due to the response of tokamak plasmas to non-axisymmetric magnetic field perturbations. (By design, the tokamak is intended to be toroidally symmetric.) Thus, the modes are linearly stable, but nonlinearly unstable when considered as an initial-value problem. In order to understand the size scaling of the plasma response, plasmas with only ohmic heating and identical ρ_*, β, ν_* and q were probed with non-axisymmetric magnetic fields with $n = 1$ and similar poloidal mode spectra on Alcator C-Mod and JET. Neither the profiles nor the global averages of these quantities are given, so it is not possible to assess the quality of the match. The hypothesis was that the ratio of the applied non-axisymmetric field to the magnitude of the total magnetic field at the onset of the locked modes should be the same for plasmas with identical dimensionless parameters. This comparison was not shown directly, but the variation of the density at which locked modes appeared with applied non-axisymmetric field was consistent between the two experiments when the identity scaling is applied. Two caveats are noted in [190]. First, the intrinsic non-axisymmetric fields ('error' fields) in each machine must either be ignorable or taken into account. In the Alcator C-Mod analysis, the effect of these error fields was included in the analysis using results from other experiments, while the error fields in JET were evidently taken to be negligible. Second, the plasma rotation is not taken into account in the analysis. Screening of the non-axisymmetric fields in rotating plasmas by the skin effect should reduce the size of the perturbation in the plasma. The rotation was not controlled to give an identity match in the two machines, nor was the perturbation amplitude corrected for any screening. Analysis of the parametric dependences in these experiments using the constraint that the scaling should be dimensionless (similar to that discussed in section 4.1) indicated that the size scaling was favorable, in that larger machines should be less sensitive to non-axisymmetric fields.

5.4.2. Fast ion modes. A first attempt at a dimensionless scaling approach for Alfvén waves destabilized by fast particles has been made using DIII-D and NSTX [191]. These two machines are physically similar in their poloidal cross-section and minor radius, but have significantly different aspect ratios. It was also possible to operate DIII-D at low β, similar to typical NSTX values. The neutral beam injectors used for destabilization of the Alfvén waves on both devices have similar acceleration voltage and geometry. The experiment yielded quite interesting data, with parameters close to similar; however, in the end, the analysis was done on the basis of comparison with theoretical predictions.

One of the main goals was to verify formulae that predict an increase in the toroidal mode number n that is most unstable in burning plasmas, compared with present-day experiments. The formulae indicate NSTX should be unstable at n near 1, while DIII-D should have higher n ($\sim$5), and ITER still higher n ($n \sim$ 10–20). The experiment did corroborate the given formulae, but putting them into a form using dimensionless parameters suggests a more definitive experiment that could be done in a single tokamak. Two formulae that predict the n at which the modes are most unstable were specified in [191]. These are transformed here into dimensionless form. The first is

$$n_{\max} = aBZ_{\mathrm{f}}e/qc(8E_{\mathrm{f}}m_{\mathrm{f}})^{1/2} = (\beta_{\mathrm{i}}^{1/2}/8^{1/2}qM_{\mathrm{A}}\rho_{*\mathrm{i}})(Z_{\mathrm{f}}/Z_{\mathrm{i}})(m_{\mathrm{i}}/m_{\mathrm{f}}), \qquad (5.2)$$

where M_A is the ratio of the fast ion velocity to the Alfvén velocity, and the quantities with subscripts f and i refer to the fast ions and the bulk ions, respectively. The second formula is

$$n_{max} = (aZ_f e/cq^2)(\pi m_i n_e/m_f^2)^{1/2} = (\beta_i^{1/2}/8^{1/2}q^2\rho_{*i})(m_i/m_f)^{1/2}(n_e/n_i)^{1/2}. \quad (5.3)$$

Both formulae clearly indicate that the n of the most unstable mode will increase from NSTX to DIII-D to ITER due to the inverse ρ_{*i} dependence under otherwise similar conditions. This should be straightforward to test by scanning ρ_{*i} while holding the rest of the dimensionless parameters fixed. The two predictions can be distinguished experimentally by determining the q dependence or the M_A dependence of the most unstable n, again while holding the remaining dimensionless parameters fixed. Writing these formulae in dimensionless variables indicates directly the methods by which the important scalings can be tested.

5.5. Summary and discussion

In moving the application of dimensionless parameter scaling beyond the realm of transport to other important problems of magnetic confinement fusion, two significant new issues are encountered. For phenomena in the edge, it is no longer a good assumption that the ions are fully stripped or that neutral particle densities are negligible. These issues bring in a whole host of new physical variables. Dimensional analysis can provide no insight about some of these new variables (for example, ratios of densities of various charge states); in other cases, the new variables bring in extreme experimental difficulties (for example, ionization potentials). New situations also arise, such as plasma stability or the L–H transition threshold power, where the quantity whose scaling is desired is not a continuous variable but the boundary between two distinct states. The techniques to be used to deal with these new issues are still under development, and the experiments reported here are commendable as the first attempts to deal with them. In both the L–H threshold scaling and the stability of the plasma to tearing mode, identity experiments have been attempted to validate the approaches chosen. Potential improvements have been identified for future experiments examining threshold behavior and the stability of the plasma to modes driven by fast ions. These new horizons for the dimensionless parameter scaling techniques, while very challenging, also represent an opportunity to refine and improve the methods reviewed here.

6. Conclusions

Analysis in terms of dimensionless parameters has been shown to be a powerful tool in many areas of physics and engineering, particularly in the field of fluid mechanics. The results reviewed here indicate that the method is beginning to have a significant impact on experimental investigations in the field of plasma physics as well. The methods, as outlined in section 2, allow the determination of the number of independent dimensionless parameters and the algebraic relationship among the dimensional parameters from which the dimensionless parameters are composed. It is possible to begin either from an assumption of a theoretical description of the governing equations (using scale invariance) or from physical intuition about the processes of interest (dimensional analysis).

Evaluating the dimensionless parameters found by these methods for the situation of interest can reveal which parameters are essential (and which are negligible) for a description of the process of interest. More importantly, since these dimensionless parameters are

combinations of the observable or measurable quantities, the scaling of the phenomenon of interest with a physical variable that cannot be varied experimentally can be uniquely determined by variations of appropriate combinations of the dimensionless variables. The chief example of this capability discussed in this review is the determination of the size scaling of energy transport in magnetic fusion devices by scaling experiments in a single device. From the scale invariance approach, it is also possible to make a connection between the observed scalings and the physical mechanisms underlying the process. An example reported here is the lack of variation of the energy transport with β, the ratio of the kinetic pressure to the magnetic pressure. From this, it is likely that the dominant transport in present-day magnetic fusion devices arises from the fluctuating electrostatic ($\boldsymbol{E} \times \boldsymbol{B}$) drifts in the plasma turbulence, rather than the fluctuations of the magnetic field. This has long been asserted on theoretical grounds, but until the methods reviewed here were applied to experiments, there was no clear way to validate this assertion. Scaling with dimensionless parameters is proving to be a powerful tool in the understanding of plasma processes and the prediction of performance in future devices.

While the primary application of the dimensionless parameter methods has been in the area of energy and particle transport in magnetized plasmas, experimental work is beginning in the equally difficult and important areas of the stability of magnetized plasmas and the physics of the boundary layer between closed and open magnetic field lines. Work is just beginning in these areas, as discussed in section 5. It is still too early to see whether these methods will have the same impact as in the transport physics area. The essential step of validating the dimensionless parameter set by means of 'identity experiments' has just started in the stability area.

Even though these methods are quite powerful, they have clear limitations. The basic methods of dimensional analysis give no information about the importance of dimensionless parameters that are ratios of like quantities, such as the surface roughness of a sphere moving in air or the geometric quantities that describe the cross-sectional shape of a tokamak. The importance of ratios of like quantities must be determined experimentally, as in the examples of q, A and $T_\mathrm{i}/T_\mathrm{e}$ dependence discussed in section 3. These quantities are known to be essential to their respective problems, but the dimensionless parameter methods discussed here cannot identify them or quantify their importance.

As with all powerful and useful tools, the success of the concept of dimensionless parameter scaling has spawned many imitators that are not valid applications of the technique. A typical example of this is an experiment that varies only one physical variable, such as the dependence of transport on density, but quotes the result in terms of a dimensionless quantity, such as a dependence on collisionality. This is simply an inappropriate transformation of variables, not a dimensionless scaling experiment, since the other dimensionless variables (in this case, ρ_* and β) also vary. The reader is encouraged to read critically the works that lay claim to measure a scaling with respect to a dimensionless quantity to see if the method was correctly applied. Time, space and discretion have prevented the review here of all such works in the plasma physics literature.

In conclusion, the final lines of Buckingham's landmark paper [2] seem still to be a fitting ending for a discussion of dimensionless parameter scaling:

> 'It is hoped that the few sample illustrations [of dimensional analysis] which have been given will prove interesting to physicists who have not been in the habit of making much use of dimensional reasoning; but if this paper merely helps a little toward dispelling the metaphysical fog that seems to be engulfing us, it will have attained its object.'

Acknowledgments

The work of TCL and CCP was supported by the U.S. Department of Energy under DE-FC02-04ER54698. The work of JGC was supported jointly by the United Kingdom Engineering and Physical Research Council and EURATOM. The authors gratefully acknowledge comments on the manuscript and the production of figure 34 by D C McDonald.

References

[1] Tolman R C 1914 *Phys. Rev.* **3** 244
[2] Buckingham E 1914 *Phys. Rev.* **4** 345
[3] Rayleigh J W S 1915 *Nature* **95** 66
[4] Bridgman P W 1922 *Dimensional Analysis* (New Haven: Yale University Press)
[5] Lamb H 1932 *Hydrodynamics* (Cambridge: Cambridge University Press)
[6] Sedov L I 1959 *Similarity and Dimensional Methods in Mechanics* (London: Infosearch)
[7] Allen J 1947 *Scale Models in Hydraulic Engineering* (New York: Longmans, Green)
[8] Kadomtsev B B 1975 *Sov. J. Plasma Phys.* **1** 295
[9] Kadomtsev B B 1992 *Tokamak Plasma: A Complex Physical System* (Bristol: Institute of Physics Publishing)
[10] Connor J W and Taylor J B 1977 *Nucl. Fusion* **17** 1047
[11] Connor J W 1988 *Plasma Phys. Control. Fusion* **30** 619.
[12] Beiser A and Raab B 1961 *Phys. Fluids* **4** 177
[13] Lacina J 1971 *Plasma Phys.* **13** 303
[14] Waltz R E, DeBoo J C and Rosenbluth M N 1990 *Phys. Rev. Lett.* **65** 2390
[15] Hinton F L and Hazeltine R D 1976 *Rev. Mod. Phys.* **48** 239
[16] Hirshman S P and Sigmar D J 1981 *Nucl. Fusion* **21** 1079
[17] Kovrizhnykh L M 1984 *Nucl. Fusion* **24** 851
[18] Liewer P C 1985 *Nucl. Fusion* **25** 543
[19] Callen J D 1992 *Phys. Fluids* B **4** 2142
[20] Editors I P B *et al* 1999 *Nucl. Fusion* **39** 2175
[21] Kaye S M *et al* 1997 *Nucl. Fusion* **37** 1303
[22] Goldston R J *et al* 1990 *Proc. 17th EPS Conf. on Controlled Fusion and Plasma Heating (Amsterdam, The Netherlands)* p 134
[23] Perkins F W *et al* 1993 *Phys. Fluids* B **5** 477
[24] Scott S D *et al* 1991 *Plasma Physics and Controlled Nuclear Fusion Research 1990 (Washington, DC, USA)* vol 1 p 235
[25] Petty C C *et al* 1998 *Phys. Plasmas* **5** 1695
[26] Luce T C *et al* 2002 *Nucl. Fusion* **42** 1193
[27] Thomsen K *et al* 1998 *Proc. 25th EPS Conf. on Controlled Fusion and Plasma Physics (Praha, Czech Republic)*
[28] Christiansen J P *et al* 1999 *Fusion Energy 1998 (Yokohama, Japan)* (Vienna: IAEA) vol 2 p 765
[29] Greenwald M 2002 *Plasma Phys. Control. Fusion* **44** R27
[30] Petty C C *et al* 2004 *Plasma Phys. Control. Fusion* **46** A207
[31] Christiansen J P *et al* 1993 *Nucl. Fusion* **33** 863
[32] Alexander M *et al* 1996 *Proc. 23rd EPS Conf. on Control. Fusion and Plasma Physics* vol 20C (ECA) Pt. I p 103
[33] Stroth U *et al* 1993 *Phys. Rev. Lett.* **70** 936
[34] Jernigan T C *et al* 1995 *Phys. Plasmas* **2** 2435
[35] Yamada H *et al* 2001 *Nucl. Fusion* **41** 901
[36] Yamada H *et al* 2000 *Phys. Rev. Lett.* **84** 1216
[37] Petty C C, Luce T C and Pinsker R I 1994 *Radio Frequency Power in Plasmas* (New York: AIP) p 165
[38] Petty C C *et al* 1995 *Phys. Rev. Lett.* **74** 1763
[39] Shirai H *et al* 1995 *J. Phys. Soc. Japan* **64** 4209
[40] Zou X L *et al* 1996 *Proc. 23rd EPS Conf. on Controlled Fusion and Plasma Physics (Kiev, Ukraine)* p 392
[41] Petty C C *et al* 1995 *Phys. Plasmas* **2** 2342
[42] Luce T C *et al* 1995 *Plasma Physics and Controlled Nuclear Fusion Research 1994 (Sevilla, Spain)* (Vienna: IAEA) vol 1 p 319
[43] Cordey J G *et al* 1996 *Plasma Phys. Control. Fusion* **38** A67
[44] Cordey J G *et al* 2004 *Proc. 31st EPS Conf. on Plasma Physics (London, UK)* vol 28G (ECA) O1.05

[45] Ryter F *et al* 1997 *Fusion Energy 1996 (Montreal, Canada)* (Vienna: IAEA) vol 1 p 625
[46] Greenwald M *et al* 1998 *Plasma Phys. Control. Fusion* **40** 789
[47] Shirai H *et al* 2000 *Plasma Phys. Control. Fusion* **42** 1193
[48] Petty C C *et al* 2002 *Phys. Plasmas* **9** 128
[49] Cordey J G *et al* 1996 *Plasma Phys. Control. Fusion* **38** 1237
[50] Petty C C and Luce T C 1997 *Nucl. Fusion* **37** 1
[51] Waltz R E, DeBoo J C and Osborne T H 1992 *Nucl. Fusion.* **32** 1051
[52] Luce T C and Petty C C 1995 *Proc. 22nd EPS Conf. on Controlled Fusion and Plasma Physics (Bournemouth, UK)* p III-025
[53] Wade M R, Luce T C and Petty C C 1997 *Phys. Rev. Lett.* **79** 419
[54] Zastrow K-D *et al* 1999 *Nucl. Fusion* **39** 1891
[55] Zastrow K-D *et al* 2004 *Plasma Phys. Control. Fusion* **46** B255
[56] McDonald D C *et al* 2004 Particle and energy transport in dedicated ρ^*, β and ν^* scans in JET ELMy H-modes *20th IAEA Fusion Energy Conf. (Vilamoura, Portugal)* EX6-6
[57] Baker D R *et al* 2000 *Nucl. Fusion* **40** 799
[58] Waltz R E, Kerbel G D and Milovich J 1994 *Phys. Plasmas* **1** 2229
[59] Ryter F and H Mode Database Working Group 1996 *Nucl. Fusion* **36** 1217
[60] Imbeaux F, Ryter F and Garbet X 2001 *Plasma Phys. Control. Fusion* **43** 1503
[61] Baker D R and Rosenbluth M N 1998 *Phys. Plasmas* **5** 2936
[62] McKee G R *et al* 2001 *Nucl. Fusion* **41** 1235
[63] Hennequin P *et al* 2004 *Plasma Phys. Control. Fusion* **46** B121
[64] Stroth U *et al* 2004 *Phys. Plasmas* **11** 2558
[65] Toi K *et al* 2002 *Proc. 29th EPS Conf. on Plasma Physics and Controlled Fusion (Montreux, Switzerland)* P-4.061
[66] Ramisch M *et al* 2005 *Phys. Plasmas* **12** 032504
[67] Waltz R E *et al* 1997 *Phys. Plasmas* **4** 2482
[68] Snyder P B and Hammett G W 2001 *Phys. Plasmas* **8** 744
[69] Candy J and Waltz R E 2003 *J. Comput. Phys.* **186** 545
[70] Kim J Y, Horton W and Dong J Q 1993 *Phys. Fluids* B **5** 4030
[71] Gao Z *et al* 2001 *Phys. Plasmas* **8** 2816
[72] Bourdelle C *et al* 2003 *Phys. Plasmas* **10** 2881
[73] Connor J W and Wilson H R 1994 *Plasma Phys. Control. Fusion* **36** 719
[74] Petty C C and Luce T C 1997 *Proc. 24th EPS Conf. on Controlled Fusion and Plasma Physics (Berchtesgaden, Germany)* p 1085
[75] Luce T C *et al* 1997 *Fusion Energy 1996 (Montreal, Canada)* (Vienna: IAEA) vol 1 p 611
[76] Petty C C *et al* 1998 *Nucl. Fusion* **38** 1183
[77] Cordey J G *et al* 1997 *Fusion Energy 1996 (Montreal, Canada)* (Vienna: IAEA) vol 1 p 603
[78] Candy J 2005 *Phys. Plasmas* **12** 072307
[79] Christiansen J P, Cordey J G and Thomsen K 1990 *Nucl. Fusion* **30** 1183
[80] Christiansen J P and Cordey J G 1998 *Nucl. Fusion* **38** 1757
[81] Petty C C *et al* 2004 *Phys. Plasmas* **11** 2514
[82] McDonald D C *et al* 2004 *Plasma Phys. Control. Fusion* **46** A215
[83] Scott S D *et al* 1993 *Plasma Physics and Controlled Nucl. Fusion Research 1992 (Würzburg, Germany)* (Vienna: IAEA) vol 3 p 427
[84] Wilgen J B *et al* 1993 *Phys. Fluids* B **5** 2513
[85] Carreras B A and Diamond P H 1989 *Phys. Fluids* B **1** 1011
[86] Harris J H *et al* 1989 *Phys. Rev. Lett.* **63** 1249
[87] Yamada H *et al* 2001 *Plasma Phys. Control. Fusion* **43** A55
[88] Zou X L *et al* 1997 *Proc. 24th EPS Conf. on Controlled Fusion and Plasma Physics (Berchtesgaden, Germany)* p I-169
[89] Zou X L *et al* 1999 *Fusion Energy 1998 (Yokohama, Japan)* (Vienna: IAEA) vol 2 p 805
[90] Lin Z *et al* 1999 *Phys. Rev. Lett.* **83** 3645
[91] Hahm T S *et al* 2000 *Plasma Phys. Control. Fusion* **42** A205
[92] Hassam A B 1992 *Phys. Fluids* B **4** 1846
[93] Greenwald M *et al* 1988 *Nucl. Fusion* **28** 2199
[94] Paccagnella R, Romanelli F and Briguglio S 1990 *Nucl. Fusion* **30** 545
[95] Fröjdg M, Liljeström M and Nordman H 1992 *Nucl. Fusion* **32** 419
[96] Dominguez R R and Staebler G M 1993 *Nucl. Fusion* **33** 51

[97] Petty C C and Luce T C 1999 *Phys. Plasmas* **6** 909
[98] Hogeweij G M D *et al* 2000 *Proc. 27th EPS Conf. on Controlled Fusion and Plasma Physics (Budapest, Hungary)* p 944
[99] Schachter J M 1997 Local transport analysis for the Alcator C-Mod Tokamak *PhD Thesis, Report* PSFC/RR-97-12 (Cambridge, MA: Plasma Science and Fusion Center)
[100] Valovic M *et al* 1999 *Proc. 26th EPS Conf. on Controlled Fusion and Plasma Physics (Maastricht, The Netherlands)* p 149
[101] Fielding S J *et al* 2001 *Nucl. Fusion* **41** 909
[102] Diamond P H *et al* 2005 *Plasma Phys. Control. Fusion* **47** R35
[103] McCarthy D R *et al* 1992 *Phys. Fluids* B **4** 1846
[104] Waltz R E *et al* 1995 *Phys. Plasmas* **2** 2408
[105] Petty C C *et al* 1999 *Fusion Energy 1998 (Yokohama, Japan)* (Vienna: IAEA) vol 2 p 789
[106] Petty C C, Kinsey J E and Luce T C 2004 *Phys. Plasmas* **11** 1011
[107] Luce T C, Petty C C and Kinsey J E 2001 *Proc. 28th EPS Conf. on Control. Fusion and Plasma Physics (Funchal, Portugal)* p 1377
[108] Rhodes T L *et al* 2002 *Phys. Plasmas* **9** 2141
[109] Sydora R D, Decyk V K and Dawson J M 1996 *Plasma Phys. Control. Fusion* **38** A281
[110] Kinsey J E *et al* 1995 *Phys. Scr.* **52** 428
[111] Waltz R E and Miller R L 1999 *Phys. Plasmas.* **6** 4265
[112] Anderson J A *et al* 2000 *Plasma Phys. Control. Fusion* **42** 545
[113] Cordey J G *et al* 1999 *Nucl. Fusion* **39** 1763
[114] Cordey J G *et al* 2000 *Plasma Phys. Control. Fusion* **42** A127
[115] Cordey J G *et al* 1999 *Nucl. Fusion* **39** 301
[116] Jacquinot J *et al* 1999 *Nucl. Fusion* **39** 235
[117] Zarnstorff M C *et al* 1995 *Plasma Physics and Controlled Nuclear Fusion Research 1994 (Sevilla, Spain)* (Vienna: IAEA) vol 1 p 183
[118] Synakowski E J *et al* 1995 *Proc. 22nd EPS Conf. on Controlled Fusion and Plasma Physics (Bournemouth, UK)* p III-013
[119] Scott S D *et al* 1997 *Fusion Energy 1996 (Montreal, Canada)* (Vienna: IAEA) vol 1 p 573
[120] McDonald D C *et al* 2004 *Plasma Phys. Control. Fusion* **46** 519
[121] Konings J A *et al* 1997 *Nucl. Fusion* **37** 199
[122] Batha S H *et al* 1997 *Proc. 24th EPS Conf. on Controlled Fusion and Plasma Physics (Berchtesgaden, Germany)* p 1057
[123] Petty C C *et al* 1999 *Phys. Rev. Lett.* **83** 3661
[124] Garbet X and Waltz R E 1996 *Phys. Plasmas* **3** 1898
[125] Beklemishev A D and Horton W 1992 *Phys. Fluids* B **4** 200
[126] Hahm T S and Tang W M 1996 *Phys. Plasmas* **3** 242
[127] Garbet X *et al* 1999 *Nucl. Fusion* **39** 2063
[128] Kardaun O J W F 2005 *Classical Methods of Statistics: With Applications in Fusion-Oriented Plasma Physics* (New York: Springer)
[129] Bickerton R J and London H 1958 *Proc. Phys. Soc.* **72** 116
[130] Goldston R J 1984 *Plasma Phys. Control. Fusion* **26** 87
[131] Yushmanov P N *et al* 1990 *Nucl. Fusion* **30** 1999
[132] Cordey J G, *et al* 1991 *Plasma Physics and Controlled Nuclear Fusion Research 1990 (Washington, DC, USA)* (Vienna: IAEA) vol 3 p 443
[133] Christiansen J P *et al* 1992 *Plasma Phys. Control. Fusion* **34** 1881
[134] Thomsen K *et al* 1994 *Nucl. Fusion* **34** 131
[135] Petty C C *et al* 2003 *Fusion Sci. Technol.* **43** 1
[136] Cordey J G *et al* 2005 *Nucl. Fusion* **45** 1078
[137] Kardaun O J W F *et al* 2003 private communication, poster presentation at the 2003 H-mode Workshop, San Diego, CA
[138] Wilson H R *et al* 2004 *Nucl. Fusion* **44** 917
[139] Dose V, Preuss R and von der Linden W 1998 *Nucl. Fusion* **38** 571
[140] Dose V, Preuss R and von der Linden W 1998 *Phys. Rev. Lett.* **81** 3407
[141] Preuss R, Dose V and von der Linden W 1999 *Nucl. Fusion* **39** 849
[142] Budny R V *et al* 2000 *Phys. Plasmas* **7** 5038
[143] Fisch N J 1987 *Rev. Mod. Phys.* **59** 175
[144] Carlstrom T N *et al* 1996 *Plasma Phys. Control. Fusion* **38** 1231

[145] Snipes J A and ITER H-mode Threshold Database Working Group 1997 *Proc. 24th EPS Conf. on Controlled Fusion and Plasma Physics (Berchtesgaden, Germany)* p III-961
[146] Itoh K and Itoh S-I 1989 *Plasma Phys. Control. Fusion* **31** 487
[147] Cordey J G, Kerner W and Pogutse O 1995 *Plasma Phys. Control. Fusion* **37** 773
[148] Chankin A V 1997 *Plasma Phys. Control. Fusion* **39** 1059
[149] Suttrop W *et al* 2002 *19th IAEA Fusion Energy Conf. (Lyon, France)* EX/P5-07
[150] Kadomtsev B B 1989 *Comment. Plasma Phys. Control. Fusion* **13** 57
[151] Lackner K 1994 *Comment. Plasma Phys. Control. Fusion* **15** 359
[152] Suttrop W *et al* 2002 *Proc. 29th EPS Conf. on Plasma Physics and Controlled Fusion (Montreux, Switzerland)* P-1.030
[153] Fukuda T *et al* 1997 *Nucl. Fusion* **37** 1199
[154] Mukhovatov V *et al* 2003 *Plasma Phys. Control. Fusion* **45** A235
[155] Groebner R J and Osborne T H 1998 *Phys. Plasmas* **5** 1800
[156] Leonard A W *et al* 2003 *Phys. Plasmas* **10** 1765
[157] Wade M R *et al* 2005 *Phys. Plasmas* **12** 056120
[158] Ferron J R and Snyder P B 2005 *Fusion Sci. Technol.* **48** 931
[159] Snyder P B *et al* 2004 *Plasma Phys. Control. Fusion* **46** A131
[160] Mahdavi M A *et al* 2002 *Proc. 29th EPS Conf. on Plasma Physics and Controlled Fusion (Montreux, Switzerland)* P2.098
[161] Chankin A V and Saibene G 1999 *Plasma Phys. Control. Fusion* **41** 913
[162] Hatae T *et al* 2000 *Plasma Phys. Control. Fusion* **42** A283
[163] Yamada H *et al* 2002 *Plasma Phys. Control. Fusion* **44** A245
[164] Kallenbach A *et al* 2002 *Nucl. Fusion* **42** 1184
[165] Mossessian D A *et al* 2003 Phys. Plasmas **10** 689
[166] Stangeby P C 2003 *J. Phys. D: Appl. Phys.* **36** 2784
[167] LaBombard B *et al* 2000 *Nucl. Fusion* **40** 2041
[168] Groth M and Porter G D 2005 *Proc. 32nd EPS Conf. on Controlled Fusion and Plasma Physics (Tarragona, Spain)* P4.015
[169] Fenstermacher M E *et al* 2005 *Nucl. Fusion* **45** 1493
[170] Saibene G *et al* 2004 *Plasma Phys. Control. Fusion* **46** A195
[171] Catto P J, Knoll D A and Krasheninnikov S I 1996 *Phys. Plasmas* **3** 3191
[172] Catto P J, Krasheninnikov S I, Connor J W 1996 *Phys. Plasmas* **3** 927
[173] Hutchinson I H and Vlases G C 1996 *Nucl. Fusion* **36** 783
[174] Connor J W *et al* 1999 *Nucl. Fusion* **39** 169
[175] Wobig H 1972 *Plasma Phys.* **14** 403
[176] Montgomery D 1992 *Plasma Phys. Control. Fusion* **34** 1157
[177] Montgomery D 1993 *Plasma Phys. Control. Fusion* **35** B105
[178] Cappello S and Escande D F 2000 *Phys. Rev. Lett.* **85** 3838
[179] Thyagaraja A 1994 *Plasma Phys. Control. Fusion* **36** 1037
[180] Montgomery D 1994 *Plasma Phys. Control. Fusion* **36** 2095
[181] Troyon F *et al* 1984 *Plasma Phys. Control. Fusion* **26** 209
[182] Sykes A *et al* 1983 *Proc. 10th EPS Conf. on Controlled Fusion and Plasma Physics (Aachen, Germany)* Pt. II p 363
[183] Stambaugh R D *et al* 1985 *Plasma Physics Controlled Nuclear Fusion Research 1984 (London, UK)* (Vienna: IAEA) vol 1 p 217
[184] Strait E J 1994 *Phys. Plasmas.* **1** 1415
[185] Lao L L *et al* 1996 *Phys. Plasmas* **3** 1951
[186] Hender T C *et al* 2004 *Nucl. Fusion* **44** 788
[187] La Haye R J *et al* 2000 *Phys. Plasmas* **7** 3349
[188] Buttery R J *et al* 2003 *Nucl. Fusion* **43** 69
[189] Buttery R J *et al* 2004 *Nucl. Fusion* **44** 678
[190] Wolfe S M *et al* 2005 *Phys. Plasmas* **12** 056110
[191] Heidbrink W W *et al* 2003 *Plasma Phys. Control. Fusion* **45** 983